# The Role of Conglomerate Crystallization in Spontaneous Resolution and Chiral Amplification

Reajean Sivakumar

A Thesis
in
The Department
of
Chemistry and Biochemistry

Presented in Partial Fulfillment of the Requirements
for the Degree of Master Science (Chemistry) at
Concordia University
Montréal, Québec, Canada

September 2016

**CONCORDIA UNIVERSITY**

**School of Graduate Studies**

This is to certify that the thesis prepared

By: Reajean Sivakumar

Entitled: The Role of Conglomerate Crystals in Spontaneous Resolution and Chiral Amplification

and submitted in partial fulfillment of the requirements for the degree of

**Master of Science (Chemistry)**

complies with the regulations of the University and meets the accepted standards with respect to originality and quality.

Signed by the final examining committee:

| | |
|---|---|
| Dr. Rafik Naccache | Chair |
| Dr. Yves Gélinas | Examiner |
| Dr. Xavier Ottenwaelder | Examiner |
| Dr. Louis A.Cuccia | Supervisor |

Approved by _____
Chair of Department or Graduate Program Director

_____ 20____ _____
Dean of Faculty

## ABSTRACT

The Role of Conglomerate Crystals in Spontaneous Resolution and Chiral Amplification

Reajean Sivakumar

The mystery of the origin of homochirality in Nature has been thoroughly investigated due to the essential role it plays in Chemistry, Biochemistry and Biology. For example, enantiopure compounds are often essential in the pharmaceutical and agrochemical industries. New aspects of chemistry and chirality can be explored by effectively utilizing the unique nature of conglomerate crystals. In some cases, conglomerate crystals can be easily resolved by carefully observing the features of the crystals. Resolution is possible through observation of hemihedrism, macromorphology, circular polarization or various surface features.

Cytosine and 1,2-bis(N-benzoyl-N-methylamino)benzene are two examples of compounds that form centrosymmetric monohydrate racemic crystals but non-centrosymmetric anhydrous conglomerate crystals.[1] Herein, a novel approach to asymmetric amplification by coupling conglomerate crystal formation *via* dehydration, with subsequent Viedma ripening (*i.e.* attrition-enchanced deracemization) is being explored. [2,3] A systematic search of the Cambridge Crystallographic Database for other crystal systems which can undergo desolvation and subsequent chiral amplification is ongoing.

Enantiomer-specific oriented attachment, an essential process in Viedma ripening, was also investigated in guanidine carbonate crystals. Simply boiling or shaking powdered racemic guanidine carbonate in saturated solution leads to the formation of large crystalline clusters. These clusters, characterized by solid-state circular dichroism and X-ray powdered diffraction, were found to be nearly homochiral. Enantiomer-specific oriented attachment can be thought of as a mesoscale analogue of conglomerate crystallization.

## DEDICATION

I would like to first thank my research supervisor, Dr. Louis A. Cuccia. My first encounter with Dr. Cuccia was during his stereochemistry course 4 years ago. I thoroughly enjoyed his class, and appreciated his knowledge and teaching methods. His lasting impression, led me to enquire about the possibility of carrying out my MSc. with him and luckily he accepted me as a student. In the last two years, he became a great mentor and friend. I thank him for his relentless support, encouragement and his extreme attention to detail. His persistence and kindness have been a great factor on my growth as a scientist and as a person.

To all my current and former lab mates, fellow graduate students and friends, thank you for your support, help and friendship that you have provided me with over the last few years. My friends at Concordia University have been a second family to me. Staying at Concordia has allowed me to forge new friendships which I will appreciate forever. To all the personnel and technical staff, thank you for putting up with my many requests over the past few years. Dr. Rolf Schmidt has been extremely helpful; I was able to appreciate his ability to combine his expertise with a slight touch of humour.

I would also like to thank the various professionals that I've had a chance to work with. Dr. Cristóbal Viedma, Dr. Pedro Cintas, Dr. Xavier Ottenwaelder, Dr. Jeanne Paquette, Dr. D.Scott Bohle, Dr. Simon Woo and Munendra Yadav who have all contributed to my development as a scientist. Their knowledge and insight have been essential to the completion of my research. Additional thanks to Dr. Yves Gélinas and Dr. Xavier Ottenwaelder for their continuous support and help throughout the research project.

Finally, I would like to thank my parents. My father taught me to be the best man that I could be. My mother is the definition of a strong woman. Although faced with many obstacles, my mother was able to unconditionally love and raise three children to the best of her abilities and for that I'm forever grateful. I could have not possibly gotten to this stage of my life without her.

# Table of Contents

# List of figures

# List of tables

# List of equations

# Preface. Contributions of Authors

The manuscript, *"Homochiral Crystal Generation via Sequential Dehydration and Viedma Ripening*" was completed with the help of Mohammad S. Askari, Dr. Simon Woo, Carolin Madwar, Dr. Xavier Ottenwaelder, Dr. D. Scott Bohle and Dr. Louis A. Cuccia.

Mohammad S. Askari and Dr. Xavier Ottenwaelder carried out single-crystal X-ray diffraction on achiral and chiral crystals of 1,2-bis(*N*-benzoyl-*N*-methylamino)benzene and chiral crystals of 1,2-bis-(*N*-benzenesulfonyl-*N*-methylamino)benzene. Synthetic procedure for the aforementioned compounds was facilitated with the aid of Dr. Simon Woo, who provided great insight and guidance. Carolin Madwar provided guidance during thermogravimetric analysis and differential scanning calorimetry. Dr. Louis A. Cuccia and Dr. D. Scott Bohle supervised the research project and were instrumental in the writing the published paper.

The manuscript, *"Enantiomer-Specific Oriented Attachment of Guanidine Carbonate Crystals"* was completed with the help of Amaury Fouret, Julien Kwiatoszynski, Thi Phuong Thao Nguyen, Parsram Ramrup, Pui Shan Monica Cheung, Dr. Pedro Cintas, Dr. Cristóbal Viedma and Dr. Louis A. Cuccia. Preliminary results for boiling and shaking were obtained by Amaury Fouret, Julien Kwiatoszynski and Parsram Ramrup. Preliminary results were also obtained by Thi Phuong Thao Nguyen and Pui Shan Monica Cheung. Dr. Louis A. Cuccia carried out SEM analysis of guanidine carbonate clusters. The paper was written with the help of Dr. Pedro Cintas, Dr. Cristóbal Viedma and Dr. Louis A. Cuccia.

Simon Woo
4707 Rue Villeret
Pierrefonds, QC H9K 1P7
Canada

I, Simon Woo, give copyright clearance for the inclusion of the following manuscript, of which I am a co-author, into Reajean Sivakumar's M.Sc. thesis:

Sivakumar, R.; Askari, M. S.; Woo, S.; Madwar, C.; Ottenwaelder, X.; Bohle, D. S.; Cuccia, L. A. *CrystEngComm* **2016**, *18*, 4277–4280.

Signature

July 26, 2016
Date

Scott Bohle
801 Sherbrooke St. W.
Department of Chemistry
McGill University
Montreal H3A 0B8
Canada

I, Scott Bohle, give copyright clearance for the inclusion of the following manuscript, of which I am a co-author, into Reajean Sivakumar's M.Sc. thesis:

Sivakumar, R.; Askari, M. S.; Woo, S.; Madwar, C.; Ottenwaelder, X.; Bohle, D. S.; Cuccia, L. A. *CrystEngComm* **2016**, *18*, 4277–4280.

Signature

7/10/2016
Date

Dr. Xavier Ottenwaelder
Department of Chemistry and Biochemistry
7141 Sherbrooke street West
Montreal, QC
H4B 1R6
Canada

I, Xavier Ottenwaelder, give copyright clearance for the inclusion of the following manuscript, of which I am a co-author, into Reajean Sivakumar's M.Sc. thesis:

Sivakumar, R.; Askari, M. S.; Woo, S.; Madwar, C.; Ottenwaelder, X.; Bohle, D. S.; Cuccia, L. A. *CrystEngComm* **2016**, *18*, 4277–4280.

Signature

14 July 2016
Date

Amaury Fouret
64 rue de Strasbourg
Courbevoie, 92400
FRANCE

I, Amaury Fouret, give copyright clearance for the inclusion of the following manuscript, of which I am a co-author, into Reajean Sivakumar's M.Sc. thesis:

Sivakumar, R.; Kwiatoszynski, J.; Fouret, A.; Nguyen, T. P. T.; Ramrup, P.; Cheung, P. S. M.; Cintas, P.; Viedma, C.; Cuccia, L. A. *Cryst. Growth & Des.* **2016**, *16*, 3573–3576.

Signature

07/07/2016

Date

Pedro Cintas
Dpt. Organic & Inorganic Chemistry
Faculty of Sciences-UEX
E-06006 Badajoz
Spain

I, Pedro Cintas, give copyright clearance for the inclusion of the following manuscript, of which I am a co-author, into Reajean Sivakumar's M.Sc. thesis:

Sivakumar, R.; Kwiatoszynski, J.; Fouret, A.; Nguyen, T. P. T.; Ramrup, P.; Cheung, P. S. M.; Cintas, P.; Viedma, C.; Cuccia, L. A. *Cryst. Growth & Des.* **2016**, *16*, 3573–3576.

Signature: P. Cintas, PhD

(Chemistry Professor) Date: 11th July 2016

Mohammad Sharif Askari
801 Sherbrooke Street West
Department of Chemistry, McGill University, OM 400
Montreal, QC., H3A 0B8
Canada

I, Mohammad Sharif Askari, give copyright clearance for the inclusion of the following manuscript, of which I am a co-author, into Reajean Sivakumar's M.Sc. thesis:

Sivakumar, R.; Askari, M. S.; Woo, S.; Madwar, C.; Ottenwaelder, X.; Bohle, D. S.; Cuccia, L. A. *CrystEngComm* **2016**, *18*, 4277–4280.

Signature

01/08/2016
Date

Carolin Madwar
10 st Jacques apt 308
Montreal, Quebec, H2Y 1L3
Canada

I, Carolin Madwar, give copyright clearance for the inclusion of the following manuscript, of which I am a co-author, into Reajean Sivakumar's M.Sc. thesis:

Sivakumar, R.; Askari, M. S.; Woo, S.; Madwar, C.; Ottenwaelder, X.; Bohle, D. S.; Cuccia, L. A. *CrystEngComm* **2016**, *18*, 4277–4280.

Signature

24/08/2016

Date

Cristobal Viedma
Universidad Complutense
Madrid 28040
Spain

I, Cristóbal Viedma, give copyright clearance for the inclusion of the following manuscript, of which I am a co-author, into Reajean Sivakumar's M.Sc. thesis:

Sivakumar, R.; Kwiatoszynski, J.; Fouret, A.; Nguyen, T. P. T.; Ramrup, P.; Cheung, P. S. M.; Cintas, P.; Viedma, C.; Cuccia, L. A. *Cryst. Growth & Des.* **2016**, *16*, 3573–3576.

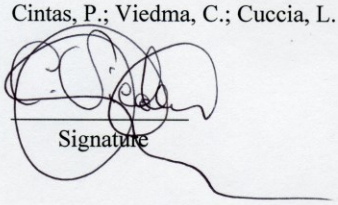

Signature

07-12-16

Date

Pui Shan Monica Cheung
9320 Av. Oligny
Brossard, Québec J4Y 3A6
Canada

I, Pui Shan Monica Cheung, give copyright clearance for the inclusion of the following manuscript, of which I am a co-author, into Reajean Sivakumar's thesis:

Sivakumar, R.; Kwiatoszynski, J.; Fouret, A.; Nguyen, T. P. T.; Ramrup, P.; Cheung, P. S. M.; Cintas, P.; Viedma, C.; Cuccia, L. A. *Cryst. Growth & Des.* **2016**, *16*, 3573–3576.

Monica Cheung
Signature

July 10, 2016
Date

Louis Cuccia
310 Parkwood Circle
Dorval, Québec
CANADA
H9S 3A3

I, Louis A.Cuccia, give copyright clearance for the inclusion of the following manuscripts, of which I am a co-author, into Reajean Sivakumar's M.Sc. thesis:

Sivakumar, R.; Askari, M. S.; Woo, S.; Madwar, C.; Ottenwaelder, X.; Bohle, D. S.; Cuccia, L. A. *CrystEngComm* **2016**, *18*, 4277–4280.

Sivakumar, R.; Kwiatoszynski, J.; Fouret, A.; Nguyen, T. P. T.; Ramrup, P.; Cheung, P. S. M.; Cintas, P.; Viedma, C.; Cuccia, L. A. *Cryst. Growth & Des.* **2016**, *16*, 3573–3576.

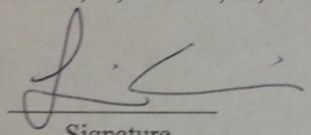

Signature

August 22, 2016

Date

Parsram Ramrup
2790 Modugno
Ville Saint-Laurent, QC H4R1V7
Canada

I, Parsram Ramrup, give copyright clearance for the inclusion of the following manuscript, of which I am a co-author, into Reajean Sivakumar's M.Sc. thesis:

Sivakumar, R.; Kwiatoszynski, J.; Fouret, A.; Nguyen, T. P. T.; Ramrup, P.; Cheung, P. S. M.; Cintas, P.; Viedma, C.; Cuccia, L. A. *Cryst. Growth & Des.* **2016**, *16*, 3573–3576.

P. Ramrup
Signature

August 22, 2016
Date

# Chapter 1. Introduction

## *1.1. Chirality*

*"I call any geometric figure, or group of points, chiral, and say it has chirality, if its image in a plane mirror, ideally realized, cannot be brought to coincide with itself."*- Lord Kelvin (Sir William Thomson), Robert Boyle Lecture at the Oxford University Junior Scientific Club in 1893 (1893).[4,5]

An object which is nonsuperposable with its mirror image is chiral. Chirality and its origins have preoccupied chemists, physicists and biologists since the very beginnings of molecular chemistry.[6] The highly sought-after understanding of the origin of homochirality is more than likely due to the fact that it is inexorably linked to the origin of life itself, since almost all chiral biological molecules are homochiral.[6] In relation to this thesis, chirality has been undeniably associated to crystals since the very early investigations of chiral phenomena, beginning with Iceland spar, quartz and, of course, sodium ammonium tartrate tetrahydrate.[7–9]

The polarizing ability of crystals of Iceland spar (*i.e.* calcite) is believed to have guided the Vikings on overcast days as they navigated the North Atlantic using the sun.[7] In 1669, Erasmus Bartholinus showed that crystals of Iceland spar exhibit double refraction (*i.e.* images viewed through calcite crystals are doubled).[10] This double refraction is the splitting of unpolarized light into two orthogonal rays of polarized light, and is due to the anisotropic nature of calcite. Huggens (1677) and Sir Isaac Newton (1704) investigated the properties of Iceland spar and remarked that the light emerging from the crystal did not behave in the same way as the incident light.[10] In 1808, Etienne-Louis Malus coined the term polarization for the change light undergoes when reflected off a surface.[10,11] Calcite prisms are still among the best polarizers available in scientific equipment requiring polarized light.[12]

In 1801, the French mineralogist René Haüy (1801) observed small faces on quartz crystals that reduced their overall symmetry.[13,14] These are known as hemihedral faces since the crystal is lacking half the planes required for complete symmetry of the holohedral form.[8,15] He noticed that these faces sometimes pointed to the left and sometimes pointed to the right, but he never reported the mirror image relationship of these faces. In 1811, Arago and Biot observed

'optical rotation' of quartz crystals viewed along the optic axis using a calcite prism, and noted that the optical rotation of polarized light was proportional to the thickness of the quartz plate and inversely proportional to the square of the wavelength of light.[16] The resulting color change, known as optical rotatory dispersion, of quartz plates is particularly insightful in that it shows that there are two forms of quartz, one that is *levorotatory* (left-handed) and one that is *dextrorotatory* (right-handed) (Figure 1).[4,15,17–20]

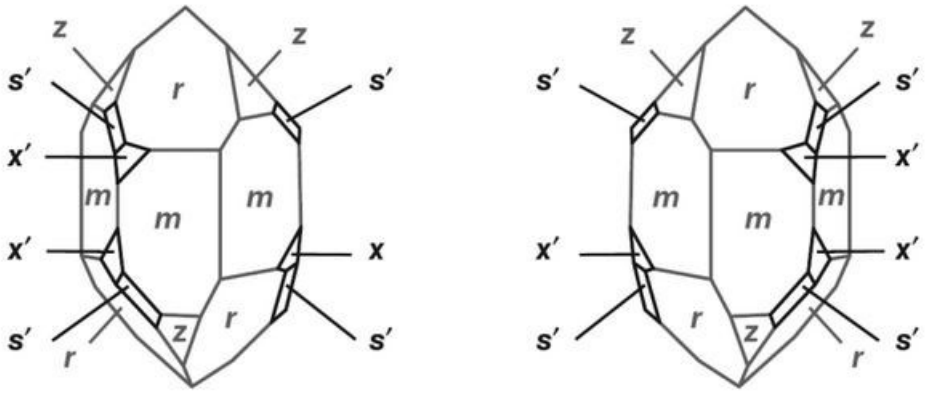


**Figure 1.** Left and right-handed enantiomorphic crystals of quartz. x' and s' are the hemihedral faces. Reprinted with permission from Glaser, R. *Symmetry, Spectroscopy, and Crystallography: The Structural Nexus*; Wiley, 2015.[15]

Biot (1815) also noted that non-crystalline natural products, such as turpentine, camphor and solutions of sucrose, can rotate polarized light (*i.e.* are optically active).[21] Furthermore, Biot's analysis of turpentine vapors allowed him to deduce that the optical rotation was a molecular property. Biot quantified optical rotation measurements and determined that optical rotation was proportional to concentration and the path length of the sample and he, "recognized that the rotation of plane polarized light was a function of the nature of dissolved molecules in liquids, while it was a function of the physical properties of the crystallized forms of minerals."[15]

In 1820, John Herschel made the connection that there was a relationship between the left- or right-pointing hemihedral faces of quartz crystals (*i.e.* the crystal form) observed by Haüy and its optical rotation investigated by Biot.[13] He examined seven quartz crystals, and noted that three were left-handed and four were right-handed.[22,23] Analysis of the hemihedral forms of

quartz by Haüy, Herschel and Biot proved to be invaluable to Louis Pasteur's investigation of sodium ammonium tartrate tetrahydrate crystals.[24]

Sodium ammonium tartrate tetrahydrate was a source of confusion in the early 1830s. This confusion stemmed from Eilhard Mitscherlich's analysis of solutions of tartaric acid and racemic acid (racemic acid was a form of tartaric acid obtained from exposure to excess heat and was also known as paratartaric acid).[25] Mistcherlich observed optical activity in solutions of tartaric acid but solutions of racemic acid were optically inactive. Mitscherlich's misunderstanding was further reinforced due to the identical appearance of both tartaric acid and racemic acid as well as their identical chemical formula.[8] Biot (1836) also investigated the optical rotation of tartaric acid, where all samples gave positive rotation, and also noted that racemic acid was optically inactive.[26] Louis Pasteur continued the work of Biot and his breakthrough occurred when he took a closer look at the crystals of sodium ammonium tartrate tetrahydrate. In 1848, he noticed, based on careful observation of hemihedral faces, that there were two crystal forms present in the samples of racemic acid. These crystals were nonsuperposable mirror images of each other (*i.e.* their morphology was enantiomorphous).[27] With tweezers and a microscope, to observe the asymmetry of the hemihedral faces, Pasteur was able to separate racemic acid into two mirror image forms.[24] Analysis of these crystals in solution by polarimetry confirmed that racemic acid was, in fact, an equal mixture of *levorotatory* tartaric acid and *dextrorotatory* tartaric acid. This approach enabled Pasteur to deduce that there was a relationship between hemihedrism and optical activity.[24] Biot knew that a molecular property was involved in the optical rotation of substances in the non-crystalline state, and his student Pasteur was the first to propose the concept of molecular chirality (*i.e. la dissymétrie moléculaire*).[20,28]

The early investigations of the chiral properties in crystals of Iceland spar, quartz and sodium ammonium tartrate tetrahydrate paved the way for a better understanding of molecular *and* solid-state chirality.

## *1.2. Chirality in Crystals*

### 1.2.1. Conglomerate Crystallization

Solid-state chirality can emerge from achiral or chiral building blocks. A racemic mixture of chiral molecules can form racemic, pseudoracemic or conglomerate crystals (Figure 2).[29] Racemic and pseudoracemic crystals are made up of equal amounts of both enantiomers in an ordered or disordered arrangement, respectively. However, conglomerate crystals of chiral molecules have only one enantiomer present within individual crystals.[30] Conglomerate crystals are formed when a molecule has a higher affinity for itself as opposed to its mirror image.[30]

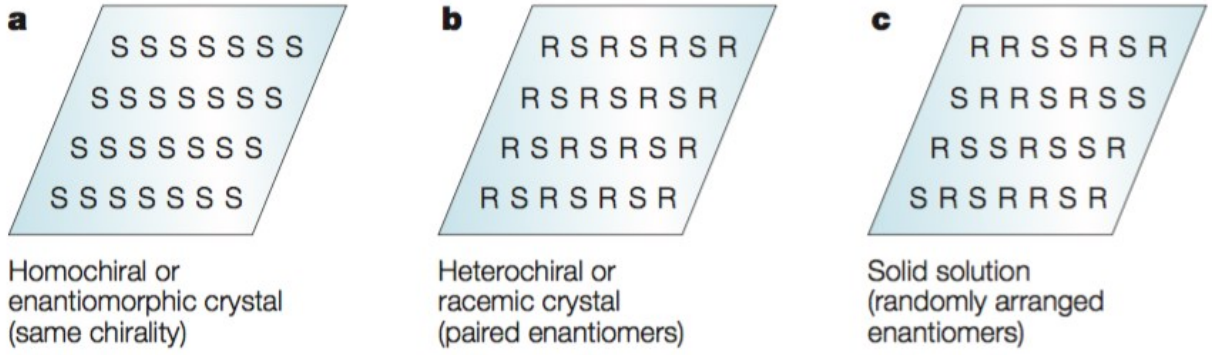


**Figure 2.** Representation of conglomerate, racemic and pseudoracemic crystals. Reprinted with permission from Datta, S.; Grant, D. J. *Nat. Rev. Drug Discov.* **2004**, *3*, 42–57.[29]

Achiral molecules can form either achiral crystals or chiral conglomerate crystals. Chirality in conglomerate crystals formed from achiral building blocks is due either to adopting a chiral conformation or chiral packing in the solid state. The chirality of these crystals resides solely in the solid-state. Note that in the case of atropisomers, chiral conformations can have a finite lifetime in solution.[31] X-ray crystallography, solid-state circular dichroism and polarized light microscopy can be used to probe the chirality of conglomerate crystals originating from achiral molecules.[3,32]

There are 230 crystallographic space groups which can be divided into two sets: (*i*) 165 space groups that can accommodate achiral crystal structures and (*ii*) 65 space groups that can accommodate chiral crystal structures. Conglomerate crystals must crystallize in one of the 65 non-centrosymmetric Sohncke space groups (*i.e.* these 65 space groups lack a center of

inversion). These 65 space groups can be further divided into two sets. There are 43 'acentric' space groups which can contain chiral structures and there are 22 truly chiral space groups that are found as 11 enantiomorphic pairs. In these 22 space groups, the absolute configuration of a molecule can be specifically assigned .[33,34]

Statistical analysis of conglomerate crystallization has been previously carried out. In 1999, Hager *et al*. showed that 80% of conglomerates crystallize in the $P2_1$ and $P2_12_12_1$ space groups.[35] There are several reports that explore the propensity of achiral molecules to crystallize as chiral crystals. The percentage of chiral crystals that are formed from achiral molecules has been determined to be 8% (2005), 8.7% (2005) and 10% (2012) by Matsuura *et al*., Pidcock *et al*. and Dryzun *et al*., respectively.[36–38]

### 1.2.2. Spontaneous Resolution

Conglomerate crystallization is also commonly referred to as spontaneous resolution. Upon spontaneous resolution, a racemic mixture separates into a physical mixture of enantiomorphic crystals.[39] The most notable example of spontaneous resolution is Louis Pasteur's separation of sodium ammonium tartrate tetrahydrate crystals. Pasteur carried out this manual resolution procedure by simply using a pair of tweezers and visualizing the crystals under a microscope.[9] Pasteur's interest in sodium ammonium tartrate tetrahydrate stemmed from his mentor Biot, who observed optical activity for tartaric acid but no optical activity for racemic acid.[26] Upon close analysis, Pasteur separated the crystals based on the asymmetry of the hemihedral faces. Pasteur was somewhat lucky with his investigation of sodium ammonium tartrate tetrahydrate crystals, as: (*i*) they formed conglomerate crystals rather than racemic crystals (Figure 3) and (*ii*) that conglomerate crystallization, in this case, only occurs below 26 °C.[9,15] The separated conglomerate crystals now had optical activity (with equal intensity but opposite sign) and he concluded that racemic acid was in fact an equal mixture of left- and right-handed tartaric acid. This is, in fact, the origin of the now more general stereodescriptor, 'racemic', an equal mixture of left- and right-handed enantiomers. Pasteur's manual separation of these conglomerate crystals was the first example of a resolution of a racemic mixture. This manual separation of crystals became known as 'resolution by triage' or 'Pasteurian resolution'.[9,13,24] It is important to note that this discovery is even more impressive given that

neither the structure of tartaric acid nor the tetrahedral geometry of carbon were known at that time.

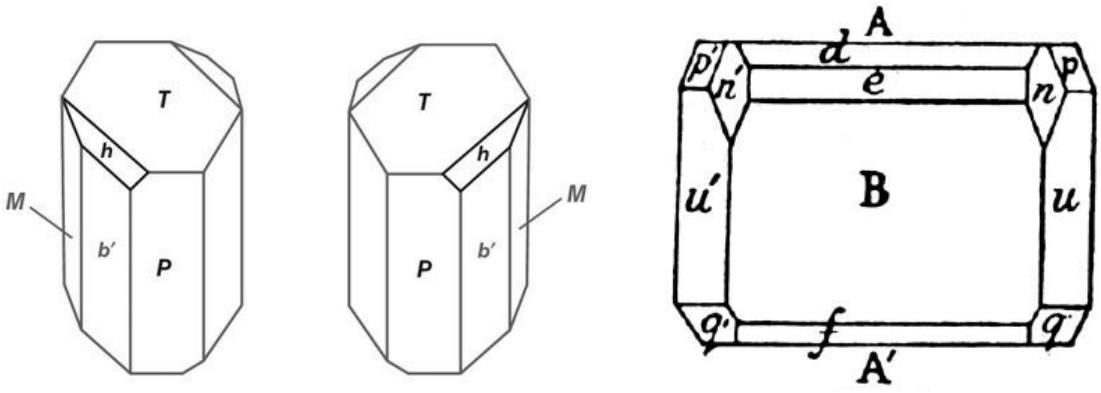


**Figure 3.** Left: Conglomerate crystals of sodium ammonium tartrate tetrahydrate, where *h* is the hemihedral face. Reprinted with permission from Glaser, R. *Symmetry, Spectroscopy, and Crystallography: The Structural Nexus*; Wiley, 2015 Right: Racemic crystal of sodium ammonium tartrate tetrahydrate. Reprinted with permission from Kauffman, G. B.; Myers, R. D. *J. Chem. Educ.* **1975**, *52*.[9,15]

## *1.3. Viedma Ripening*

Conglomerate crystallization can be exploited in various chiral amplification methods to obtain homochiral crystals. Chiral amplification is extensively studied due to the importance of chiral purity in various industries such as the pharmaceutical and agrochemical industries.[40–43] Viedma ripening is a deracemization technique discovered by Cristóbal Viedma in 2005. Viedma's seminal experiments simply involved grinding racemic mixtures of enantiomorphic sodium chlorate crystals. His initial experiment involved ten flasks containing racemic mixtures of enantiomorphic sodium chlorate crystals in saturated solution. After stirring each solution for 10 days he noticed that the sodium chlorate in one flask was homochiral. He was surprised with this result and repeated the experiment, and once again the sodium chlorate in the same flask was homochiral. Repeating the experiment for a third time and changing the location of this unique flask, resulted again in homochiral sodium chlorate only in this one flask. On closer inspection, Viedma noted that the stir bar in only this flask had a ring around the center whereas the others were smooth. Viedma deduced that this ring allowed for grinding of crystals to take place such that the stir bar in only this flask was acting like a mill. To test this hypothesis, glass beads were

added to all the flasks. With this change, the sodium chlorate in all flasks was amplified to homochirality.[2,44,45]

Viedma ripening is an attrition-enchanced deracemization process which is carried out in saturated solution with grinding media (Figure 4).[30] Under these grinding conditions, a racemic mixture of enantiomorphic crystals becomes homochiral. Essential for this process is that one begins with a compound that forms conglomerate crystals. It is important to note that Viedma ripening is a chiral amplification process – as such, the mirror symmetry of the initial system is already broken. Although we state that a racemic mixture is used, in the case of conglomerate crystals, there will always be some degree of broken symmetry with respect to quantity or crystal size (*i.e.* the starting point is not truly racemic in the strictest sense). Viedma ripening relies on three main stages: (*i*) attrition enhanced Ostwald ripening, where crystal attrition speeds up the dissolution process (*i.e.* according to the Gibbs-Thomson effect, smaller crystals are more soluble than the larger crystals) (*ii*) molecules in solution can transform to either enantiomorph to feed crystal growth (through racemization in solution for chiral molecules) and (*iii*) amplification of the initial chiral imbalance by enantiomer-specific oriented attachment. The probability of crystal growth *via* enantiomer-specific oriented attachment is higher for the major enantiomorph whereas the probability for dissolution is higher for the minor enantiomorph. As such, Viedma ripening is an autocatalytic process that ultimately amplifies a racemic mixture of conglomerate crystals to homochirality.[2,3,32]

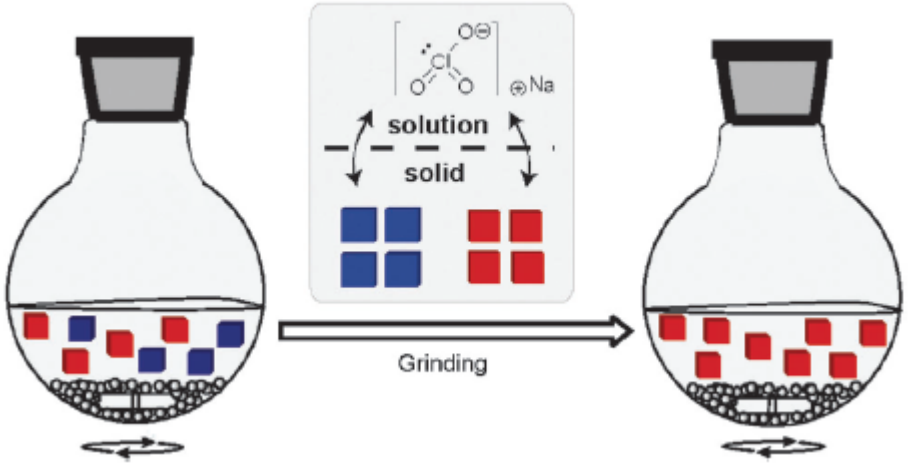

**Figure 4.** Schematic representation of the Viedma ripening of sodium chlorate. Reprinted from Sögütoglu, L.-C.; Steendam, R. R. E.; Meekes, H.; Vlieg, E.; Rutjes, F. P. J. T. *Chem. Soc. Rev.* 2015, *44*, 6723–6732. Published by the Royal Society of Chemistry.[30]

## *1.4. Crystal-to-Crystal Transitions*

Solid-state molecular motion can lead to a change in bulk material properties that can prove beneficial for various applications.[46] This includes crystal-to-crystal transitions that can be exploited to induce chirality within crystals.[47,48]

Although Viedma ripening is an efficient chiral amplification technique, it requires the use of conglomerate crystals. Only 10% of chiral organic molecules form conglomerate crystals.[49,50] Investigating alternative routes of conglomerate crystallization can expand the number of compounds that can undergo Viedma ripening. In 2014, Vlieg *et al.* used the formation of salt derivatives to achieve conglomerate crystallization for subsequent Viedma ripening.[49] Only three out of the twenty proteinogenic amino acids can form conglomerate crystals (*i.e.* threonine, glutamic acid hydrochloride and aspartic acid monohydrate).[49] Alanine is a chiral amino acid which forms racemic crystals, however, alanine 4-chlorobenzenesulfonic acid can form conglomerate crystals. This salt derivative was able to undergo chiral amplification using Viedma ripening.[49] Similarly, crystal-to-crystal transitions can be exploited to form conglomerate crystals. For example, some hydrated achiral crystals can be converted to chiral conglomerate crystals through thermal dehydration or reduced pressure conditions.[47,48] Soai *et al.* carried out the face selective dehydration-triggered chirogenesis of cytosine crystals. In this case, the chirality of hydrated cytosine crystals can be *absolutely* directed by heating a pair of enantiotopic faces (Figure 5).[48] The achiral crystals were cleaved at the (010) plane to reveal enantiotopic faces. The Miller Index is a notation system used to describe lattice planes in crystals. There are different notations for describing points (*h*, *k*, l), directions [*hkl*] and planes (*hkl*) (Figure 6).[51] This crystal-to-crystal transition enabled the formation of conglomerate crystals from achiral crystals.

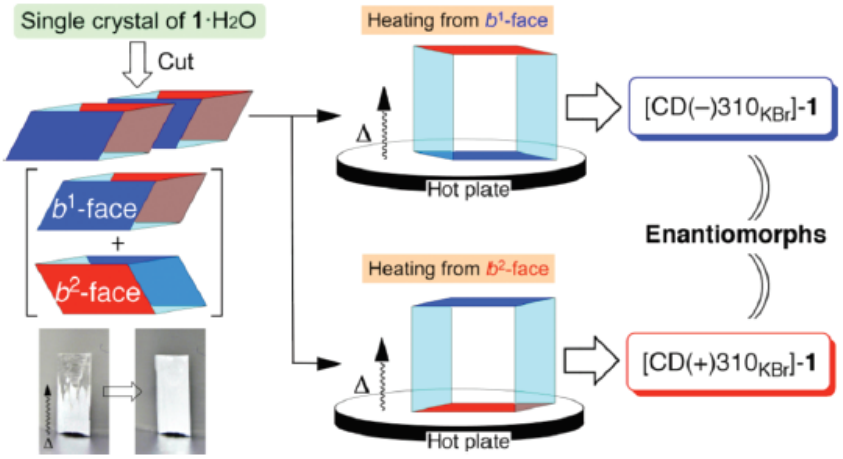


**Figure 5.** Large achiral crystals of cytosine monohydrate were grown and cleaved at the (010) plane. The (010) or (0-10) face was then placed on a hot plate and carefully heated. Heating either face results in dehydration and the formation of opposite enantiomorphs, which was validated by subsequent solid-state circular dichroism spectroscopy. Reprinted with permission from Kawasaki, T.; Hakoda, Y.; Mineki, H.; Suzuki, K.; Soai, K. *J. Am. Chem. Soc.* **2010**, *132*, 2874–2875. [48]

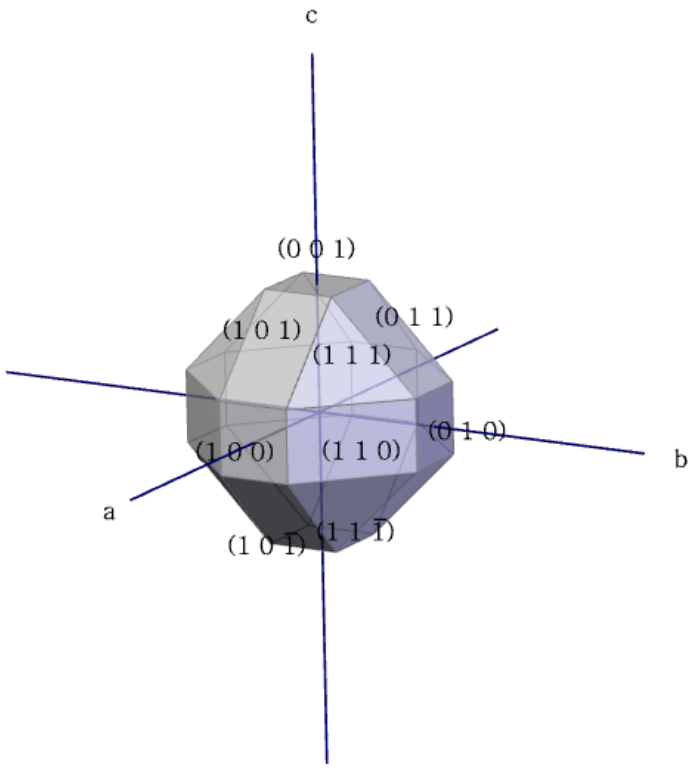


**Figure 6.** Representation of Miller Indices**.** [48]

## *1.5. Classical and Non-Classical Crystal Growth*

Classical crystallization involves the formation of a crystalline solid from a saturated solution, melt or vapour through nucleation and sequential crystal growth, where the incorporation of atoms, molecules or ions ultimately leads to the formation of stable crystalline structures.[52,53] Ostwald ripening is a process often observed during classical crystallization.[53] During Ostwald ripening, larger crystals grow at the expense of smaller ones.[54,55] This crystal growth mechanism is due to the diffusion of ionic or molecular species from the more soluble crystals to the less soluble crystals,[56,57] and can occur during longer growth periods due to a decrease in solvent supersaturation.[53] During crystallization through evaporation, the speed of the evaporation process will affect crystal nuclei formation. Fast evaporation will induce the formation of multiple crystal nuclei whereas slow evaporation will result in the formation of fewer nuclei. Very fast crystallization can result in the formation of amorphous crystals, which are crystals with a disordered arrangement (*i.e.* the lattice structure is filled with many dislocations).[58] Amorphous crystals typically show a halo-effect in the X-ray powder diffraction pattern. [32] In some cases, a chemical substance can crystallize with different crystalline structures (*i.e.* polymorphs). Polymorphism is the ability for a single compound to have different arrangements of its molecules in the solid state, thereby resulting in different crystalline structures (*i.e.* polymorphs give different X-ray powder diffraction patterns).[52,59,60]

The non-classical phenomenon of crystal growth by oriented attachment was noticed by both Gaubert (1896) and Liesegang (1910). Gaubert observed crystal aggregates in lead nitrate solutions whereas Liesegang was investigating the coarsening of silver halide single crystals in photographic emulsions.[61,62] Liesegang attributed aggregation as the cause of coarsening of crystals, and stated that, "two or more undissolved fragments would be cemented together by intermediary dissolved material." [62,63] In 1998, Penn and Banfield investigated the nanoscale oriented attachment at specific faces of titanium dioxide nanoparticles using high-resolution TEM, which showed alignment of lattice fringes of neighboring crystals (Figure 7). [64,65] This oriented attachment was further corroborated *via* single crystal X-ray diffraction experiments. They proposed that primary particles attach to one another in an irreversible and highly oriented fashion to produce new single crystals or pseudocrystals.[64,65] During oriented attachment there is

a reduction in surface energy attributed to the removal of unsatisfied bonds at the crystal-air or crystal-fluid interface.[66,67]

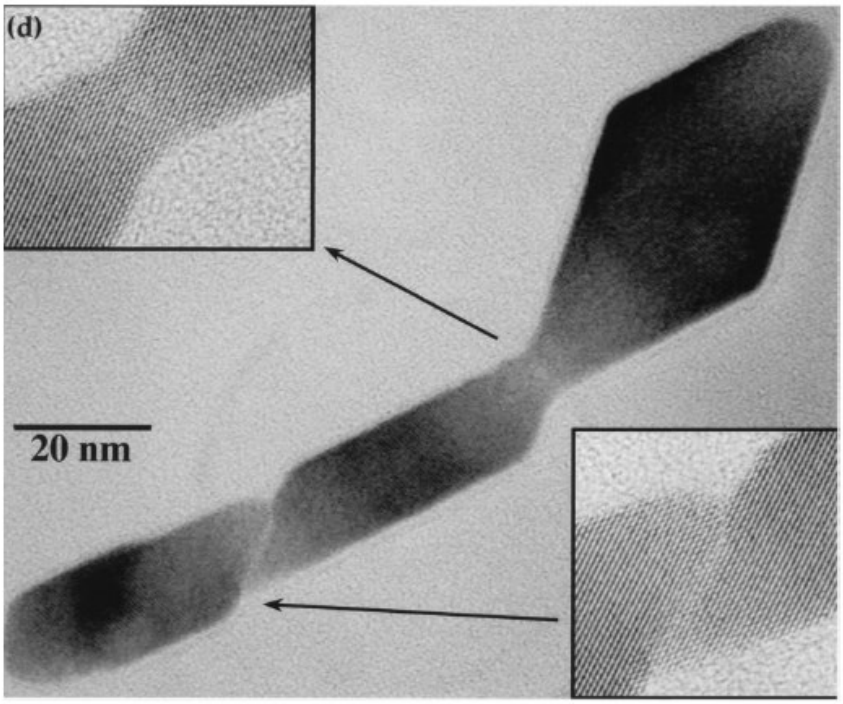


**Figure 7.** TEM image of a composite single crystal of titanium dioxide. Inset – The crystal is composed of multiple crystals with aligned lattice fringes. Reprinted with permission from Penn, R. L.; Banfield, J. F. *Geochim. et Cosmochim. Acta* **1999**, *63*, 1549–1557.[64]

Oriented attachment can be considered a two-step process which includes elements of both classical and non-classical crystallization. Through classical crystallization, molecules can undergo crystal growth to form initial crystals. The crystals can then spontaneously self-assemble at common crystallographic orientations to form mesocrystals (Figure 8).[67,68] Mesocrystals are superstructures formed from a highly ordered arrangement of individual building blocks.[53,69] During oriented attachment, the crystals make transient contact with one another at many points and orientations. The crystals will collide until a preferential crystallographic orientation is attained.[55,65] In some cases, a highly efficient oriented attachment process may give the illusion that a crystal was formed through classical crystallization.[70]

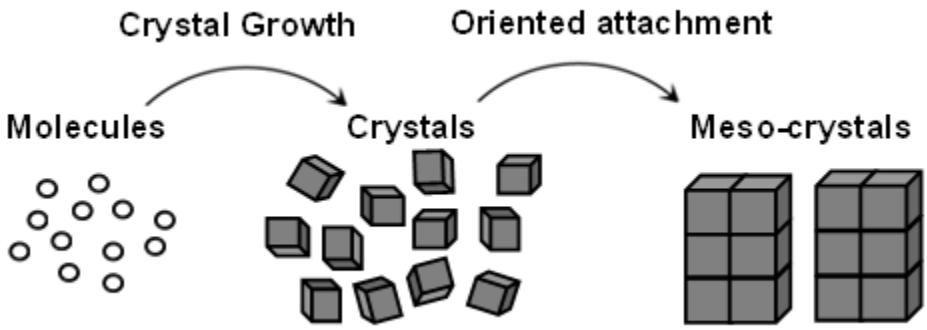


**Figure 8.** Representation of oriented attachment. Molecules undergo crystal growth that can spontaneously self-assemble at common orientations to form mesocrystals.

Introducing enantiomer-specificity to the mechanism of oriented attachment can lead to the formation of a racemic conglomerate of mesocrystals (Figure 9). The phenomenon of enantiomer-specific oriented attachment was proposed in 2004 by Uwaha to model the Viedma ripening process. He stated that there are minimum size clusters that possess chirality and that the growth of chiral crystals was due to the addition of achiral molecules as well as chiral units.[71]

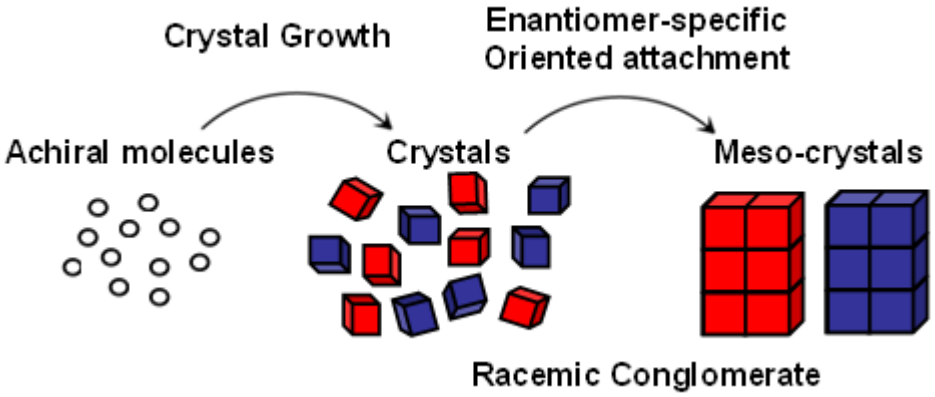


**Figure 9.** Representation of enantiomer-specific oriented attachment. Molecules undergo crystal growth to form a racemic conglomerate of crystals which can spontaneously self-assemble at common crystallographic orientations to form a racemic conglomerate of mesocrystals (*i.e.* a physical mixture of enantiomorphic mesocrystals).

In 2013, Viedma *et al.* studied enantiomer-specific oriented attachment in clusters of sodium bromate and sodium chlorate.[63] For example, an aqueous suspension of racemic sodium bromate (*ca.* 20 g in 6 mL water) was heated at 160 °C to yield centimeter-sized clusters within 24 h. These composite crystals were homochiral (or very nearly homochiral) as viewed between

polarizing filters (Figure 10, left). Similar results were observed when shaking sodium chlorate crystals in saturated solution.[63] Enantiomer-specific oriented attachment was also observed from boiling racemic threonine conglomerate crystals. In this case, the aggregates themselves had either left- or right-handed helicity and the enantiomeric excess of these clusters was confirmed using polarimetry (Figure 10, right). [63]

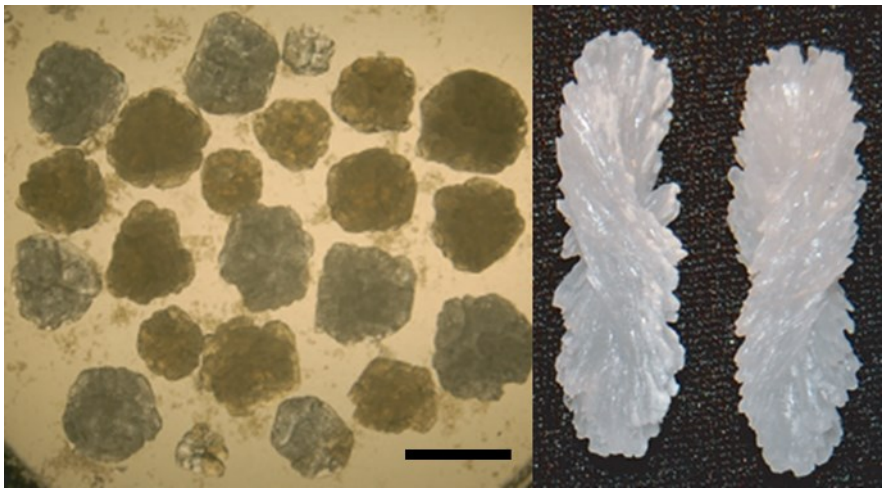

**Figure 10.** Left: Clusters of sodium bromate grown through boiling experiments. Scale bar: 0.5 mm. Right: Crystal aggregates of L- and D-threonine. Reprinted with permission from Viedma, C.; McBride, J. M.; Kahr, B.; Cintas, P. *Angew. Chem. Int. Ed.* **2013**, *52*, 10545–10548. [63]

## *1.6. Objectives*

The objective of this thesis is to explore the role of conglomerate crystallization in spontaneous resolution and chiral amplification. The phenomenon of conglomerate crystallization will be examined in three chapters which focus on different aspects of spontaneous resolution or chiral amplification. Chapter 2 investigates the rare cases of conglomerate crystallization where spontaneous resolution is possible by observing the features of the crystal. Crystal resolution based on hemihedrism, macromorphology, circular polarization and surface characteristics/topographic features are probed. Chapter 3 focuses on the role of conglomerate crystallization in chiral amplification by attrition-enhanced chiral amplification (*i.e.* Viedma ripening). In this case, thermal dehydration is explored as a means to transform achiral crystals to conglomerate crystals, which are subsequently amplified by Viedma ripening. In chapter 4, enantiomer-specific oriented attachment, an essential part of the Viedma ripening process, is explored in guanidine carbonate crystals.

# Chapter 2. Resolution by Triage

## *2.1. Abstract*

Louis Pasteur's elegant resolution of sodium ammonium tartrate tetrahydrate by visual inspection (*i.e.* triage) remains one of his most vital contributions to chemistry. The hemihedral faces of sodium ammonium tartrate tetrahydrate were critical for the distinction of *dextrorotatory* crystals from *levorotatory* crystals. This seminal experiment laid the foundation for the theories of molecular chirality that still hold today. Inspired by Pasteur's manual separation, a literature survey was conducted to find other systems that could undergo triage-based resolution. To our surprise, finding examples of resolution by triage has been challenging and only a handful of examples have been identified. A compilation of compounds which can be separated by triage found to date is presented below.

## *2.2. Introduction*

The first and most notable example of enantiomeric resolution was Louis Pasteur's resolution of sodium ammonium tartrate tetrahydrate. Pasteur was investigating the curious absence of optical activity in hemihedral paratartaric acid (*i.e.* racemic acid) crystals. Through analysis under a microscope, Pasteur noticed a subtle difference in the hemihedral faces of paratartaric acid when compared to pure tartaric acid. Using a microscope, Pasteur separated the crystals into groups which contained left- or right-pointing hemihedral faces. Remarkably, the separated crystals now had optical activity. Pasteur's separation of sodium ammonium tartrate tetrahydrate crystals using hemihedral faces was the first example of a resolution of a racemic mixture. Pasteur deduced that the paratartaric acid was actually an equal mixture of left-handed and right-handed tartaric acid.[9,13] This type of manual separation of crystals is often referred to as 'Pasteurian resolution' or 'resolution by triage'. Currently, there is continual pressure from the pharmaceutical and agrochemical industries to develop techniques that can prepare chiral substances in an enantiomerically pure form.[72] The development of simpler resolution techniques, such as preferential crystallization and formation of diastereomeric salts, has made the application of Pasteur's original method quite sporadic.[73,74] Although resolution by triage is a tedious process, it still remains a fundamental and effective form of resolution that takes full advantage of conglomerate crystallization.

Pasteur's simple but elegant resolution method can be applied to other compounds as well. This literature survey will focus on both achiral and chiral molecules that crystallize as conglomerates. These crystals must reside in one of the 65 non-centrosymmetric Sohncke space groups.[3] In most cases, observations carried out by visual inspection have been validated by secondary techniques. For chiral molecules, optical rotation of the dissolved enantiomorphic crystals can be evaluated. Whereas for achiral molecules, solid-state circular dichroism or single-crystal X-ray diffraction can often be used to further analyze the chirality of conglomerate crystals.[3] In some cases, surface topography of crystals can be investigated to verify the efficacy of the resolution. Our preliminary search for compounds was based on keywords such as conglomerate crystals, resolution by triage, manual sorting, resolution/hemihedrism, uniaxial crystals, hand-picking, enantiomorphous crystals and Pasteurian resolution. To date, our current list has 59 examples of crystals that can undergo resolution by triage and it is continuously growing. The results of this preliminary literature search are organized into crystal resolution based on: (*i*) hemihedral faces, (*ii*) macromorphology, (*iii*) circular polarization and (*iv*) surface characteristics/topographic features. Remarkably, sodium chlorate crystals can be separated by all the aforementioned methods of triage. As such, sodium chlorate will be used as the model example throughout this chapter.

## *2.3. Hemihedral Faces*

Hemihedral faces have only half the required planes for complete symmetry of the holohedral form.[8,15] Hemihedrism played the central role in Louis Pasteur's (1848) resolution of sodium ammonium tartrate tetrahydrate crystals, which ultimately led to his proposal of molecular disymmetry.[75] Before this seminal discovery, René Haüy (1801) and Louis-Nicolas Vauquelin (1806) identified the hemihedral facets in quartz and asparagine crystals, respectively.[13,14,76] Quartz crystals are enantiomorphic and they often present hemihedral faces (Figure 11).[13] It is important to note that the term "enantiomorphs" is used to describe nonsuperposable mirror image objects whereas "enantiomers" is used to describe nonsuperposable mirror image molecules.[15]

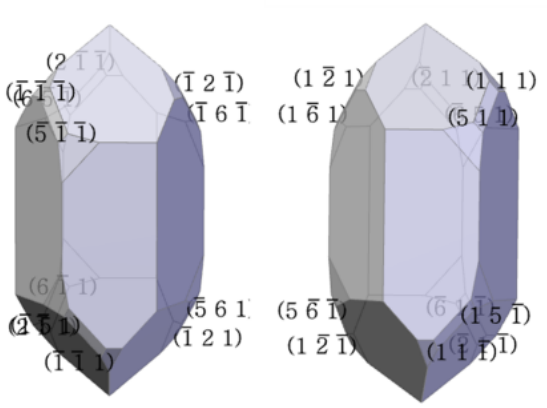

**Figure 11.** Crystal morphology of left- and right-handed quartz crystals viewed along the a-axis. Miller Indices highlight the hemihedral faces of quartz**.**

Sodium ammonium tartrate tetrahydrate is an example of a chiral molecule that forms either conglomerate crystals or racemic crystals depending on the crystallization temperature (Figure 12). The racemic crystals are holohedral and exhibit all the faces required for complete symmetry.[9] The conglomerate crystals, however, have hemihedral faces. Pasteur carried out the crystallization of sodium ammonium tartrate tetrahydrate below 26 °C, which enabled the formation of conglomerate crystals rather than racemic crystals, which form above 26 °C. [9]

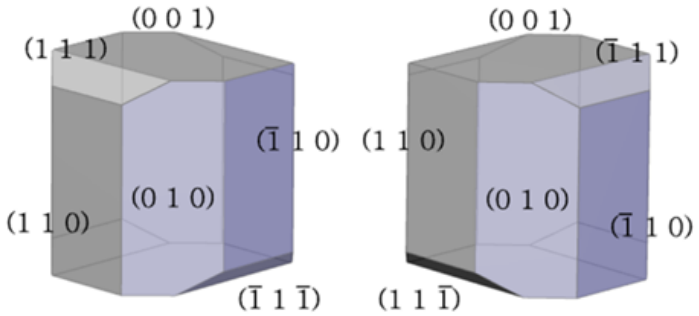

**Figure 12.** Crystal morphology of enantiomorphic crystals of sodium ammonium tartrate tetrahydrate viewed along the b-axis. Miller Indices are indicated**.**

The presence of hemihedral faces in crystals can be influenced by various factors such as temperature, the crystallization solvent and the presence of additives or impurities.[77] Hemihedral faces can be found on conglomerate crystals that belong to various space groups. The probability of finding hemihedral faces is greater in space group $P2_1$, compared to the other Sohncke space groups.[32,35] Space groups $P2_12_12_1$ and $P2_1$ account for 80% of chiral crystals.

The crystal class of a compound can dictate the hemihedral face(s) observed upon crystallization. The internal atomic arrangement or morphology can be used to arrange crystals into crystal classes which represent 32 unique combinations of symmetry operations. The crystal classes can be further grouped into six crystal systems based on similar symmetry operations.[52,60] For example, in crystal class 2, there is only a two-fold rotation axis. As a result, any face subject to this symmetry element converts (*hkl*) to(-*hk*-*l*). A face is hemihedral in this crystal class if $k \neq 0$, therefore, the probability of finding hemihedral faces in this crystal class remains the highest.[78] In crystal class 222, a face is hemihedral if $h \neq 0$ , $k \neq 0$ and $l \neq 0$, whereas in crystal class 422 a face is hemihedral if $h \neq 0$ , $k \neq 0$ , $l \neq 0$ and $h \neq k$ .[78,79] A crystal can have multiple hemihedral faces as long as they follow the criteria for their respective crystal class. The (211) face has been previously reported to be the hemihedral face in magnesium sulfate heptahydrate crystals.[80] During crystallization of magnesium sulfate heptahydrate in our lab, the (211) face was not expressed whereas the (111) face, which is also hemihedral, was present. In the case of sodium chlorate, hemihedral faces have been previously observed in rare cases.[20,81] Thus far, we have identified 46 literature examples of crystals with reported hemihedrism (Table 1).

**Table 1.** Conglomerate crystals showing hemihedral faces.

| Name | Space Group | Ref |
|---|---|---|
| N,N′-(1,1-dimethylethyl)-3,3′-dimethoxy-N,N′-dimethyl-2,2′dibenzamide | $P2_1$ | 82,83 |
| 1,2-bis(N,N′-benzoyl-N,N′-methylamino)benzene | $P2_12_12_1$ | 84,85 |
| 1,8-bis(dimethylamino)-2-(α-hydroxy-α-phenylethyl)naphthalene | $P2_12_12_1$ | 86,87 |
| 2,3-bis-fluoren-9-ylidenesuccinic acid/acetone Inclusion crystal | $P2_12_12_1$ | 88,89 |
| 2-(cyclohex-2-enyl)-2,2-diphenylethanol | $P2_1$ | 90 |
| 5-methyl-5-(4-methylphenyl)-hydantoin | $P2_12_12_1$ | 77 |
| Ammonium hydrogen malate | $P2_12_12_1$ | 81,91 |
| L-asparagine monohydrate | $P2_12_12_1$ | 76,92 |
| β-lactam/ 4-oxoazetidin-2yl benzoate inclusion crystal | $P2_12_12_1$ | 93 |

| | | |
|---|---|---|
| β-lactam/4-phenylazetidin-2-one inclusion crystal | NA | [93] |
| Camphoric acid | $P2_1$ | [92] |
| Camphoethylic acid | NA | [92] |
| Cane sugar (Sucrose) | P2 | [92,94,95] |
| CFA-1 $[Zn_5(OAc)_4(bibta)_3]$ | P321 | [96] |
| Chiral ammonium salt $Me(Et)N^+(All)PhI^-*CHCl_3$ | $P2_12_12_1$ | [97] |
| Cinnabar | $P3_221/P3_121$ | [98] |
| Formyl-dl-neomenthylamine | NA | [99] |
| dl-isohydrobenzoin | $P2_1$ | [100,101] |
| Glucosate of sea-salt | NA | [102] |
| Hexa-o-phenylene | P1 | [103–105] |
| Hydrocarbon fichetelite | $P2_1$ | [94] |
| Hydroveratroin | $P6_2$ | [104–106] |
| Lithium sulphate | $P2_1$ | [94,107,108] |
| Malic acid | $P2_1$ | [92] |
| Magnesium sulfate heptahydrate | $P2_12_12_1$ | [80] |
| $[M(H_3L)](NO_3)_2•MeOH$<br>M=Mn, Fe, Co, Ni, Zn | $P2_12_12_1$ | [109] |
| Milk sugar (Lactose) | $P2_1$ | [92,94] |
| Morphine monohydrate | $P2_12_12_1$ | [92] |
| Potassium bichromate | P1 | [110] |
| Potassium *dextro*-tartrate | $P2_12_12_1$ | [94] |
| Polyoxometalate $([CH_3)_2NH_2]_{10}$<br>$[Zr(PW_{11}O_{39})_2]_.*H_2O$ | $P2_1$ | [111] |
| Quercite | $P2_1$ | [94] |
| Salt derivative of BNDA | $P2_1$ | [35] |
| Sodium Ammonium Tartrate | $P2_12_12_1$ | [75] |
| Sodium chlorate | $P2_13$ | [102] |
| Stronium formate | $P2_12_12_1$ | [102] |
| Tartaric acid | $P2_1$ | [9,78,92,94,112,113] |
| Tartramide | $P2_12_12_1$ | [81,92] |
| Tartramic acid | $P2_12_12_1$ | [92] |
| Tetraphenylethylenes | $P2_1$ | [114] |
| Quartz | $P3_121/P3_221$ | |
| Quinic acid | $P2_1$ | [92] |

## *2.4. Macromorphology*

There are alternative methods of manual triage that can be carried out when hemihedral faces are not present. The relationship between other faces can sometimes be used to determine the chirality of crystals. The faces in question are not hemihedral but their position relative to other

faces within the crystal can be used as an indicator of chirality. For example, sodium chlorate can be separated using macromorphology (Figure 13). The presence of the (110), (111) and (210) faces can be used to distinguish between enantiomorphic crystals.[115] The chirality can also be determined in the absence of the (110) face, where the unsymmetrical nature of the (111) face (with respect to the (210) face) can be used to distinguish between enantiomorphic crystals. Similarly, magnesium sulfate heptahydrate crystals can be separated using macromorphology. If crystals are oriented with the (110) face pointing upwards, the enantiomorphic crystals can be separated by the position of the (010) face.

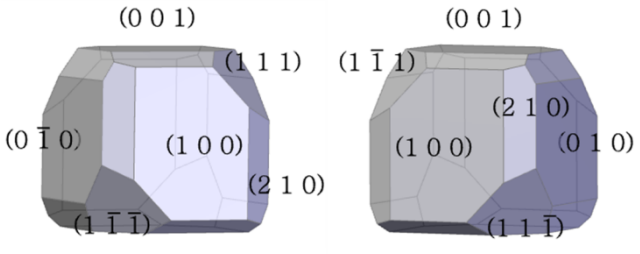


**Figure 13.** Crystal morphology of *d*-$NaClO_3$ (left) and *l*-$NaClO_3$ (right) *viewed along the a-axis*.

## 2.5. Circular Polarization

The chirality of a crystal can be determined through optical rotatory dispersion, a color transition observed along the optic axis, where the change in color will be opposite for enantiomorphic crystals.[92]

> "If, in order to make these follow in their natural order—red, orange, yellow, green, blue, violet—it is necessary to turn the analyser to the right—that is to say, in the direction of the hands of a watch—the substance is said to exhibit right-handed or positive circular polarization, which is usually indicated by the sign ↱ or + : if, on the contrary, the analyser must be turned to the left to produce the same result, the polarization is left-handed, or negative, and the sign ↰ or − is employed."

- J. H. Gladstone (1861)[92], J. Chem. Soc., 1861, 13, 254–270.

Gladstone's transition can be seen in ethylenediammonium sulfate (EDS) crystals, the *dextrorotatory* crystal transforms from blue-to-violet-to-red-to-amber-to-clear (Figure 14). The *levorotatory* crystal transforms from yellow-to-amber-to-violet-to-blue-to-clear (Figure 15). Figure 16 shows the circular polarization of benzil crystals viewed along the optic axis. The *levorotatory* crystal transforms from amber-to-blue-to-clear, while the *dextrorotatory* crystal transforms from blue-to-amber-to-clear on rotating the analyzer clockwise

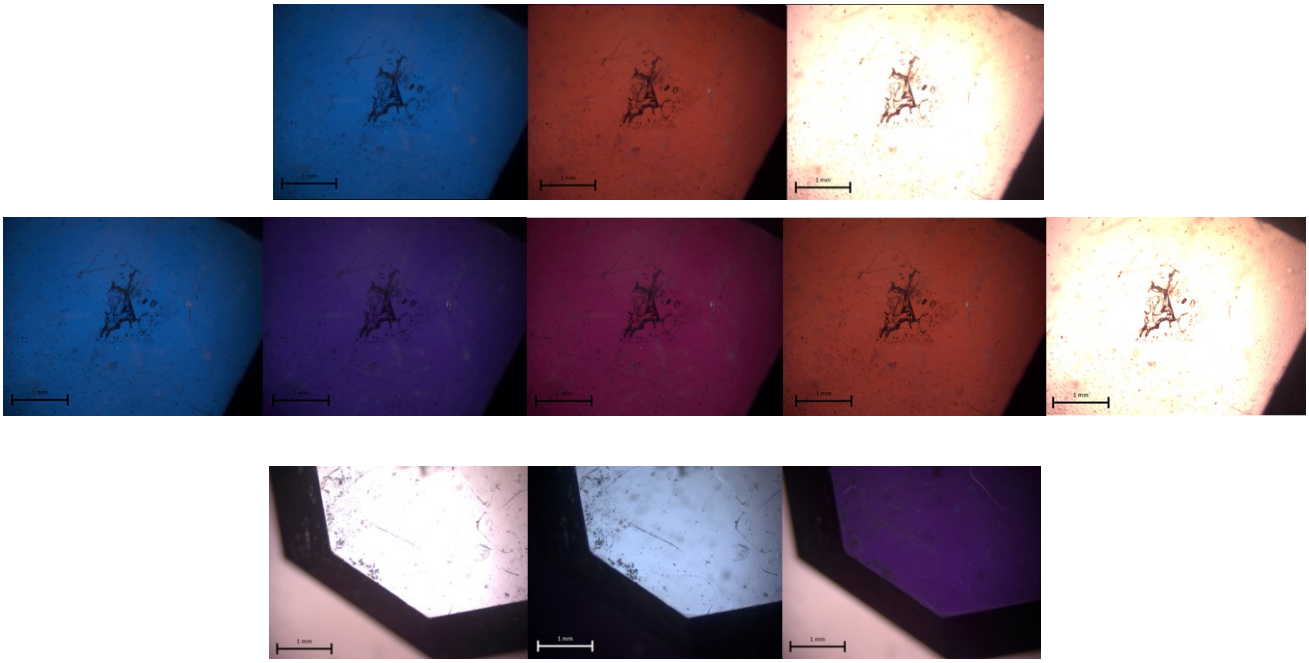

**Figure 14.** Color transitions observed for *dextrorotatory* crystal of EDS using polarized light microscopy (rotating the analyzer clockwise). Blue-to-amber-to-clear crystal (top row, according to Cuccia, L. A. *et al.*, M. *J. Chem. Educ.* **2005**, *82*.), blue-to-violet-to-red-to-orange-to-clear (middle-row, according to J. H. Gladstone., *J. Chem. Soc*., 1861, 13, 254), decreasing brightness according to clockwise rotation of the polarizer (bottom row, according to Matsumoto, A. *et al*. *Chem. Lett.* 2015, *45*, 526). Scale bar = 1 mm**.**

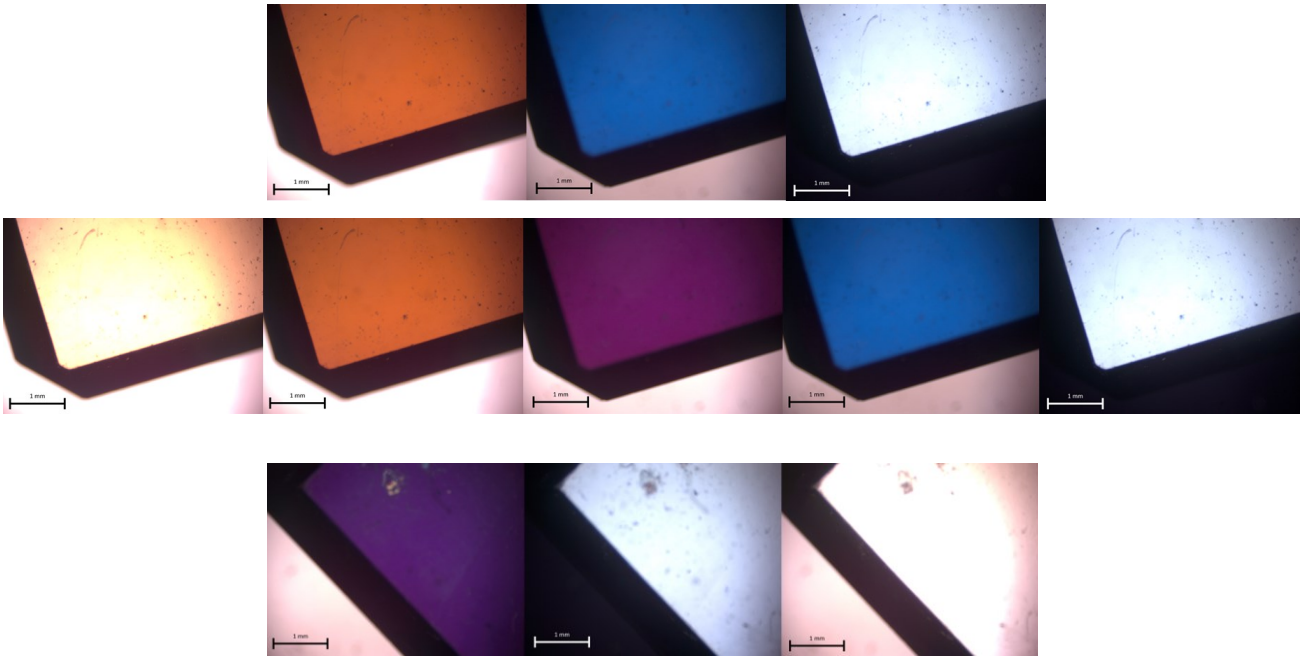

**Figure 15.** Color transitions observed for *levorotatory* crystal of EDS using polarized light microscopy (rotating the analyzer clockwise). Amber-to-blue-to-clear crystal (top row, according to Cuccia, L. A. *et al.*, M. *J. Chem. Educ.* **2005**, *82*.), yellow-to-orange-to-violet-to-blue-to-clear middle-row, according to according to J. H. Gladstone., *J. Chem. Soc*., 1861, 13, 254), increasing brightness according to clockwise rotation of the polarizer (bottom row, according to Matsumoto, A. *et al*. *Chem. Lett.* 2015, *45*, 526). Scale bar = 1 mm**.**

Crystals can belong to one of 7 crystal systems. These crystal systems can be separated into two groups, isotropic and anisotropic. The cubic crystal system is the only isotropic crystal system and the velocity of light is same in all crystal orientations. Therefore, crystals residing in the cubic crystal system are ideal for investigation by circular polarization measurements. The remaining crystal systems are anisotropic, where the velocity of light varies with different crystallographic orientations.[52,60] Uniaxial crystals reside in the tetragonal or hexagonal (trigonal) crystal systems, whereas biaxial crystals reside in the orthorhombic, monoclinic or triclinic crystal systems. Uniaxial crystals have one optic axis whereas biaxial crystals have two. The optic axis in uniaxial crystals is perpendicular to the (001) face, which facilitates analysis using polarized light microscopy.[116]

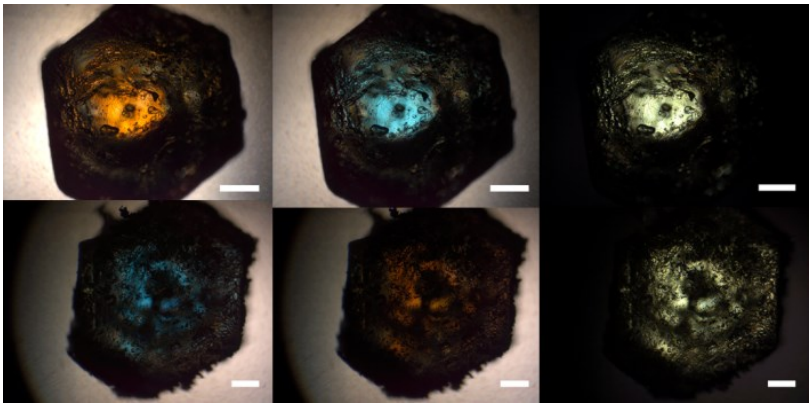

**Figure 16.** Color transitions observed for enantiomorphic crystals of benzil using polarized light microscopy (rotating the analyzer clockwise). *levorotatory* (-) crystal (top row), *dextrorotatory* (+) crystal (bottom-row). Scale bar = 0.5 mm**.**

Guanidine carbonate is an example of a compound that crystallizes in the enaniomorphic $P4_12_12/P4_32_12$ space groups. These uniaxial crystals can be resolved using optical rotatory dispersion viewed along the (001) face (Figure 17).[117] Sodium chlorate, a crystal which resides in the cubic crystal system can also be resolved by polarized light microscopy at any orientation. *Dextrorotatory*-$NaClO_3$ crystals display an optical rotatory dispersion of blue-to-violet-to-yellow whereas *levorotatory*-$NaClO_3$ crystals display an optical rotatory display dispersion of yellow-to-violet-to-blue when the analyzer is rotated clockwise.[118] For simplicity, only isotropic and uniaxial crystals that can be resolved by triage are shown in Table 2.

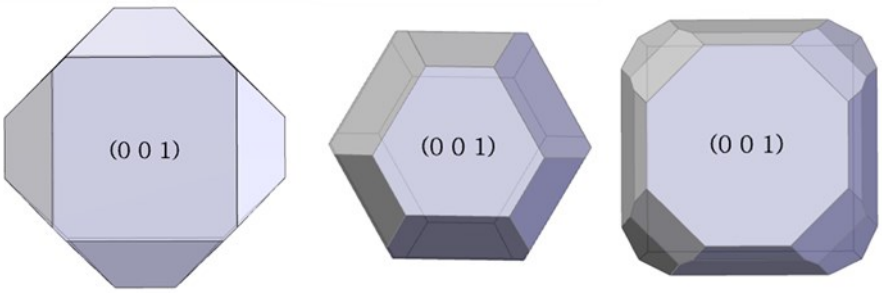


**Figure 17.** Crystal morphology of guanidine carbonate (left), benzil (BENZIL) (middle) and ethylenediammonium sulfate (ETDAMS) (right) with Miller Indices *highlighted along the c-axis***.**

Table 2. Conglomerate crystals that can be resolved using circular polarization

| Name | Space Group | Ref |
|---|---|---|
| 1,1-binaphthyl | $P4_12_12$ / $P4_32_12$ | 79 |
| 1,2-bis-(N-benzenesulfonyl-N-methylamino)benzene | $P4_13_12$/$P4_33_12$ | 32,119 |
| Benzil | $P3_121$ / $P3_221$ | 120 |
| Ethylenediammonium sulfate | $P4_1$ | 121 |
| Guanidine carbonate | $P4_12_12$ / $P4_32_12$ | 122 |
| Sodium bromate | $P2_13$ | 63,123 |
| Sodium chlorate | $P2_13$ | 115,123 |
| Trinitroiodbenzol | $P4_12_12$ / $P4_32_12$ | 79 |

## *2.6. Topographic Features*

The morphology of crystals can be used to distinguish and ultimately resolve enantiomorphic crystals. The morphology can be investigated at different levels depending on the method used. As such, distinguishing enantiomorphic crystals can be based on observations ranging from the nanoscale to the macroscale.

Surface topography is an intriguing property because it can be used as a primary method to resolve enantiomorphic crystals or it can be used to validate other triage methods. Magnesium sulfate heptahydrate crystals display hemihedral faces. The (111) face is present in left-handed crystals whereas the (1-11) face is present in right-handed crystals (Figure 18).

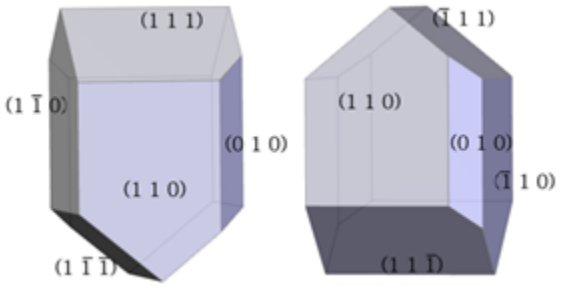


**Figure 18.** : Experimental left-handed and right-handed crystals of magnesium sulfate heptahydrate**.**

If the left-handed crystals is rotated 180° along the axis perpendicular to the (110) face, the difference between both crystals appears to be the position of the (010) face. However, there also exists the possibility of the development of the (100) face. This additional face can add an

element of confusion, because the (100) face of the right-handed crystal can be easily mistaken for the (010) face of the left-handed crystal. In such cases, the use of surface topography (*e.g.* etch pits or growth hillocks (*vide infra*)) can be used to reveal the difference between the (100) and (010) faces. Figure 19 shows crystals of the same chirality but displaying either the (100) or (010) face, which can easily give the impression that these crystals are enantiomorphic.

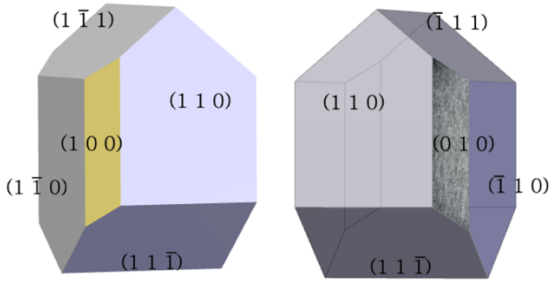


**Figure 19.** : Right-handed crystals of magnesium sulfate heptahydrate with either the (100) or the (010) face present appear to be enantiomorphic**.**

Chemical etching and the use of chiral additives can result in distinct patterns at the nanoscale that can help distinguish between enantiomorphic crystals. By hindering the deposition of layers of molecules on crystals, chiral additives can be used to create morphological differences between enantiomorphic crystals. This allows crystals to be separated manually by triage.[124–127] For example solutions of aspartic acid can be used as etchants on crystals of asparagine monohydrate. (*R*)-aspartic acid forms etch pits on the (010) face of the R-crystals while the S-crystals remain unchanged. On the other hand, the (*S*)-asparagine crystals are etched by solutions of (*S*)-aspartic acid while the (*R)*-asparagine crystals remain unchanged. This subtle difference in morphology enables the separation of enantiomorphic crystals.[124]

Chemical etchants that form mirror image etch pits, or growth hillocks can be used to separate enantiomorphic crystals.[128] In the case of sodium chlorate, various solvents were used as chemical etchants. Etching using formic acid, acetic acid, methanol or a 1:1 mixture of acetone:water resulted in the formation of mirror image etch pits on the (100) face of enantiomorphic crystals. Etch pits that can be used to resolve enantiomorphic crystals were also seen on the (110), (210) and (111) faces using formic acid (Figure 20).[128]

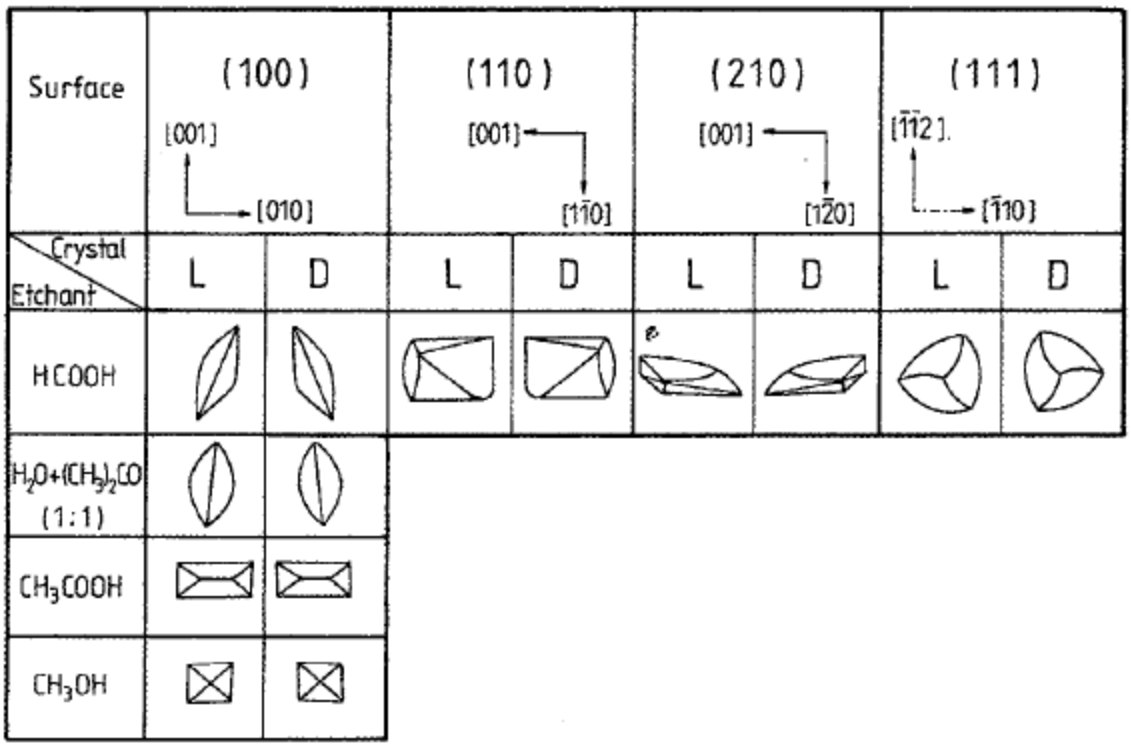


**Figure 20.** : Morphology of etch pits on various faces of enantiomorphic crystals of sodium chlorate. Reprinted with permission from Szurgot, M. *Cryst. Res. Technol.* **1995**, *30*, 621–628. [128]

Conglomerate crystals can also be exposed to the vapours of optically active reagents that can result in a different visible coating for enantiomorphic crystals.[105] For example, single crystals of tartaric acid, mandelic acid and 2,2-diphenyl-cyclopropane-1-carboxylic acid were exposed to vapours of (+)- or (-)-1-phenylethylamine. The vapours exhibited enantiospecificity in their interactions with enantiomorphic crystals (*i.e* (+)-1-phenylethylamine altered the morphology of (+)-crystal whereas the (-)-crystal remained unchanged whereas (-)-1-phenylethylamine altered the morphology of (-)-crystal whereas the (+)-crystal remained unchanged).[129]

Alternatively, the morphology of enantiomorphous crystals can be influenced at the macroscale using various additives. Due to adsorption-growth inhibition, the morphology of enantiomorphic crystals can be altered. Addadi *et al*., have previously shown that the morphology of enantiomorphic crystals of L-asparagine monohydrate, glutamic acid hydrochloride and threonine can be changed using certain "tailor-made" additives.[125–127] For

example, conglomerate crystals of glumatic acid hydrochloride grown in the presence of increasing concentrations of L-lysine cause the L-enantiomorph to crystallize as a powder, while the D-enantiomorph, which remains unaffected, crystallizes as thin plates.[125–127,130] Table 3 shows eight examples of conglomerate crystals that can be separated using surface characteristics or topographic features. (Table 3).

**Table 3.** Conglomerate crystals that can be resolved using surface characteristics or topographic features.

| Name | Space Group | Ref |
|---|---|---|
| 2,2-diphenyl-cyclopropane-1-carboxylic acid | $P2_1$ | 129 |
| L-asparagine monohydrate | $P2_12_12_1$ | 124–127 |
| Glutamic acid hydrochloride | $P2_12_12_1$ | 125–127 |
| Mandelic acid | $P2_1$ | 129 |
| Potassium bichromate | P1 | 110 |
| Sodium chlorate | $P2_13$ | 128 |
| Tartaric acid | $P2_1$ | 129 |
| Threonine | $P2_12_12_1$ | 125–127 |

# Chapter 3. Enantiomer-specific oriented attachment of guanidine carbonate crystals

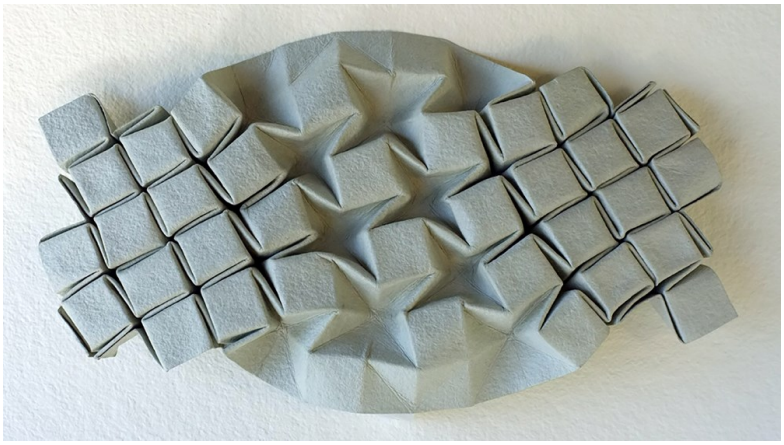



## *3.1. Abstract*

Oriented attachment, a non-classical crystallization phenomenon, describes the spontaneous self-assembly of adjoining crystals with common crystallographic orientations. Introducing chiral recognition between crystals during oriented attachment enables enantiomer-specificity and the formation of homochiral structures. Herein, we report efficient enantiomer-specific oriented attachment for suspended crystals of guanidine carbonate to form mesoscale homochiral or enantioenriched aggregates under boiling or shaking conditions. These aggregates display polyhedral macrostructures and their chirality was monitored using circular dichroism and polarized light microscopy.

## *3.2. Main Text*

Strategies devoted to the preparation of chiral substances, often in enantiomerically pure form, constitute a thriving area of chemical research, instrumental to the pharmaceutical or agrochemical industries.[40–43] Exploiting conglomerate crystallization (*i.e.* spontaneous resolution),[34,131,132] represents an appealing avenue to mediate chiral amplification, often bypassing the inherent limitations of classical resolution techniques.[133] Attrition-enhanced

deracemization of conglomerate-forming crystals, which has been dubbed *'Viedma ripening'*, is an unprecedented technique that leads to enantioseparation and chiral amplification from an essentially racemic mixture.[2,30,134,135] Still waiting for an industrial application, especially in drug innovation, the protocol has proven to be robust and has been applied to both achiral and chiral molecules alike.[2,3,136] To date, there are over 35 reported examples of chiral and achiral molecules that can undergo this sort of enantioseparation (Table 5). Crystallization in a non-centrosymmetric Sohncke space group (*i.e.* conglomerate crystallization) and racemizing conditions in solution (in the case of chiral molecules) appear to be the principal requirements for this attrition-enhanced chiral amplification process.[3] From a theoretical viewpoint, an in-depth understanding of the underlying mechanism behind attrition-enhanced deracemization remains elusive as yet,[71,135,137–143] although it relies on Ostwald ripening and homochiral cluster recognition, presumably by enantiomer-specific oriented attachment.[71,135,137–143] In short, it is generally believed that there are three major steps involved: (*i*) the increased solubility of crystals through crystal attrition (*i.e.* small crystals are more soluble than large crystals according to the Gibbs-Thomson effect) and the growth of larger crystals at the expense of smaller crystals;[144] (*ii*) the transformation of chiral crystals to their enantiomorphs through this dissolution-growth process (with concomitant racemization in solution in the case of chiral molecules),[30] and (*iii*) the reincorporation of crystallites by enantiomer-specific oriented attachment into larger crystals. Combined, these processes lead to the autocatalytic amplification to a homochiral crystal population.[53]

Non-classical crystallization mechanisms are implicated in the formation of elegant and complex nanoscale superstructures. Oriented attachment appears to be the distinctive feature of non-classical crystallization phenomena, which dominate natural processes such as biomineralization and are usually overlooked in classical mechanisms of crystallization.[56,145–147] Although thought to be fairly modern, Liesegang postulated non-classical crystallization routes as early as 1911.[44,62] He suggested that non-classical crystallization can be achieved by incorporating larger-scale aggregation involving two or more undissolved fragments combined with intermediary dissolved material.[62] Even from a historical context, the first indications, though vague, could be traced to the work of French mineralogist Gaubert, who in 1896 reported the formation of crystal aggregates from lead (II) nitrate solutions.[61] Over the last two decades, oriented attachment has garnered much attention and has been beautifully visualized by electron microscopy, as most, if

not all, examples have centered on micro and nanoparticles.[68,148] This non-classical crystal growth relies on, *"spontaneous self-organization of adjacent particles with a common crystallographic orientation, followed by joining of these particles at a planar interface"*. [70]

Recently, Viedma *et al.* were able to move the phenomenon from the submicron scale to the mesoscale, where large crystal aggregates of $NaClO_3$ and $NaBrO_3$ were obtained through shaking and boiling experiments, respectively, and visible to the naked eye.[63] Remarkably, most aggregates exhibited homochirality or significant enantiomeric imbalances; thereby being the first indication of enantiomer-specific oriented attachment. Interestingly, enantiomer-specific oriented attachment, in the form of helical aggregates, was also observed in conglomerate threonine crystals, an essential and proteinogenic amino acid.[63] An origami tessellation enables intuitive 2D visualization of enantiomer-specific oriented attachment (Figure 21, left).

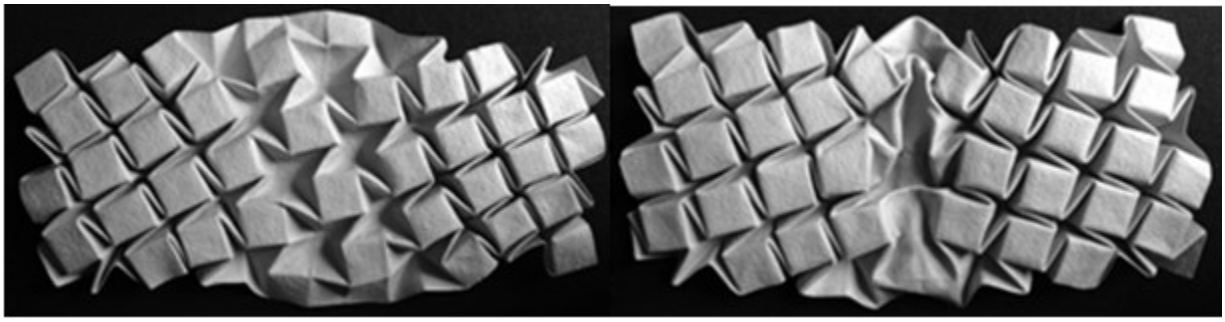

**Figure 21.** Left: Origami representation of enantiomer-specific oriented attachment. The tessellations on the left and the right have the same handedness and merge perfectly at the interface. One can envisage the central unfolded, yet chiral, region linking the 'crystalline' domains acting as a 'chiral glue' *to* attract the two halves together. Right: The tessellations on the left and the right are mirror images of each other and are unable to join at the interface**.**

Herein we report, in detail, the spontaneous aggregation or clustering of guanidine carbonate crystals (Scheme 1) through enantiomer-specific oriented attachment that occurs during boiling or shaking experiments. Like the sodium halates, guanidine carbonate is an achiral molecule which forms chiral conglomerate crystals in the enantiomorphic $P4_12_12$ or $P4_32_12$ chiral space groups, being therefore susceptible to resolution *via* attrition-based deracemization.[3] Guanidine carbonate crystallizes in a tetragonal uniaxial crystal system and displays an optical rotation of +/- 14°/mm with its optic axis along the c-axis.

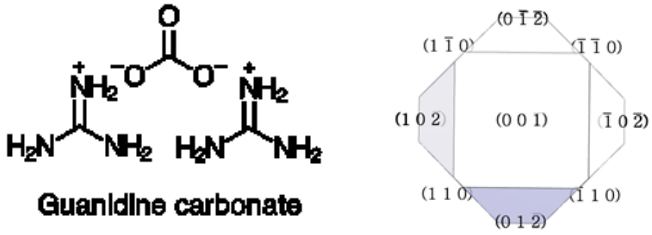


Scheme 1: Left: Chemical structure of guanidine carbonate. Right: Crystal morphology with the Miller indices highlighted *along the c-axis*.[149]

Conglomerate crystals of guanidine carbonate can be analyzed using optical rotatory dispersion or solid-state circular dichroism. A crystal with (+) CD signal correlates to an optical rotatory dispersion from blue-to-amber-to-clear whereas a crystal with (-) CD signal correlates to an optical rotatory dispersion from amber-to-blue-to-clear with clockwise rotation of the polarizer. Ripening under attrition afforded a homochiral population after *ca.* 2 days (Figure 22).

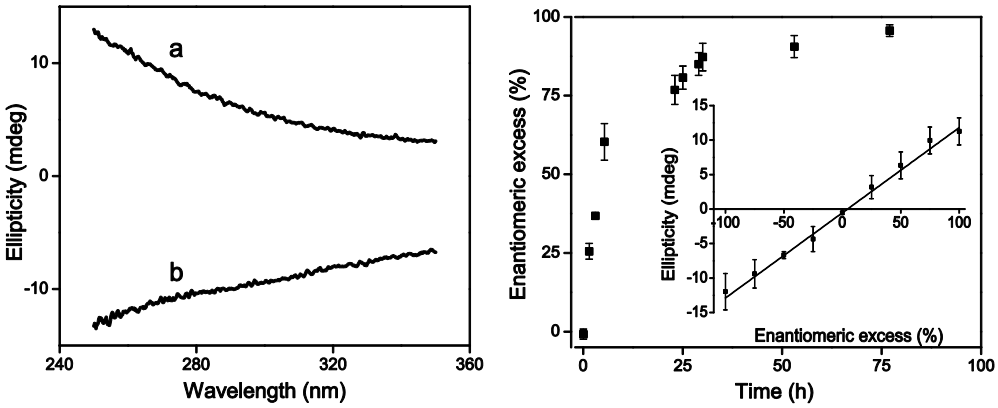


**Figure 22.** Left: Solid-state CD spectra of guanidine carbonate single crystals in Nujol, (a): [CD(+)250 nm], (b): [CD(-)250 nm]. Right: Kinetics of attrition-based deracemization of guanidine carbonate using 0.25 g of chiral crystals suspended in 1 mL of saturated solution in distilled water with 3 g of ceramic grinding media (0.8 mm) and stirring at 2400 rpm for *ca.* 60 hours. Inset: enantiomeric excess CD calibration curve of guanidine carbonate in Nujol prepared from mixtures of homochiral crystals ([CD(±)250 nm]).

Boiling and shaking experiments with guanidine carbonate crystals in saturated solution were carried out to investigate enantiomer-specific oriented attachment. Boiling a physical racemate of guanidine carbonate crystallites in suspension in a saturated aqueous solution at 190 °C resulted in the formation of clusters within 17 to 24 hours. Larger clusters formed in a 100 mL round

bottom flask in comparison to a 23 mm diameter reaction tube (Figure 23). The delay in cluster formation suggests that powdered guanidine carbonate crystallites undergo Ostwald ripening to a suitable size prior to cluster formation. The guanidine carbonate clusters are remarkably similar in appearance to $NaBrO_3$ clusters obtained under similar boiling conditions.[63]

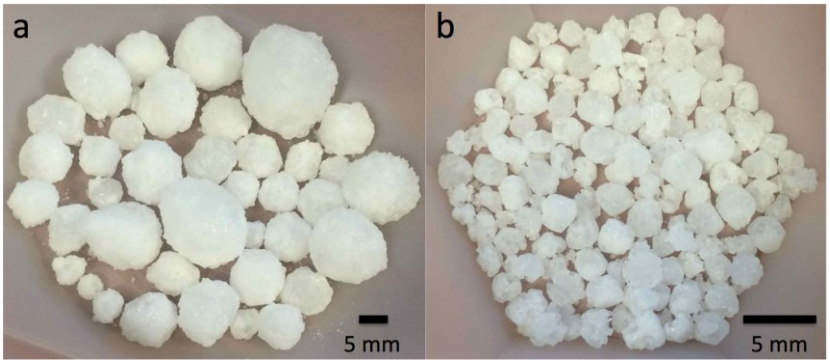


**Figure 23.** Guanidine carbonate clusters from boiling experiments at 190 °C. a: in a 100 mL round bottom flask b: in 23 x 150 mm reaction tubes.

The extent of enantiomer-specific oriented attachment of the guanidine carbonate was determined using solid-state circular dichroism of crushed individual clusters. Of 39 clusters isolated from one boiling experiment (Figure 24a), there were 23 (+) clusters and 16 (-) clusters. The crystalline enantiomeric excess varied from cluster to cluster, but in most cases was significantly higher than that of the starting material (Figure 24). Commercial guanidine carbonate was scalemic and the starting enantiomeric excess for this experiment was *ca.* 9% [CD(-)250 nm]. In fact, it was generally observed that in boiling experiments, cluster formation was more prevalent when scalemic guanidine carbonate was used as starting material. CD analysis of select clusters from boiling experiments carried out in reaction tubes (Figure 23b) showed similar results (Figure 34).

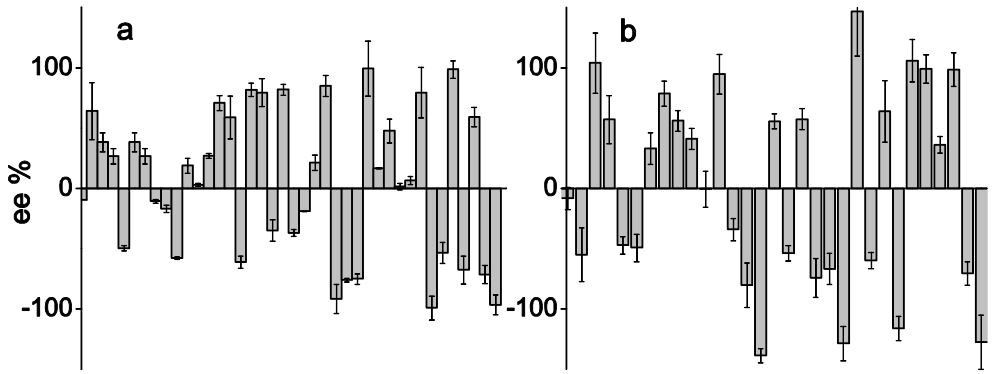


**Figure 24.** Enantiomeric excess of guanidine carbonate clusters obtained from a: A boiling experiment at 190 °C in a 100 mL bottom flask (initial enantiomeric excess: ca. 9 % [CD(-)250 nm]) and b: Shaking experiments (1000 rpm) at 69 °C in 2 mL centrifuge tubes (initial enantiomeric excess ca. 8% [CD(-)250 nm]).

Shaking experiments at 1000 rpm for *ca.* 24 hours in a 2.0 mL microcentrifuge tube (at 69 °C) also resulted in the formation of clusters ranging in size from 2 to 5 mm. Clusters were randomly selected from numerous tubes (*ca.* 3 clusters per tube) and the enantiomeric excess was determined using solid-state circular dichroism of crushed individual clusters. Of 30 clusters isolated at random, there were 15 (+) clusters, 14 (-) clusters and 1 racemic cluster (Figure 24b). In most cases the enantiomeric excess was significantly higher than that of the starting material. Once again, optimal clustering was observed when starting from a scalemic starting material. Clustering was hardly observed within 24 hours when the initial crystalline mixture was racemic. In this case, it is believed that a longer period of time is required for optimal homochiral interactions to take place. However, using the commercial scalemic mixture (*ca.* 8% [CD(-)250 nm]) resulted in cluster formation within 24 hours. A shaking experiment was also carried out using homochiral guanidine carbonate as the starting material and, as expected, the clusters that formed were homochiral with the same chirality as the starting material.

The majority of clusters from shaking and boiling experiments exhibited some degree of faceting that could be correlated to those of guanidine carbonate single crystals (Figure 25a). Remarkably, in some cases single crystals were isolated, but whether they originated from late stages of enantiomer specific oriented attachment or simply Ostwald ripening is uncertain (Figure 25b).

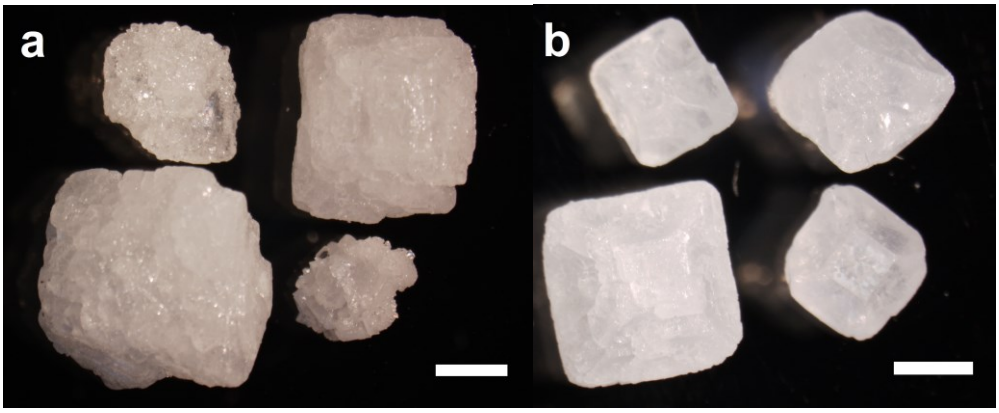


**Figure 25.** Guanidine carbonate from shaking experiments a: cluster-like b: single crystal-like. Scale bar = 2 mm.

The (001) and (012) faces were the most prevalent, especially in the smaller clusters obtained in the shaking experiments. This assignment was supported by measuring the interfacial angle between the (001) and the (012) faces of crystal aggregates from shaking experiments with a value 54 ± 2° (theoretical value: 54.58°). In some cases, the transparency of the (001) face of the constituent crystals enabled the visualization of cluster chirality *via* optical rotatory dispersion (Figure 26).

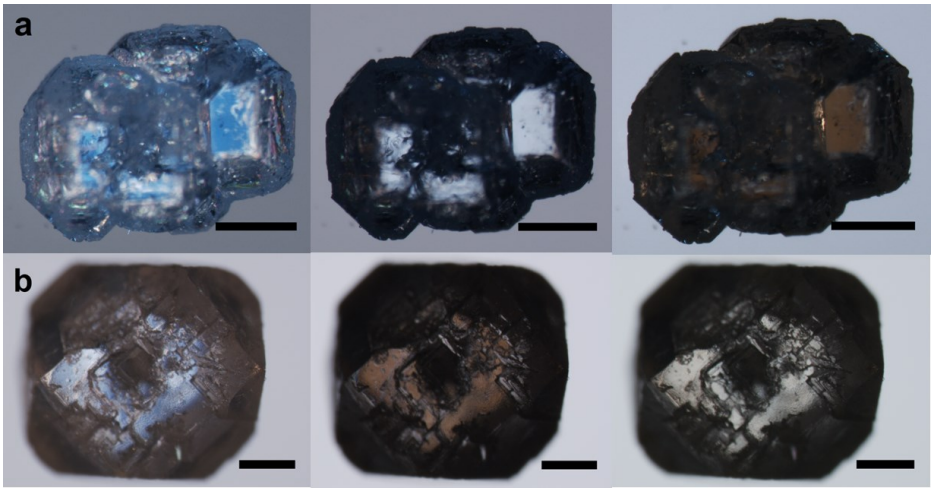


**Figure 26.** Optical rotatory dispersion of guanidine carbonate clusters viewed in the [001] direction upon rotating the analyzer clockwise. a:- clusters with an optical rotatory dispersion from blue-to-clear-to-amber ([CD(-) 250 nm]). b: clusters with an optical rotatory dispersion from blue-to-amber-to-clear ([CD(+) 250 nm]). Scale bar = 0.5 mm.

SEM analysis of the clusters obtained from both boiling and shaking experiments are in agreement with oriented attachment at the microscopic level. Once again, the (001) and (012)

faces are the most prominent within the clusters (*i.e.* the relative orientation of these faces are parallel with respect to each other; Figure 27). These SEM results, in combination with our investigation of cluster chirality, strongly support our hypothesis for enantiomer-specific oriented attachment of guanidine carbonate. Furthermore, evidence of crystal fusion is clearly visible (Figure 27b and Figure 37), suggesting that heterogeneous nucleation of a 'chiral glue' between crystals may facilitate enantiomer-specific oriented attachment.[23]

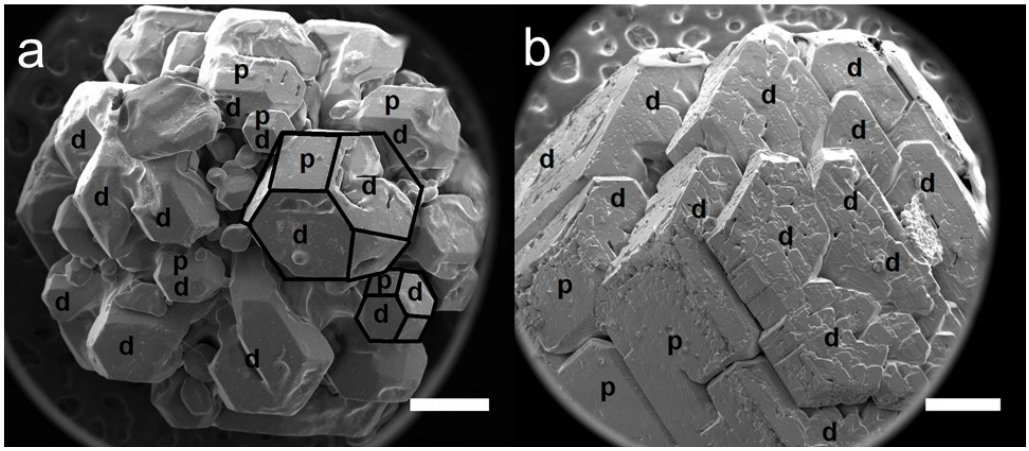


**Figure 27.** SEM images of guanidine carbonate clusters from, a: boiling and b: shaking experiments. p and d denote the (001) and the (012) faces, respectively. Scale bar: 0.5 mm.

There is also a possibility that certain surfaces of one enantiomorph could recognize clusters of the opposite enantiomorph. In their elegant work on the use of 'tailor-made' chiral polymers for the inhibition of lamellar twinning of conglomerate crystals, Lahav, Zbaida and coworkers have suggested that, "the epitaxial-like deposition of molecular clusters of a single handedness onto the surface of a crystal of opposite handedness as a secondary nucleation step might account for the formation of lamellar twins."[150,151] *Heterochiral* enantiomer-specific oriented attachment would have common features with *homochiral* enantiomer-specific oriented attachment, although it would undoubtedly lead to a different final result, the segregation of the two enantiomers within the same crystal. In the case of guanidine carbonate, our results are consistent with a preference for homochiral enantiomer-specific oriented attachment (*i.e.* solid-state homochiral interactions are favored).

Our investigations of guanidine carbonate under crystal clustering conditions demonstrate homochiral enantiomer-specific oriented attachment. The formation of homochiral and

enantioenriched aggregates of scalemic guanidine carbonate through enantiomer-specific oriented attachment at the mesoscale is remarkably analogous to conglomerate crystallization at the molecular level. The degree of enantiomer-specific oriented attachment was quantified using CD measurements and validated using polarized light microscopy. SEM images also displayed a microscopic view of the oriented attachment within the clusters. Understanding the phenomenon of enantiomer-specific oriented attachment at the molecular level will be enabled by exploring the generality of this process in other conglomerate crystal systems.

# Chapter 4. Homochiral Crystal Generation via Sequential Dehydration and Viedma Ripening

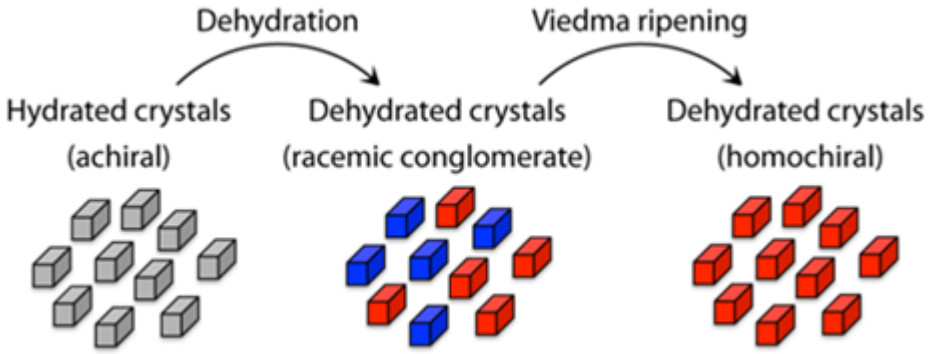


Reproduced with permission from: Sivakumar, R.; Askari, M. S.; Woo, S.; Madwar, C.; Ottenwaelder, X.; Bohle, D. S.; Cuccia, L. A. *CrystEngComm* 2016, *18*, 4277–4280 with permission from Royal Society of Chemistry.

## *4.1. Abstract*

1,2-bis(*N*-benzoyl-*N*-methylamino)benzene (2) forms centrosymmetric hydrate crystals but non-centrosymmetric anhydrous crystals. Dehydration of this hydrate (30 min at 140 °C for 2•*x*$H_2O$) resulted in the formation of chiral crystals (*i.e.* a physical racemate of the conglomerate crystals) as verified using solid-state circular dichroism and powder X-ray diffraction. Subsequent attrition-enhanced deracemization, also known as Viedma ripening, was used to obtain homochiral crystals of 2 within 5 h.

## *4.2. Main Text*

The outstanding mystery of the origin of homochirality in nature has been thoroughly investigated due to the essential role it plays in chemistry, biochemistry and biology. The mechanism to generate homochiral populations can be generally separated into two steps: (*i*) the formation of an initial chiral imbalance (*i.e.* mirror symmetry breaking) and (*ii*) its subsequent amplification to homochirality. The initial imbalance may be caused by statistical fluctuations, the parity violation energy difference (PVED), the influence of circularly polarized light or selective adsorption on chiral mineral surfaces.[20] In conglomerate crystal systems, this initial

imbalance can be amplified through, for example, the eutectic model,[152] Kondepudi's model[153,154] and more recently, Viedma ripening.[2]

Generating chirality in the absence of chiral reagents (*i.e.* spontaneous absolute asymmetric induction) is an attractive route to obtain chiral materials and has clear implications with regards to the origins of biological homochirality.[155] Mirror symmetry breaking and chiral amplification can be achieved by effectively utilizing the unique nature of conglomerate crystals. More specifically, attrition-enchanced deracemization, or Viedma ripening, has proven to be an effective method to obtain homochiral populations of conglomerate-forming crystals from an initial racemic state.[2,3,156,157] The remarkably simple process involves grinding a conglomerate crystal mixture in saturated solution. Both chiral and achiral molecules that crystallize as conglomerates, in non-centrosymmetric space groups, can undergo Viedma ripening, albeit the former require racemizing conditions in solution.[30,136] The initial broken mirror symmetry is a result of conglomerate crystallization, where the chirality of the system resides intimately and sometimes solely in the solid state. Conglomerate crystallization is often referred to as spontaneous resolution even though the chiral crystals are not physically separated.[154] In the extreme case of an achiral conglomerate-forming molecule under optimal Ostwald ripening conditions, one can envisage the formation of one homochiral crystal.[158–160]

Chiral or achiral molecules that form conglomerates must crystallize in one of the 65 non-centrosymmetric Sohncke space groups.[34,131] Our group is particularly interested in the latter case, where it was estimated in 2005 that 8-10% of chiral crystal structures are formed from achiral molecules.[36–38] A more recent survey of the Cambridge Structural Database (CSD 5.36; 2015) estimates that 5 ± 2% of chiral crystal structures are formed from achiral molecules (see Appendix 8.2).[161] Out of the 127 397 structures (chiral and achiral molecules) in a Sohncke space group, the majority crystallize in the $P2_1$ (31%) and $P2_12_12_1$ (44%) space groups. Out of these structures in the $P2_1$ and $P2_12_12_1$ space groups, 9% and 14% are formed from achiral molecules, respectively (Appendix 8.2). These statistics represent a maximum frequency since a common early crystallographic error was to miss assign space groups to lower symmetry.[162] Marsh has noted that these errors have dropped significantly but still arise with alarming regularity.[163]

Through the 'manipulation' of crystalline structures in the solid-state, crystal chirogenesis can be achieved to obtain homochiral populations. For example, crystals that incorporate solvent molecules or host-guest inclusion crystals can undergo a crystal-to-crystal transition from centrosymmetric hydrates or solvates to non-centrosymmetric anhydrous or non-solvated crystals.[84,88] Along these lines, Soai *et al.* have elegantly demonstrated the generation of absolute crystal chirality by the face-selective removal of crystal water from *individual* achiral cytosine monohydrate crystals *via* thermal dehydration or reduced pressure conditions.[47,48]

Scheme 2

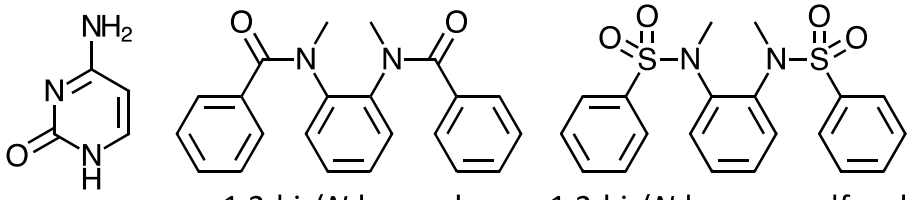


Cytosine **1** | 1,2-bis(*N*-benzoyl-*N*-methylamino)benzene **2** | 1,2-bis(*N*-benzenesulfonyl-*N*-methylamino)benzene **3**

Herein, we address the *bulk* conversion from an achiral crystalline sample into a homochiral sample using two compounds: cytosine, **1** and 1,2-bis(N-benzoyl-N-methylamino)benzene, **2** (Scheme 2).[1,47,48,84,85] Specifically, centrosymmetric hydrate crystals of **1**•$H_2O$ and **2**•$xH_2O$ were subjected to thermal dehydration. Viedma ripening was subsequently used to obtain homochiral crystal populations of **1** and **2** (Figure 28).[3,84] Our approach is somewhat reminiscent to that of Vlieg *et al.*, where Viedma ripening of alanine and phenylalanine was achieved by non-centrosymmetric salt formation, while the deracemization of glutamic acid was enabled *via* a metastable conglomerate.[49,164]

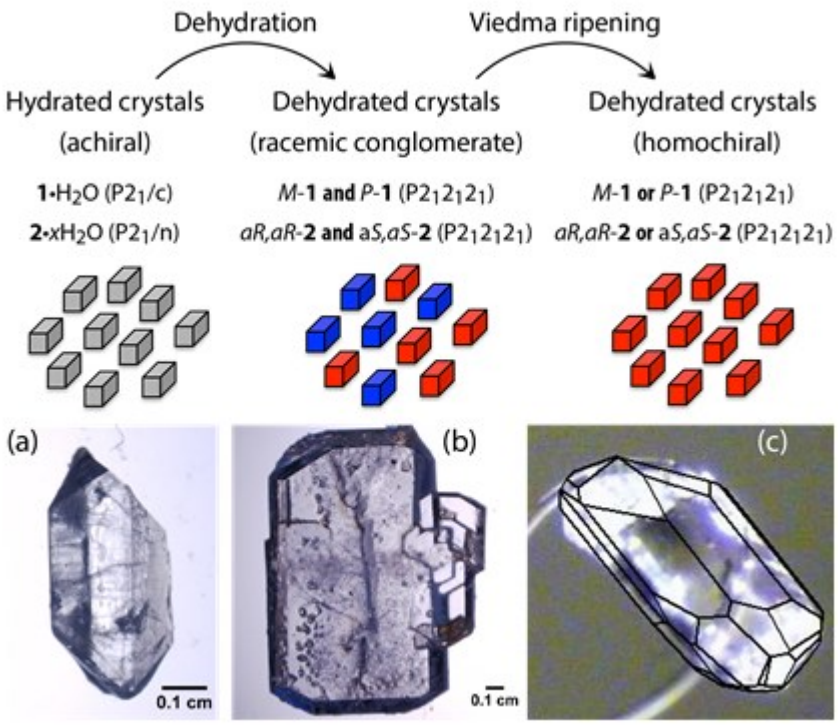


**Figure 28.** Top - general scheme. Bottom - (a) achiral hydrated crystal of **2**•*x*$H_2O$, (b) chiral crystal and (c) indexed chiral single crystal of **2**.

Anhydrous **1** was commercially available, while **2** was synthesized through generation of a secondary anilide followed by *N*-methylation from *ortho*-phenylenediamine and benzoyl chloride (Figure 38).[84] 1,2-bis-(*N*-benzenesulfonyl-*N*-methylamino)benzene, **3** (Scheme 2), was synthesized using a similar procedure as that of **2**, where benzenesulfonyl chloride was substituted for benzoyl chloride as a starting reagent (Figure 39).[84,85,119] Compound **3** crystallizes in either the $P4_12_12$ or $P4_32_12$ enantiomorphic space groups. The absolute structure of **3** was determined by single-crystal X-ray diffraction (Figure 42).[119] In this case, a solvated crystal structure of **3** has not been reported.[119] Viedma ripening at 2400 rpm for *ca.* 24 hours yielded homochiral crystals of **3**.

Compounds **1** and **2** can form either achiral or chiral crystals depending on the solvent used during crystallization. Crystallization of compound **1** from water results in the formation of achiral crystals of **1**•$H_2O$ with space group $P2_1/c$, whereas crystallization in anhydrous methanol yields chiral crystals of **1** with space group $P2_12_12_1$.[47,48] Similarly, crystallization of compound **2** from water-saturated ethyl acetate or aqueous ethanol results in the formation of achiral crystals

of **2**•$x$H$_2$O with space group P2$_1$/n. Different scanning calorimetry (DSC) measurements of **1**•H$_2$O and **2**•$x$H$_2$O confirm the loss of water with broad endothermic peaks at *ca.* 96°C and 152°C, respectively. The non-stoichiometric water occupancy in **2**•$x$H$_2$O was determined by thermogravimetric (TGA) analysis ($x$ = 0.67) and is in agreement with the values estimated from single-crystal X-ray diffraction ($x$ = 0.59 to 0.78 for an old and a freshly picked crystal, respectively; Appendix 8.2†). Crystallization of **2** from dry solvents, such as anhydrous ethyl acetate, absolute ethanol, benzene and chloroform, yields chiral crystals of **2** with space group P2$_1$2$_1$2$_1$.[1,84] Upon crystallization of these achiral molecules, a racemic mixture of enantiomorphic conglomerate crystals should be obtained. However, the commercial sample of **1** used in these experiments was found to be scalemic (6% ee [CD(−)290 nm]).[3] Similarly, slow crystallization of **2** (from anhydrous ethyl acetate in the presence of a drying tube, Appendix 8.2) resulted in a unequal distribution of chiral crystals, as observed by Azumaya *et al.*.[84] In our hands, separate crystallization dishes typically yielded crystals of only one chirality of **2**. This non-stochastic mirror symmetry breaking observed in **1** and **2** can be attributed to crystallization in a cryptochiral environment.[156,157,165–168]

Achiral crystals of **1**•H$_2$O and **2**•$x$H$_2$O were converted to anhydrous chiral crystals through dehydration using a heating mantle (*i.e.* 3 h at 90 °C for **1**•H$_2$O and 30 min at 140 °C for 2•$x$H$_2$O; Figure 28). Starting from finely ground material reduced the time required for the crystals to transform from the centrosymmetric to non-centrosymmetric space groups. A visual indication of the transformation was possible for **1**, as **1**•H$_2$O crystals were initially transparent but became opaque upon dehydration. The phase transition from centrosymmetric to non-centrosymmetric space group was validated through X-ray powder diffraction (XRPD, Figures 29 and 30). Experimental XRPD data for all compounds was compared with XRPD patterns simulated from single-crystal X-ray diffraction data, either from the CSD (for **1**•H$_2$O and **1**, Figure 29) or remeasured (for **2**•$x$H$_2$O and **2**, Figure 30, see Appendix 8.2† for experimental details). Finally, dehydration of **1**•H$_2$O and **2**•$x$H$_2$O yielded physical racemates, as confirmed by baseline solid-state circular dichroism (CD) signals. Our attempts at face-selective dehydration from individual achiral **2**•$x$H$_2$O were unsuccessful (see Appendix 8.2†).[48]

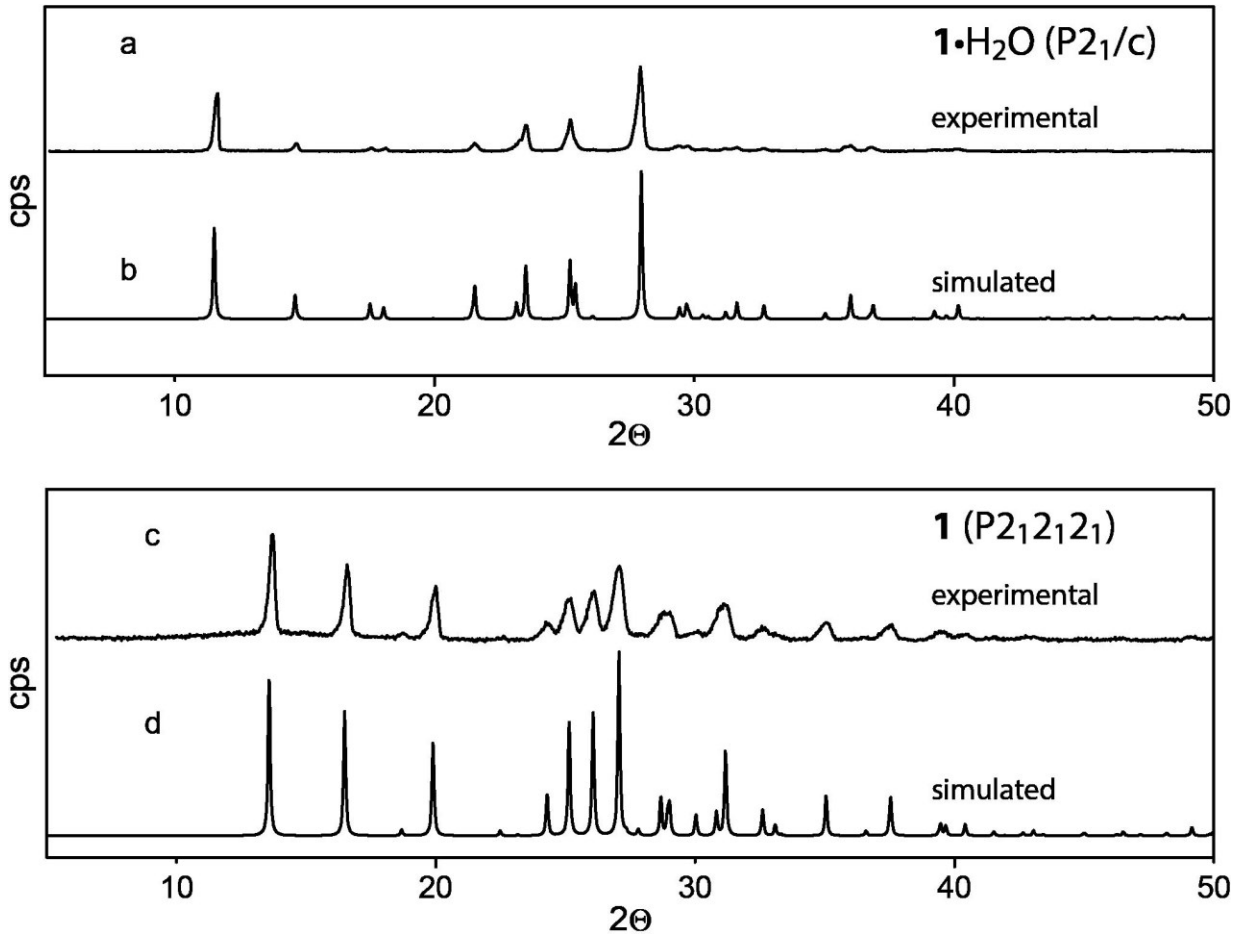


**Figure 29.** Transformation of **1**•$H_2O$ ($P2_1/c$) to **1** ($P2_12_12_1$). (a) Experimental XRPD for **1**•$H_2O$, (b) XRPD of **1**•$H_2O$ generated from the CSD (CYTOSM), (c) Experimental XRPD for **1** and (d) XRPD of **1** generated from the CSD (CYTSIN).

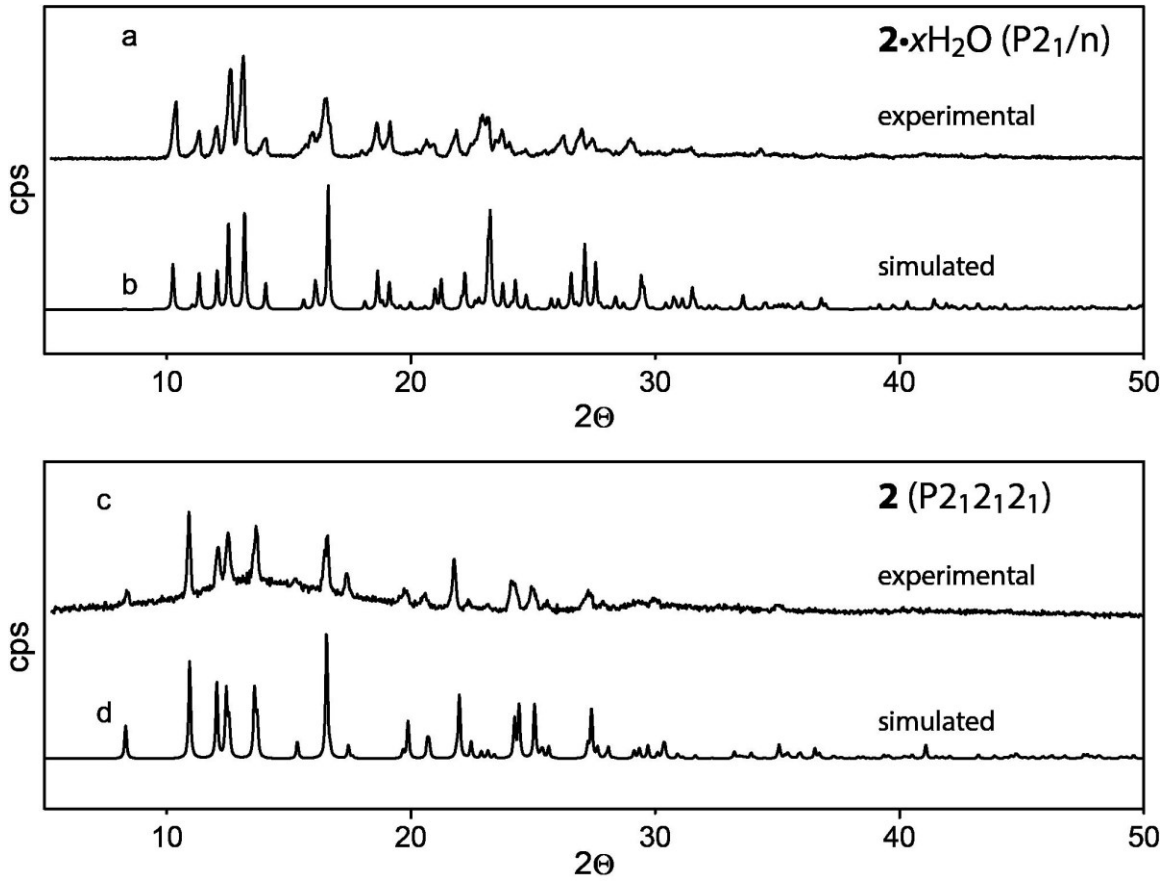


**Figure 30.** Transformation of **2**•$x$H$_2$O (P2$_1$/n) to **2** (P2$_1$2$_1$2$_1$) (a) Experimental XRPD for **2**•$x$H$_2$O, (b) XRPD of **2**•H$_2$O generated from single crystal data, (c) Experimental XRPD for **2**, (d) XRPD of **2** generated from single crystal data.

Viedma ripening was then carried out on the racemic mixtures of **1** or **2** in an attempt to yield homochiral crystals (see Appendix 8.2 for experimental details).[3] In both cases, amplification to homochirality occurred. For **1**, five experiments yielded homochiral crystals with negative CD signal and five yielded homochiral crystals with positive CD signal at 290 nm (Figure 31). For **2**, four experiments yielded homochiral crystals with negative CD signal and one experiment yielded homochiral crystals with positive CD signal at 260 nm (Figure 32).

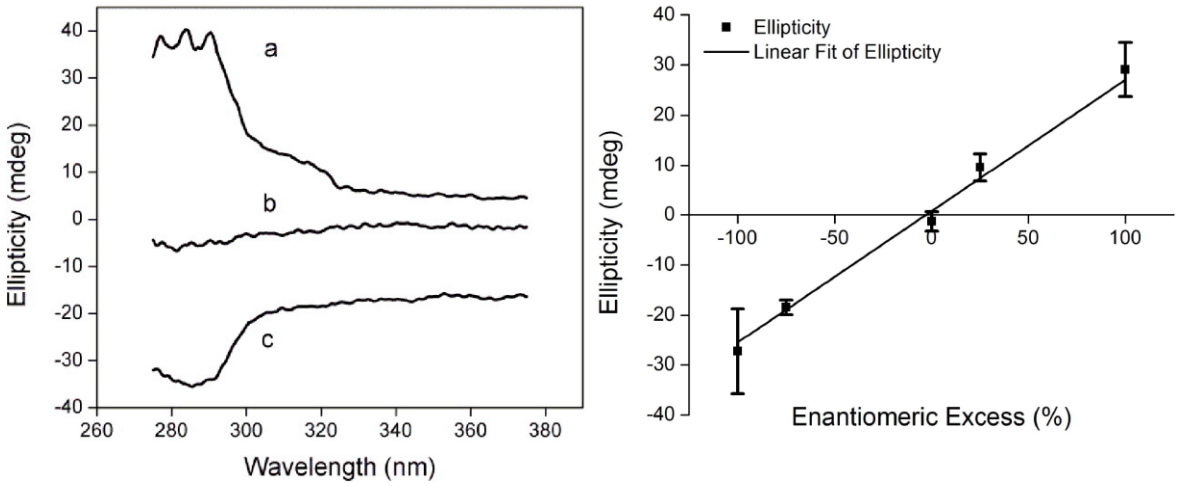


**Figure 31.** Left - Solid-state CD spectra of the chiral crystals of **1** in KBr: (b) After dehydration, (a) and (c) following Viedma ripening. Viedma ripening was carried out using 0.25 g sample suspended in 3 mL of saturated solution in anhydrous methanol with 3 g of ceramic grinding media (0.8 mm) stirring at 2400 rpm for *ca.* 65 hours. Right - CD calibration curve of **1** in KBr prepared from mixtures of homochiral crystals ([CD(±)290 nm]).

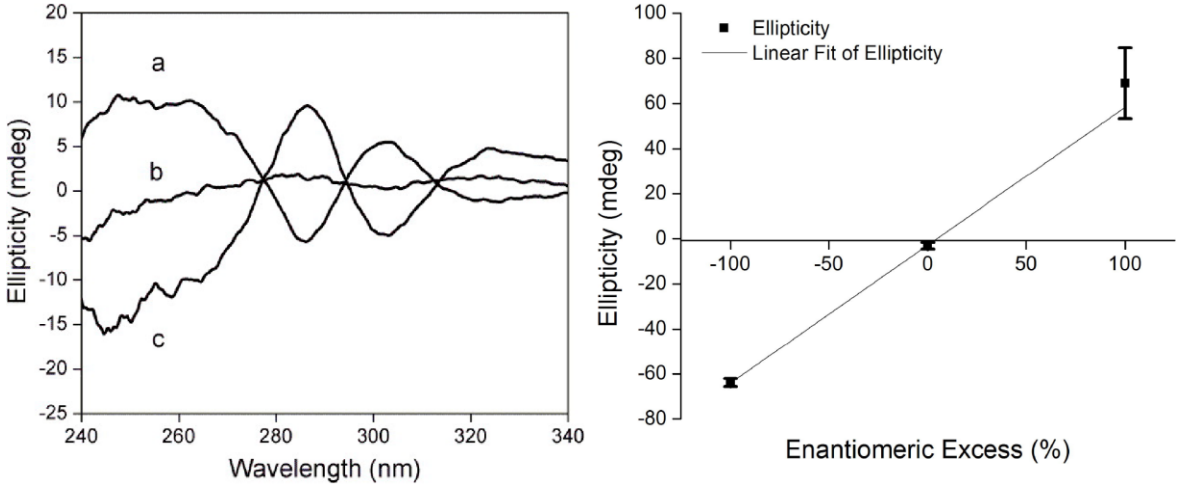


**Figure 32.** Left - Solid-state CD spectra of the chiral crystals of **2** in KBr: (b) immediately after dehydration, (a) and (c) following Viedma ripening. Viedma ripening was carried out using 0.25 g sample suspended in 3 mL of saturated solution in anhydrous ethyl acetate with 3 g of ceramic grinding media (0.8 mm) stirring at 1500 rpm for *ca.* 5 hours. Right - CD calibration curve of **2** in KBr prepared from mixtures of homochiral crystals ([CD(±)260 nm]).

The absolute structure of **2** was confirmed by single-crystal X-ray diffraction and solid-state CD carried out on the same single crystal. Since **2** only contains light atoms, the diffraction data was acquired with a Cu Kα radiation source. The correct enantiomer was validated by a low Flack

parameter of -0.03(10) and the conformation of **2** was correlated with its respective CD signal. The chirality of **2** is due to the presence of two chiral axes (Ar-N). Crystals formed from (*aS*,*aS*)-**2** resulted in a negative CD signal at 260 nm, whereas (*aR*,*aR*)-**2** would give a positive CD signal at 260 nm (see Appendix 8.2).[1,84]

To conclude, homochiral crystals can be produced through asymmetric amplification using dehydration coupled with attrition-enchanced deracemization, as exemplified here with compounds 1 and 2. We are currently probing the CSD for further examples of achiral molecules that form both solvated achiral crystals as well as the corresponding non-solvated chiral crystals.[169,170]

# Chapter 5. Conclusion

The role of conglomerate crystallization in spontaneous resolution and chiral amplification was investigated. This includes a literature survey of compounds that can undergo Pasteurian resolution. The survey included conglomerates that can be separated using hemihedrism, macromorphology, circular polarization or surface characteristics/topographic features.

Enantiomer-specific oriented attachment was investigated in guanidine carbonate crystals. This phenomenon was previously reported for sodium bromate, sodium chlorate, and threonine.[63] Boiling and shaking experiments of scalemic guanidine carbonate crystals resulted in the formation of large clusters. Based on solid-state CD measurements, these clusters had high enantiomeric excess. Furthermore, aligned crystal facets within the clusters, visualized with SEM microscopy, confirmed oriented attachment. This process can be considered analogous to mesoscale conglomerate crystallization.[117] This phenomenon of homochiral cluster recognition is believed to be essential for Viedma ripening.[32,117]

Chiral amplification through coupling thermal dehydration with Viedma ripening was demonstrated. Soai *et al.* were able to obtain homochiral conglomerate crystals through dehydrating enantiotopic faces of single achiral crystals of cytosine monohydrate. This experimental approach was further elaborated by our research group and carried out on bulk material. Achiral crystals were converted to conglomerate crystals through thermal dehydration. The dehydration process resulted in the formation of a physical racemate of conglomerate crystals which was subsequentially amplified to homochirality using Viedma ripening. This process was applied to both cytosine and 1,2-bis(*N*-benzoyl-*N*-methylamino)benzene. Conglomerate crystallization is an essential requirement for this process, without the formation of conglomerate crystals, attrition-enhanced chiral amplification would not be possible.[32]

# Chapter 6. Future Directions

Homochiral crystals can be generated by coupling thermal dehydration and chiral amplification. The experimental procedure carried out for cytosine and 1,2-bis(*N*-benzoyl-*N*-methylamino)benzene can be applied to other compounds. The compounds chosen must be able to form both achiral hydrated and chiral anhydrous crystals. The Cambridge Structural Database was probed to obtain a list of compounds that can form both hydrated and dehydrated crystal structures.[170] A script was developed in our lab which searched the CSD database for compounds that had both achiral hydrated crystals as well as chiral dehydrated crystals. There were 95 hits, including cytosine and 1,2-bis(*N*-benzoyl-*N*-methylamino)benzene. We will continue to explore the generality of this chirogenesis/chiral amplification process. For example, phloroglucinol and 5-nitrouracil were identified and tested (Appendix). Altering the script can increase the range of compounds that can undergo this assymetric amplification (i.e. a *'desolvation'* process can be applied to other solvates).[171] The transition from non-solvated achiral crystals to solvated chiral crystals will be investigated.

Investigating the phenomenon of enantiomer-specific oriented attachment in other conglomerate systems (achiral and chiral molecules) can provide further insight into enantiomer-specific oriented attachment and Viedma ripening. It can also be investigated in achiral crystals with chiral face (*e.g.* gypsum). [172]

# Chapter 7. References


(1) Azumaya, I.; Yamaguchi, K.; Okamoto, I.; Kagechika, H.; Shudo, K. *J. Am. Chem. Soc.* **1995**, *117*, 9083–9084.
(2) Viedma, C. *Phys. Rev. Lett.* **2005**, *94*, 065504–1 – 065504–4.
(3) McLaughlin, D. T.; Nguyen, T. P. T.; Mengnjo, L.; Bian, C.; Leung, Y. H.; Goodfellow, E.; Ramrup, P.; Woo, S.; Cuccia, L. A. *Cryst. Growth & Des.* **2014**, *14*, 1067–1076.
(4) Cronin, J.; Reisse, J. In *Lectures in Astrobiology*; Springer Berlin Heidelberg, 2005; pp. 473–515.
(5) Kelvin, Lord. *On the Molecular Tactics of Crystals, Baltimore Lectures, Appendix H*; C.J. Clay and Sons: London, 1904; p. 619.
(6) Blackmond, D. G. *Cold Spring Harb Perspect Biol* **2010**, *2*.
(7) Bohannon, J. The Viking Sunstone Revealed? http://www.sciencemag.org/news/2011/11/viking-sunstone-revealed (accessed Aug 10, 2016).
(8) Glusker, J. P.; Lewis, M.; Rossi, M. *Crystal Structure Analysis for Chemists and Biologists*; Wiley, 1994.
(9) Kauffman, G. B.; Myers, R. D. *J. Chem. Educ.* **1975**, *52*.
(10) Goldstein, D. H. *Polarized Light, Third Edition*; CRC Press: Boca Raton, 2016.
(11) Hall, A. R. *Isaac Newton: Adventurer in Thought*; Cambridge University Press: Cambridge, United Kingdom, 1996.
(12) Bridges, T. J.; Kluver, J. W. *Appl. Opt.* **1965**, *4*, 1121–1125.
(13) Fieser, L. F.; Fieser, M. *Organic Chemistry*; Reinhold Publishing Corporation: New York, 1956.
(14) Schreier, P.; Bernreuther, A.; Huffer, M. *Analysis of Chiral Organic Molecules: Methodology and Applications*; Walter de Gruyter: Berlin, Germany, 1995.
(15) Glaser, R. *Symmetry, Spectroscopy, and Crystallography: The Structural Nexus*; Wiley: Weinheim, Germany, 2015.
(16) Fincham, W. H. A.; Freeman, M. H. *Optics*; Elsevier Science, 2013.
(17) Glazer, A. M.; Stadnicka, K. On the Origin of Optical Activity in Crystal Structures. *Journal of Applied Crystallography*, 1986, *19*, 108–122.
(18) Kahr, B.; Arteaga, O. *ChemPhysChem* **2012**, *13*, 79–88.
(19) Palyi, G.; Zucchi, C.; Caglioti, L. *Progress in Biological Chirality*; Elsevier Science: Netherlands, 2004..
(20) Guijarro, A.; Yus, M. *The Origin of Chirality in the Molecules of Life*; The Royal Society of Chemistry: Cambridge, United Kingdom, 2009.
(21) Rocke, A. J. *Image and Reality: Kekulé, Kopp, and the Scientific Imagination*; University of Chicago Press: USA, 2010.
(22) Herschel, J. F. W. *On the Rotation Impressed by Plates of Rock Crystal on the Planes of Polarization of the Rays of Light, as Connected with Certain Peculiarities in Its Crystallization. From the Transactions of the Cambridge Philosophical Society*; J. Smith: Cambridge, United Kingdom, 1820.
(23) Herschel, J. F. W. *Camb. Philos. Soc. Trans.* **1822**, 43–52.
(24) Geison, G. L. *The Private Science of Louis Pasteur*; Princeton University Press: New Jersey, USA, 1996.
(25) Derewenda, Z. S. *Acta Crystallogr. Sect.* **2008**, *64*, 246–258.

(26) Saha, C.; Chakraborty, S. *Resonance* **2012**, *17*, 768–778.
(27) Gal, J. *Chirality* **2007**, *19*, 89–98.
(28) Pasteur, L. *Recherches sur la dissymétrie moléculaire des produits organiques naturels*; Librairie de L. Hachette: Paris, 1861.
(29) Datta, S.; Grant, D. J. *Nat. Rev. Drug Discov.* **2004**, *3*, 42–57.
(30) Sögütoglu, L.-C.; Steendam, R. R. E.; Meekes, H.; Vlieg, E.; Rutjes, F. P. J. T. *Chem. Soc. Rev.* **2015**, *44*, 6723–6732.
(31) LaPlante, S. R.; Edwards, P. J.; Fader, L. D.; Jakalian, A.; Hucke, O. *ChemMedChem* **2011**, *6*, 505–513.
(32) Sivakumar, R.; Askari, M. S.; Woo, S.; Madwar, C.; Ottenwaelder, X.; Bohle, D. S.; Cuccia, L. A. *CrystEngComm* **2016**, *18*, 4277–4280.
(33) Nespolo, M. *Cryst. Res. Technol.* **2015**, *50*, 413–413.
(34) Flack, H. D. *Helvetica Chim. Acta* **2003**, *86*, 905–921.
(35) Hager, O.; Llamas-Saiz, A. L.; Foces-Foces, C.; Claramunt, R. M.; López, C.; Elguero, J. *Helvetica Chim. Acta* **1999**, *82*, 2213–2230.
(36) Matsuura, T.; Koshima, H. *J. Photochem. Photobiol. C: Photochem. Rev.* **2005**, *6*, 7–24.
(37) Dryzun, C.; Avnir, D. *Chem. Commun.* **2012**, *48*, 5874–5876.
(38) Pidcock, E. *Chem. Commun.* **2005**, 3457–3459.
(39) Eliel, E. L.; Wilen, S. H. *Stereochemistry of Organic Compounds*; Wiley India Pvt. Limited: New Delhi, India, 2008.
(40) Kurihara, N.; Miyamoto, J.; Paulson, G. D.; Zeeh, B.; Skidmore, M. W.; Hollingworth, R. M.; Kuiper, H. A. *Pure Appl. Chem.* **1997**, *69*, 2007–2026.
(41) Blaser, H.-U.; Federsel, H.-J. *Asymmetric Catalysis on Industrial Scale: Challenges, Approaches and Solutions*; John Wiley & Sons: Weinheim, 2010.
(42) Blaser, H.-U. *Rendiconti Lince*- **2013**, *24,* 213-216.
(43) Ulrich, E. M.; Morrison, C. N.; Goldsmith, M. R.; Foreman, W. T. In *Reviews of Environmental Contamination and Toxicology Volume 217*; Springer US: Boston, MA, 2012; pp. 1–74.
(44) McBride, J. M.; Tully, J. C.; Ulas, G. *Nature* **2008**, *452*, 161–162.
(45) Viedma, C. *When "Left" and "Right" Cannot Coexist: Chiral Purity by Thermodynamic-Kinetic Feedback Near Equilibrium - Personal Communication*; Concordia University: Montreal, Canada, 2008.
(46) Bushuyev, O. S.; Tomberg, A.; Friščić, T.; Barrett, C. J. *J. Am. Chem. Soc.* **2013**, *135*, 12556–12559.
(47) Mineki, H.; Kaimori, Y.; Kawasaki, T.; Matsumoto, A.; Soai, K. *Tetrahedron: Asymmetry* **2013**, *24*, 1365–1367.
(48) Kawasaki, T.; Hakoda, Y.; Mineki, H.; Suzuki, K.; Soai, K. *J. Am. Chem. Soc.* **2010**, *132*, 2874–2875.
(49) Spix, L.; Alfring, A.; Meekes, H.; Enckevort, W. J. P. van; Vlieg, E. *Cryst. Growth & Des.* **2014**, *14*, 1744–1748.
(50) Wilmink, P.; Rougeot, C.; Wurst, K.; Sanselme, M.; Meijden, M. van der; Saletra, W.; Coquerel, G.; Kellogg, R. M. *Org. Process. Res. & Dev.* **2015**, *19*, 302–308.
(51) Patterson, J.; Bailey, B. *Solid-State Physics: Introduction to the Theory*; Springer Berlin Heidelberg, 2007.
(52) *Manual of Mineralogy (after James D. Dana)*; Dana, J. D.; Klein, C.; Hurlbut, C., Eds.; Wiley: New York, USA, 1985.

(53) Bahrig, L.; Hickey, S. G.; Eychmuller, A. *CrystEngComm* **2014**, *16*, 9408–9424.
(54) Ostwald, W. *Lehrbuch der Allgemeinen Chemie*; Engelmann: Leipzig, Germany, 1896; Vol. 2 , part 1.
(55) Xue, X.; Penn, R. L.; Leite, E. R.; Huang, F.; Lin, Z. *CrystEngComm* **2014**, *16*, 1419–1429.
(56) Zhang, H.; Penn, R. L.; Lin, Z.; Colfen, H. *CrystEngComm* **2014**, *16*, 1407–1408.
(57) Zhang, H.; Banfield, J. F. *CrystEngComm* **2014**, *16*, 1568–1578.
(58) Serway, R.; Moses, C.; Moyer, C. *Modern Physics*; Cengage Learning: USA, 2004.
(59) Brog, J.-P.; Chanez, C.-L.; Crochet, A.; Fromm, K. M. *RSC Adv.* **2013**, *3*, 16905–16931.
(60) Hurlbut Jr., C. S.; Klein, C. *Manual of Mineralogy (after James D. Dana)*; John Wiley & Sons, Inc., 1977.
(61) Gaubert, P. *Bull. de la Société française de minéralogie* **1896**, *19*, 431–434.
(62) Liesegang, R. E. *Z. Phys. Chem. Stoechiom. Verwandtschaftsl.* **1911**, *75*, 374–377.
(63) Viedma, C.; McBride, J. M.; Kahr, B.; Cintas, P. *Angew. Chem. Int. Ed.* **2013**, *52*, 10545–10548.
(64) Penn, R. L.; Banfield, J. F. *Geochim. et Cosmochim. Acta* **1999**, *63*, 1549–1557.
(65) Li, D.; Nielsen, M. H.; Lee, J. R. I.; Frandsen, C.; Banfield, J. F.; De Yoreo, J. J. *Science* **2012**, *336*, 1014–1018.
(66) Penn, R. L.; Banfield, J. F. *Science* **1998**, *281*, 969–971.
(67) Distaso, M.; Mačković, M.; Spiecker, E.; Peukert, W. *Chem. – Eur. J.* **2012**, *18*, 13265–13268.
(68) Penn, R. L.; Banfield, J. F. *Am. Miner.* **1998**, *83*, 1077–1082.
(69) Sturm (nee Rosseeva), E. V.; Colfen, H. *Chem. Soc. Rev.* **2016**.
(70) Cölfen, H.; Antonietti, M. *Mesocrystals and nonclassical crystallization*; Wiley: Chichester, UK, 2008.
(71) Uwaha, M. *J. Phys. Soc. Jpn.* **2004**, *73*, 2601–2603.
(72) Nunez, M. C.; Garcia-Rubino, M. E.; Conejo-Garcia, A.; Cruz-Lopez, O.; Kimatrai, M.; Gallo, M. A.; Espinosa, A.; Campos, J. M. *Curr. Med. Chem.* **2009**, *16*, 2064–2074.
(73) Johnson, G. *The Ten Most Beautiful Experiments*; Knopf Doubleday Publishing Group: New York, USA 2008.
(74) Leeman, M. S. Resolution of Racemates by Crystallization: Additives and Attrition, University of Groningen: Groningen, Netherlands, 2009.
(75) Tobe, Y. *Mendeleev Commun.* **2003**, *13*, 93–94.
(76) Gal, J. *Chirality* **2012**, *24*, 959–976.
(77) Coquerel, G.; Petit, S. *J. Cryst. Growth* **1993**, *130*, 173–180.
(78) Kress, R. B.; Duesler, E. N.; Etter, M. C.; Paul, I. C.; Curtin, D. Y. *J. Am. Chem. Soc.* **1980**, *102*, 7709–7714.
(79) Curtin, D. Y.; Paul, I. C. *Chem. Rev.* **1981**, *81*, 525–541.
(80) Fortes, A. D. *Axis* **2005**, *1*, 1–28.
(81) *The Chemical News*; Crookes, W., Ed.; London, 1884; Vol. XLIX.
(82) Sephton, M. A.; University, O. S. *Synthesis of Novel Ambifunctional Atropisomeric 2,2',6,6'-tetrasubstituted Biphenyls and Investigation of Their Properties and Organocatalytic Activity*; Oregon State University: USA, 2008.
(83) Sephton, M. A.; Emerson, C. R.; Zakharov, L. N.; Blakemore, P. R. *Chem. Commun.* **2010**, *46*, 2094–2096.
(84) Azumaya, I.; Okamoto, I.; Nakayama, S.; Tanatani, A.; Yamaguchi, K.; Shudo, K.;

Kagechika, H. *Tetrahedron* **1999**, *55*, 11237–11246.
(85) Azumaya, I.; Kagechika, H.; Yamaguchi, K.; Shudo, K. *Tetrahedron* **1995**, *51*, 5277–5290.
(86) Kostyanovsky, R. G.; Kadorkina, G. K.; Nabiev, O. G.; Pozharskii, A. F.; Degtyarev, A. V.; Malyshev, O. R. *Mendeleev Commun.* **2007**, *17*, 214–215.
(87) Pozharskii, A. F.; Degtyarev, A. V.; Ryabtsova, O. V.; Ozeryanskii, V. A.; Kletskii, M. E.; Starikova, Z. A.; Sobczyk, L.; Filarowski, A. *J. Org. Chem.* **2007**, *72*, 3006–3019.
(88) Tanaka, K.; Iwamoto, T.; Wada, S.-I.; Frelek, J.; Caira, M. R. *Chirality* **2006**, *18*, 483–488.
(89) Tanaka, K.; Iwamoto, T.; Caira, M. R. *New J. Chem.* **2004**, *28*, 329–331.
(90) Sohail, M.; Wang, Y.-F.; Wu, S.-X.; Zeng, W.; Guo, J.-Y.; Chen, F.-X. *Chin. Chem. Lett.* **2013**, *24*, 695–698.
(91) Suh, I.-H.; Park, K. H.; Jensen, W. P.; Lewis, D. E. *J. Chem. Educ.* **1997**, *74*.
(92) Gladstone, J. H. *Q. J. Chem. Soc.* **1861**, *13*, 254–270.
(93) Tanaka, K.; Takenaka, H.; Caira, M. R. *Tetrahedron: Asymmetry* **2006**, *17*, 2216–2219.
(94) EB Classic Encyclopaedia, 1911.
(95) Authier, A. *Early Days of X-ray Crystallography*; OUP Oxford, 2013.
(96) Schmieder, P.; Denysenko, D.; Grzywa, M.; Baumgartner, B.; Senkovska, I.; Kaskel, S.; Sastre, G.; van Wullen, L.; Volkmer, D. *Dalton Trans.* **2013**, *42*, 10786–10797.
(97) G. Kostyanovsky, R.; R. Kostyanovsky, V.; K. Kadorkina, G.; A. Lyssenko, K. *Mendeleev Commun.* **2001**, *11*, 1–5.
(98) mindat.org http://www.mindat.org/photo-334001.html (accessed Aug 22, 2016).
(99) Read, J.; Cook, A. M. R.; Shannon, M. I. *J. Chem. Soc.* **1926**, *129*, 2223–2234.
(100) Read, J. *J. Pharm. Pharmacol.* **1953**, *5*, 1–17.
(101) Pennington, W. T.; Chakraborty, S.; Paul, I. C.; Curtin, D. Y. *J. Am. Chem. Soc.* **1988**, *110*, 6498–6504.
(102) *The Encyclopædia Britannica, or, Dictionary of arts, sciences, and general literature*; Adam & Charles Black, 1858.
(103) Irngartinger, H. *Isr. J. Chem.* **1972**, *10*, 635–647.
(104) Jacques, J.; Collet, A.; Wilen, S. H. *Enantiomers, racemates, and resolutions*; Krieger Pub. Co.: New York , USA, 1994.
(105) Collet, A.; Brienne, M. J.; Jacques, J. *Chem. Rev.* **1980**, *80*, 215–230.
(106) Karlsson, O.; Lundquist, K.; Stomberg, R. *Acta Chem. Scand.* **1990**, *44*, 617–624.
(107) Swanson, H. E.; Tatge, E.; Fuyat, R. K. **1953**.
(108) Priya, R.; Krishnan, S.; Raj, C. J.; Das, S. J. *Cryst. Res. Technol.* **2009**, *44*, 1272–1276.
(109) Nagasato, S.; Katsuki, I.; Motoda, Y.; Sunatsuki, Y.; Matsumoto, N.; Kojima, M. *Inorg. Chem.* **2001**, *40*, 2534–2540.
(110) Sangwal, K.; Szurgot, M.; Szczepaniak, M. *J. Cryst. Growth* **1986**, *79*, 185–191.
(111) Cai, L.; Li, Y.; Yu, C.; Ji, H.; Liu, Y.; Liu, S. *Inorganica Chim. Acta* **2009**, *362*, 2895–2899.
(112) Lewis, W. J. *A Treatise on Crystallography*; C. J. Clay and Sons: Cambridge, United Kingdom, 1899.
(113) *J. Chem. Educ.* **2007**, *84*, 1783.
(114) Kawasaki, T.; Nakaoda, M.; Kaito, N.; Sasagawa, T.; Soai, K. *Orig. Life Evol. Biospheres* **2010**, *40*, 65–78.
(115) Szurgot, J.; Szurgot, M. *Cryst. Res. Technol.* **1995**, *30*, 71–79.

(116) Klein, C.; Hurlbut Jr, C. S. *Manual of Mineralogy (after James D. Dana)*; John Wiley & Sons, 1985.
(117) Sivakumar, R.; Kwiatoszynski, J.; Fouret, A.; Nguyen, T. P. T.; Ramrup, P.; Cheung, P. S. M.; Cintas, P.; Viedma, C.; Cuccia, L. A. *Cryst. Growth & Des.* **2016**, *16*, 3573–3576.
(118) Lan, Z.-P.; Lai, X.; Roberts, K.; Klapper, H. *Cryst. Growth & Des.* **2014**, *14*, 6084–6092.
(119) Azumaya, I.; Kato, T.; Okamoto, I.; Yamasaki, R.; Tanatani, A.; Yamaguchi, K.; Kagechika, H.; Takayanagi, H. *Org. Lett.* **2003**, *5*, 3939–3942.
(120) Brown, C. J.; Sadanaga, R. *Acta Crystallogr.* **1965**, *18*, 158–164.
(121) Cuccia, L. A.; Koby, L.; Ningappa, J. B.; Dakessian, M. *J. Chem. Educ.* **2005**, *82*.
(122) Adams, J. M.; Small, R. W. H. *Acta Crystallogr. Sect. B* **1974**, *30*, 2191–2193.
(123) Karssen, A. *Recl. des Trav. Chim. des Pays-Bas* **1923**, *42*, 904–930.
(124) Shimon, L. J. W.; Lahav, M.; Leiserowitz, L. *J. Am. Chem. Soc.* **1985**, *107*, 3375–3377.
(125) Addadi, L.; Weinstein, S.; Gati, E.; Weissbuch, I.; Lahav, M. *J. Am. Chem. Soc.* **1982**, *104*, 4610–4617.
(126) Addadi, L.; Berkovitch-Yellin, Z.; Domb, N.; Gati, E.; Lahav, M.; Leiserowitz, L. *Nature* **1982**, *296*, 21–26.
(127) Addadi, L.; Berkovitch-Yellin, Z.; Weissbuch, I.; van Mil, J.; Shimon, L. J. W.; Lahav, M.; Leiserowitz, L. *Angew. Chem. Int. Ed. Engl.* **1985**, *24*, 466–485.
(128) Szurgot, M. *Cryst. Res. Technol.* **1995**, *30*, 621–628.
(129) Lin, C.-T.; Curtin, D. Y.; Paul, I. C. *J. Am. Chem. Soc.* **1974**, *96*, 6199–6200.
(130) Weissbuch, I.; Addadi, L.; Leiserowitz, L.; Lahav, M. *J. Am. Chem. Soc.* **1988**, *110*, 561–567.
(131) Flack, H. D.; Bernardinelli, G. *Acta Crystallogr. Sect. Found. Crystallogr.* **1999**, *55*, 908–915.
(132) Perez-Garcia, L.; Amabilino, D. B. *Chem. Soc. Rev.* **2007**, *36*, 941–967.
(133) Lorenz, H.; Seidel-Morgenstern, A. *Angew. Chem.* **2014**, *53*, 1218–1250.
(134) In *Handbook of Crystal Growth*; Viedma, C.; Coquerel, G.; Cintas, P.; Nishinaga, T., Eds.; Elsevier: Amsterdam, 2015; Vol. 1A, pp. 951–1002.
(135) Noorduin, W. L.; van Enckevort, W. J. P.; Meekes, H.; Kaptein, B.; Kellogg, R. M.; Tully, J. C.; McBride, J. M.; Vlieg, E. *Angew. Chem. Int. Ed.* **2010**, *49*, 8435–8438.
(136) Noorduin, W. L.; Izumi, T.; Millemaggi, A.; Leeman, M.; Meekes, H.; Van Enckevort, W. J. P.; Kellogg, R. M.; Kaptein, B.; Vlieg, E.; Blackmond, D. G. *J. Am. Chem. Soc.* **2008**, *130*, 1158–1159.
(137) Saito, Y.; Hyuga, H. *J. Phys. Soc. Jpn.* **2009**, *78*.
(138) Skrdla, P. J. *Cryst. Growth & Des.* **2011**, *11*, 1957–1965.
(139) Iggland, M.; Mazzotti, M. *Cryst. Growth & Des.* **2011**, *11*, 4611–4622.
(140) Wattis, J. A. D. *Orig Life Evol Biosph* **2011**, *41*, 133–173.
(141) El-Hachemi, Z.; Crusats, J.; Ribó, J. M.; McBride, J. M.; Veintemillas-Verdaguer, S. *Angew. Chem. Int. Ed.* **2011**, *50*, 2359–2363.
(142) Iggland, M.; Müller, R.; Mazzotti, M. *Cryst. Growth & Des.* **2014**, *14*, 2488–2493.
(143) Blanco, C.; Ribó, J. M.; Hochberg, D. *Phys. Rev.* **2015**, *91*.
(144) De Yoreo, J. J.; Vekilov, P. G. *Rev. Mineral. Geochem.* **2003**, *54*, 57–93.
(145) De Yoreo, J. J.; Gilbert, P. U. P. A.; Sommerdijk, N. A. J. M.; Penn, R. L.; Whitelam, S.; Joester, D.; Zhang, H.; Rimer, J. D.; Navrotsky, A.; Banfield, J. F.; Wallace, A. F.; Michel, F. M.; Meldrum, F. C.; Cölfen, H.; Dove, P. M. *Science* **2015**, *349*.
(146) Teng, H. H. *Elements* **2013**, *9*, 189–194.

(147) Ivanov, V. K.; Fedorov, P. P.; Baranchikov, A. Y.; Osiko, V. V. *Russ. Chem. Rev.* **2014**, *83*.
(148) Niederberger, M.; Colfen, H. *Phys. Chem. Chem. Phys.* **2006**, *8*, 3271–3287.
(149) Kaminsky, W. *J. Appl. Crystallogr.* **2007**, *40*, 382–385.
(150) Berfeld, M.; Zbaida, D.; Leiserowitz, L.; Lahav, M. *Adv. Mater.* **1999**, *11*, 328–331.
(151) Zbaida, D.; Lahav, M.; Drauz, K.; Knaup, G.; Kottenhahn, M. *Tetrahedron* **2000**, *56*, 6645–6649.
(152) *Biochirality: Origins, Evolution and Molecular Recognition*; Cintas, P., Ed.; Springer, 2013; Vol. 333.
(153) Kondepudi, D. K.; Sabanayagam, C. *Chem. Phys. Lett.* **1994**, *217*, 364–368.
(154) McBride, J. M.; Carter, R. L. *Angew. Chem. Int. Ed. Engl.* **1991**, *30*, 293–295.
(155) Kawasaki, T.; Suzuki, K.; Shimizu, M.; Ishikawa, K.; Soai, K. *Chirality* **2006**, *18*, 479–482.
(156) Cheung, P. S. M.; Cuccia, L. A. *Chem. Commun.* **2009**, 1337–1338.
(157) Cheung, P. S. M.; Gagnon, J.; Surprenant, J.; Tao, Y.; Xu, H.; Cuccia, L. A. *Chem. Commun.* **2008**, 987–989.
(158) Noorduin, W. L.; Vlieg, E.; Kellogg, R. M.; Kaptein, B. *Angew. Chem.* **2009**, *48*, 9600–9606.
(159) Noorduin, W. L.; Meekes, H.; Bode, A. A. C.; van Enckevort, W. J. P.; Kaptein, B.; Kellogg, R. M.; Vlieg, E. *Cryst. Growth & Des.* **2008**, *8*, 1675–1681.
(160) Cartwright, J. H. E.; García-Ruiz, J. M.; Piro, O.; Sainz-Díaz, C. I.; Tuval, I. *Phys. Rev. Lett.* **2004**, *93*, 035502–1 – 035502–035504.
(161) Allen, F. H. *Acta Crystallogr. Sect. B* **2002**, *58*, 380–388.
(162) Marsh, R. E. *Acta Crystallogr. Sect. B* **2009**, *65*, 782–783.
(163) Henling, L. M.; Marsh, R. E. *Acta Crystallogr. Sect. C* **2014**, *70*, 834–836.
(164) Spix, L.; Meekes, H.; Blaauw, R. H.; van Enckevort, W. J. P.; Vlieg, E. *Cryst. Growth & Des.* **2012**, *12*, 5796–5799.
(165) Veintemillas-Verdaguer, S.; Esteban, S. O.; Herrero, M. A. *J. Cryst. Growth* **2007**, *303*, 562–567.
(166) Brewer, D. G.; Kan, K. T. *Can. J. Chem.* **1971**, *49*, 965–967.
(167) Azeroual, S.; Surprenant, J.; Lazzara, T. D.; Kocun, M.; Tao, Y.; Cuccia, L. A.; Lehn, J.-M. *Chem. Commun.* **2012**, *48*, 2292–2294.
(168) Viedma, C. *Cryst. Growth Des.* **2007**, *7*, 553–556.
(169) Van de Streek, J. *CrystEngComm* **2007**, *9*, 350–352.
(170) Van de Streek, J.; Motherwell, S. *CrystEngComm* **2007**, *9*, 55–64.
(171) Van de Streek, J. *CrystEngComm* **2007**, *9*, 350–352.
(172) Viedma, C.; Cuccia, L. A.; McTaggart, A.; Kahr, B.; Martin, A. T.; McBride, J. M.; Cintas, P. *Chem. Commun.* accepted 19-Aug-2016: Manuscript ID: CC-COM-08-2016-006353
(173) Rybak, W. K. *Tetrahedron: Asymmetry* **2008**, *19*, 2234–2239.
(174) Noorduin, W. L.; Bode, A. A. C.; van der Meijden, M.; Meekes, H.; van Etteger, A. F.; van Enckevort, W. J. P.; Christianen, P. C. M.; Kaptein, B.; Kellogg, R. M.; Rasing, T.; Vlieg, E. *Nat Chem* **2009**, *1*, 729–732.
(175) Viedma, C.; Ortiz, J. E.; Torres, T. de; Izumi, T.; Blackmond, D. G. *J. Am. Chem. Soc.* **2008**, *130*, 15274–15275.
(176) Kaptein, B.; Noorduin, W. L.; Meekes, H.; van Enckevort, W. J. P.; Kellogg, R. M.; Vlieg, E. *Angew. Chem. Int. Ed.* **2008**, *47*, 7226–7229.

(177) Noorduin, W. L.; Kaptein, B.; Meekes, H.; van Enckevort, W. J. P.; Kellogg, R. M.; Vlieg, E. *Angew. Chem. Int. Ed.* **2009**, *48*, 4581–4583.
(178) Hein, J. E.; Huynh Cao, B.; Viedma, C.; Kellogg, R. M.; Blackmond, D. G. *J. Am. Chem. Soc.* **2012**, *134*, 12629–12636.
(179) Van der Meijden, M. W.; Leeman, M.; Gelens, E.; Noorduin, W. L.; Meekes, H.; van Enckevort, W. J. P.; Kaptein, B.; Vlieg, E.; Kellogg, R. M. *Org. Process. Res. & Dev.* **2009**, *13*, 1195–1198.
(180) Tsogoeva, S. B.; Wei, S.; Freund, M.; Mauksch, M. *Angew. Chem. Int. Ed. Engl.* **2009**, *48*, 590–594.
(181) Flock, A. M.; Reucher, C. M. M.; Bolm, C. *Chem. – Eur. J.* **2010**, *16*, 3918–3921.
(182) Leeman, M.; Noorduin, W. L.; Millemaggi, A.; Vlieg, E.; Meekes, H.; van Enckevort, W. J. P.; Kaptein, B.; Kellogg, R. M. *CrystEngComm* **2010**, *12*, 2051–2053.
(183) Iggland, M.; Fernández-Ronco, M. P.; Senn, R.; Kluge, J.; Mazzotti, M. *Chem. Eng. Sci.* **2014**, *111*, 106–111.
(184) Steendam, R. R. E.; Brouwer, M. C. T.; Huijs, E. M. E.; Kulka, M. W.; Meekes, H.; van Enckevort, W. J. P.; Raap, J.; Rutjes, F. P. J. T.; Vlieg, E. *Chem. – Eur. J.* **2014**, *20*, 13527–13530.
(185) Björemark, P. M.; Olsson, S.; Kokoli, T.; Håkansson, M. *Chem. – Eur. J.* **2015**, *21*, 8750–8753.
(186) Björemark, P. M.; Jönsson, J.; Håkansson, M. *Chem. – Eur. J.* **2015**, *21*, 10630–10633.
(187) Steendam, R. R. E.; van Benthem, T. J. B.; Huijs, E. M. E.; Meekes, H.; van Enckevort, W. J. P.; Raap, J.; Rutjes, F. P. J. T.; Vlieg, E. *Cryst. Growth & Des.* **2015**, *15*, 3917–3921.
(188) Tarasevych, A. V.; Sorochinsky, A. E.; Kukhar, V. P.; Toupet, L.; Crassous, J.; Guillemin, J.-C. *CrystEngComm* **2015**, *17*, 1513–1517.
(189) Shang, X.; Li, X.; Xi, N.; Zhai, Y.; Zhang, J.; Xu, X. *Sensors Actuators B: Chem.* **2011**, *160*, 1112–1119.
(190) Amundsen, L. H. *J. Am. Chem. Soc.* **1937**, *59*, 1466–1467.
(191) Martel, P.; Powell, B. M. *Biophys. J.* **1983**, *41*, 91–93.
(192) Bruno, I. J.; Cole, J. C.; Edgington, P. R.; Kessler, M.; Macrae, C. F.; McCabe, P.; Pearson, J.; Taylor, R. *Acta Crystallogr. Sect. B* **2002**, *58*, 389–397.
(193) Macrae, C. F.; Edgington, P. R.; McCabe, P.; Pidcock, E.; Shields, G. P.; Taylor, R.; Towler, M.; van de Streek, J. *J. Appl. Crystallogr.* **2006**, *39*, 453–457.
(194) Eppel, S.; Bernstein, J. *Acta Crystallogr. Sect. B* **2008**, *64*, 50–56.
(195) Okoth, M. O.; Vrcelj, R. M.; Pitak, M. B.; Sheen, D. B.; Sherwood, J. N. *Cryst. Growth & Des.* **2012**, *12*, 5002–5011.
(196) Wallwork, S. C.; Powell, H. M. *Acta Crystallogr.* **1957**, *10*, 48–52.
(197) Braun, D. E.; Tocher, D. A.; Price, S. L.; Griesser, U. J. *J. Phys. Chem. B* **2012**, *116*, 3961–3972.
(198) Maartmann-Moe, K. *Acta Crystallogr.* **1965**, *19*, 155–157.

# Chapter 8. Appendix

## *8.1. Enantiomer-Specific Oriented Attachment in Guanidine Carbonate Crystals – Supporting Information*

### 8.1.1. Materials and Methods

Guanidine carbonate ([CAS 593-85-1]) was purchased from Acros Organics (15.5 % *ee* [CD(-)250 nm]) and Aldrich (1.7% *ee*, [CD(-) 250] and 13.5% *ee* [CD(+) 250 nm]). Nujol mineral oil [CAS 8012-95-1] was obtained from Plough Inc. CD absorption spectra were recorded using a Jasco J-710 spectropolarimeter. Polarized light microscopy was carried out using a Nikon SMZ1500 stereomicroscope. SEM images were acquired using an FEI Inspect F50 FE-SEM instrument.

### 8.1.2. Crystallization through Slow Evaporation

Single crystals of guanidine carbonate were grown through slow evaporation from water in crystallizing dishes (15 cm by 8 cm). Guanidine carbonate (*ca.* 40 g) was dissolved in distilled water (500 mL) with heating and stirring and subsequently covered with perforated aluminum foil to slow down evaporation. Slow crystallization of large single crystals occurred over several weeks. Crystals were typically 1 x 1 x 0.25 cm in size.

### 8.1.3. Viedma Ripening

Viedma ripening of samples was carried out using a modified Pine Industrial Company analytical rotator. Guanidine carbonate was dissolved in distilled water before being precipitated by addition of acetone.

Guanidine carbonate (*ca.* 0.25 g) and grinding media (3 g of 0.8 mm of YTZ® Zirconia ceramic beads) were suspended in saturated solution (1 mL) in a stoppered and sealed round bottom flask (5 mL). A magnetic stir bar (10 mm x 5 mm) was placed within the round-bottom flask and the sample was stirred at 2400 rpm until homochirality was achieved (*ca.* 60 hours). The kinetics of the Viedma ripening process was monitored by taking periodic slurry samples (100 µL).

### 8.1.4. Boiling Experiments

Boiling experiments were carried out using a round-bottom flask (100 mL) or reaction tubes (diameter: 23 mm, length: 150 mm). Ground guanidine carbonate (*ca.* 30 g) was dissolved in water (20 mL) in a round-bottom flask. This mixture was refluxed at 190 °C for *ca.* 24 hours until the formation of clusters was observed. Clusters ranged in size from 0.2 cm to 1 cm in diameter (20 mg to 1.5 g in mass).

The boiling experiments were also carried out in a carousel using reaction tubes. Ground guanidine carbonate (*ca.* 8 g) was mixed with water (5 mL) in each reaction tube and then placed into the carousel. The bottom of the tubes was heated at 190 °C for *ca*. 24 hours until cluster formation was observed (Figure 33). Clusters ranged in size from 0.2 cm to 0.7 cm in diameter (10 mg to 350 mg in mass).

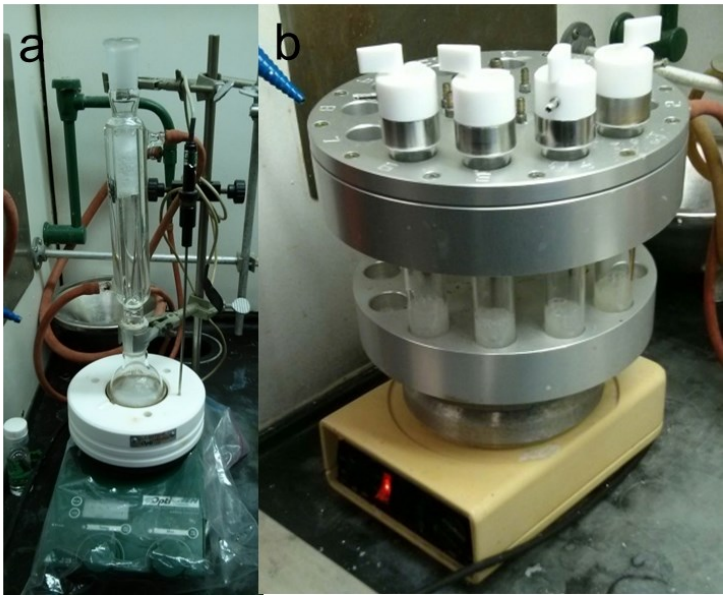


**Figure 33.** Boiling experiment apparatus, a: round-bottom flask equipped with a reflux condenser and b: tubes in a reaction carousel.

### 8.1.5. Shaking Experiments

Shaking experiments were carried out in an Eppendorf Thermomixer 5436. Ground guanidine carbonate (*ca.* 750 mg) was suspended in distilled water (500 µL) in 1.5 mL Eppendorf tubes. The mixtures were vortexed prior to placement in the Eppendorf Thermomixer

to ensure guanidine carbonate hydration. The Eppendorf tubes were heated at *ca.* 69 °C at 1000 rpm for 16 to 24 hours. Clusters ranged in size from 0.2 cm to 0.5 cm in diameter (from 17 mg to 130 mg). Solid-state circular dichroism measurements were carried out on three clusters from each Eppendorf tube.

Parameters were varied during shaking experiments to optimize cluster formation. A key factor for cluster formation was the crystalline enantiomeric excess of the starting material. Out of 5 shaking experiments using racemic guanidine carbonate, only 1 showed cluster formation within 24 hours. On the other hand, all 4 experiments with scalemic starting material had significant cluster formation within 24 hours.

### 8.1.6. Circular Dichroism

Solid-state circular dichroism was used to quantify the crystal enantiomer excess (CEE) of guanidine carbonate clusters obtained during the Viedma ripening process and from shaking and boiling experiments. The CD spectra were recorded from 250 to 350 nm using a Jasco J-710 spectropolarimeter. The resolution used was 5 points/nm and each curve generated was an average of 4 accumulations collected at a scan rate of 50 nm/min. Solid-state samples of guanidine carbonate were prepared as Nujol mulls. Guanidine carbonate was ground with a mortar and pestle and Nujol was subsequently added to obtain the desired weight percentage (20% wt/wt). The samples were mixed until a homogenous mixture was obtained. The suspended sample (10 mg) was sandwiched between two quartz plates (20 x 20 mm, 6 mm thick) such that a uniform film was obtained before being mounted onto a standard cell holder for analysis. HT voltage values were typically below 400 V at 250 nm.

### 8.1.7. Crystal Enantiomeric Excess Calibration Curves

Crystal enantiomeric excess (CEE) in single crystals and guanidine carbonate clusters were determined using calibration curves. The enantiomeric excess was determined using eq. S1, where $m_{(+)}$ and $m_{(-)}$ are the weights of CD-positive and CD-negative crystals.

$$\%ee = \frac{m_{(+)} - m_{(-)}}{m_{(+)} + m_{(-)}} \times 100\%$$

Equation 1. Determination of enantiomeric excess

Homochiral single crystals that generated either [CD(+) 250 nm] and [CD(-) 250 nm] were mixed together at various ratios while maintaining a constant total weight. The CD signal at a specific wavelength (250 nm) was determined at various enantiomeric excesses and plotted to generate the crystal enantiomeric excess calibration curve. The average CD signal and standard deviation was obtained for each CEE (typically, n = 3).

### 8.1.8. WinXMorph™

Crystal morphology of guanidine carbonate was generated using WinXMorph™ software.[149] Point symmetry (42) and the corresponding faces were used to emulate experimental crystal morphology (Table 4).

**Table 4.** Faces used to generate the crystal morphology of guanidine carbonate using WinXMorph software.[149]

| Indices | Distance |
|---|---|
| 0 0 1 | 0.4 |
| 1 1 0 | 2 |
| 1 0 2 | 1.04 |

### 8.1.9. Shape™

The theoretical value for the interfacial angle between the (001) face and the (012) face was generated using Shape™. The theoretical value was determined to be 54.58°. Interfacial angles on clusters from shaking experiments were determined by using a contact goniometer. The interfacial angle between the (001) face and the (012) face was measured on 10 different clusters.

### 8.1.10. Scanning electron microscopy

SEM images were obtained using an FEI Inspect F50 FE-SEM operating at 15 keV acceleration voltage. The apparatus was equipped with an EDAX Octane Super 60 $mm^2$ SDD, TEAM EDS

Analysis System and iXRF XBeam XRF. Guanidine carbonate clusters from boiling and shaking experiments were fixed on glass slides (7.5 cm x 2.5 cm) using double-sided conductive tape. An E6300 Bench Top Evaporator was used to apply a gold layer (*ca.* 10 nm) on the samples prior to imaging.

### 8.1.11. Supplementary Data

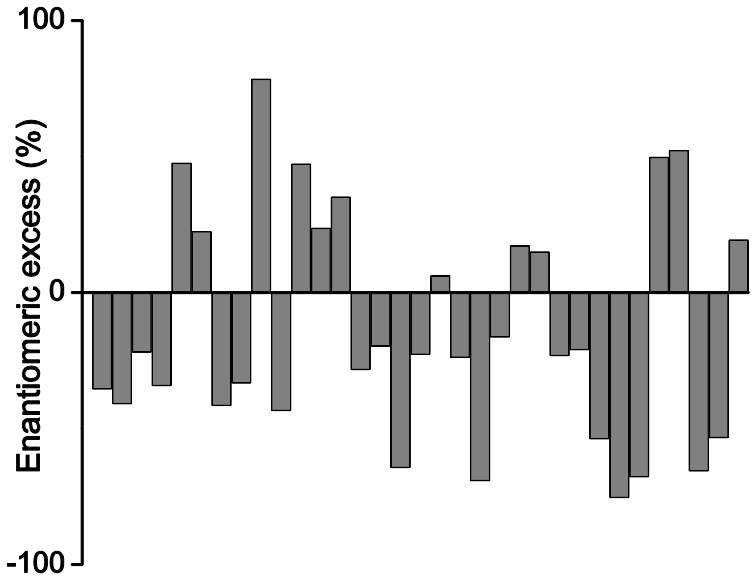


**Figure 34.** Enantiomeric excess of guanidine carbonate clusters obtained from boiling experiment using reaction tubes.

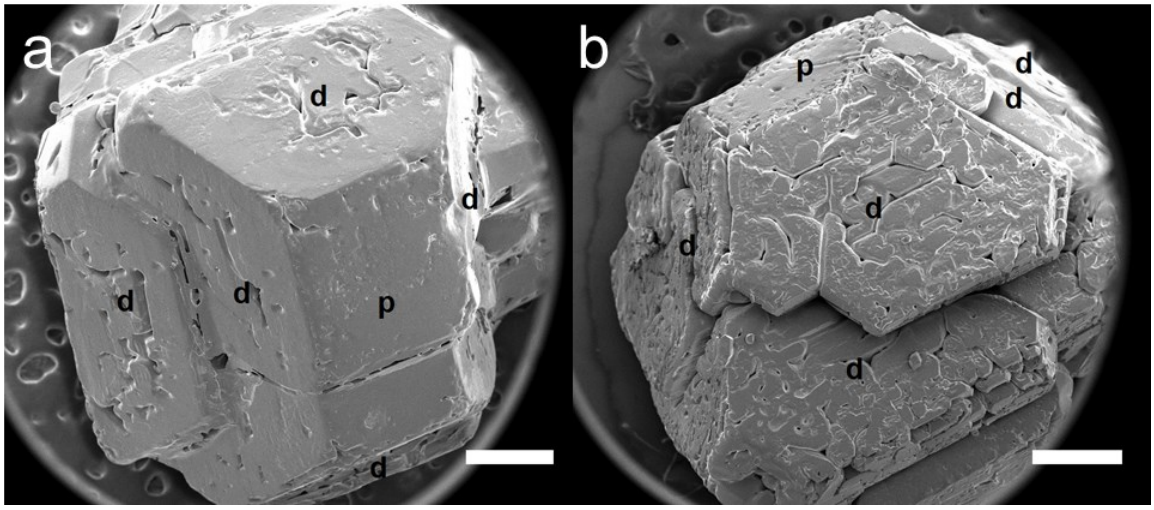


**Figure 35.** Clusters obtained from shaking experiment that display single-crystal-like appearance. p: (001) face, d: (012) face Scale bar: 0.5mm.

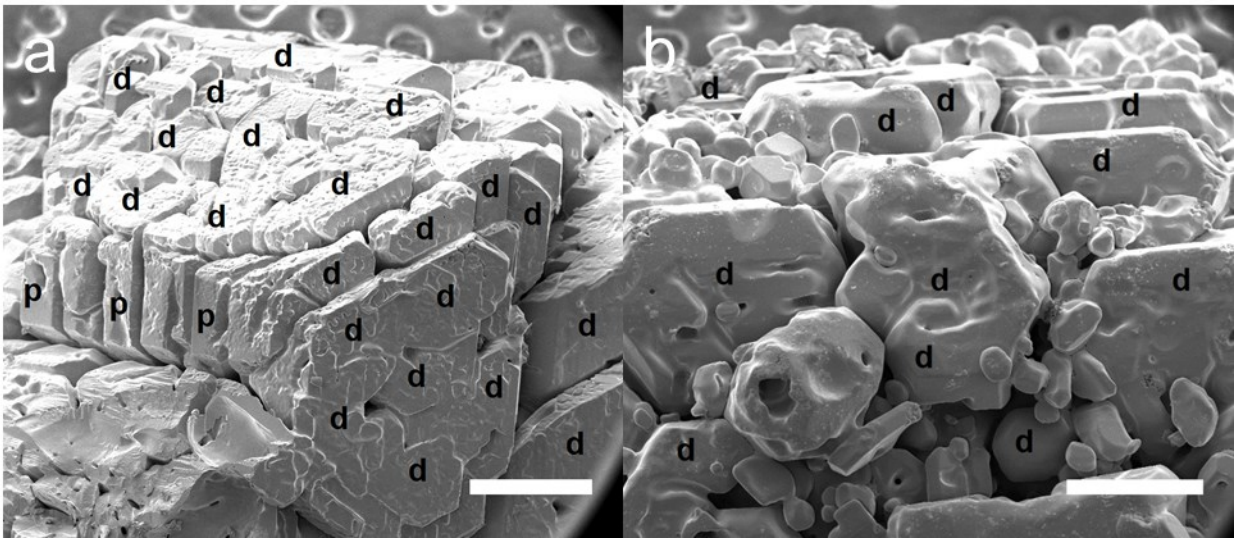


**Figure 36.** Crystal facets were present on the clusters in a highly oriented manner with respect with each other. a: Cluster obtained from shaking experiment indicating the presence of the (001) face (p) and (012) face (d). b: Cluster obtained from boiling experiment indicating the presence of (012) face (d).Scale bar: 500 μm.

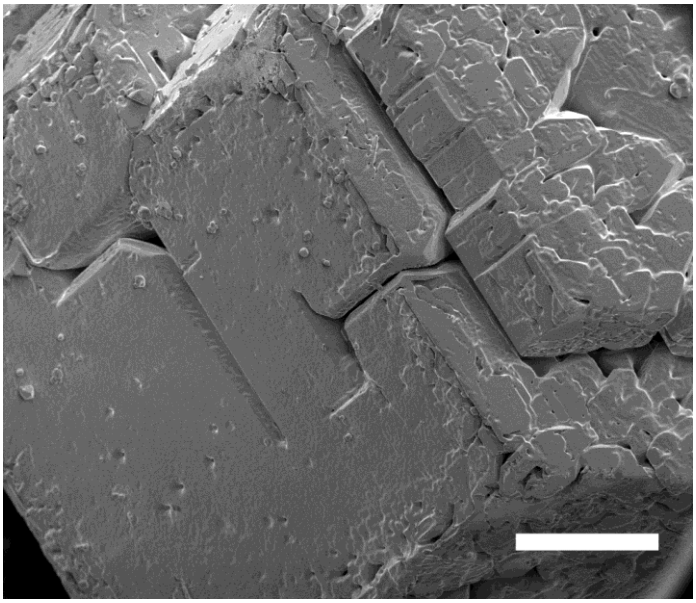

**Figure 37.** Cluster obtained from shaking experiment displaying fusion process that occurs within the clusters at the (001) face. Scale bar: 500 μm.

**Table 5.** Compounds that undergo Viedma Ripening

| Compound | Year | Ref |
|---|---|---|
| Sodium chlorate | 2005 | 2 |
| Sodium bromate | 2007 | 168 |
| Ethylenediammonium sulfate | 2008 | 157 |
| Oxo-rhenium(V) complex | 2008 | 173 |
| 2-(2-methylbenzylideneamino)-2-phenylacetamide | 2008 | 136,174 |
| Aspartic acid | 2008 | 175 |
| N-(4-chlorobenzylidene) phenylalanine methyl ester | 2008 | 176 |
| Methyl-2-(6-methoxynaphthalen-2-yl) propanoate (naproxen methyl ester) | 2009 | 177 |

| | | |
|---|---|---|
| 2-(benzylideneamino)-2-(2-chlorophenyl)acetamide | 2009 | [178,179] |
| 4-bromobenzoyl-2-[1-(ethoxycarbonyl)-3-oxobutyl]hydrazide | 2009 | [180] |
| 4-*tert*-butyl-2-[hydroxy(4-nitrophenyl)methyl]cyclohexanone | 2010 | [181] |
| 2-(2-methylbenzylideneamino) propanamide | 2010 | [182] |
| Glutamic acid | 2012 | [164] |
| Benzil | 2014 | [3] |
| Diphenyl disulfide | 2014 | [3] |
| Benzophenone | 2014 | [3] |
| Tetraphenylethylene | 2014 | [3] |
| Guanidine carbonate | 2014 | [3] |
| 2,6-di-*tert*-butyl-4-methylphenol (BHT) | 2014 | [3] |
| Benzoylaminoethanoic acid (Hippuric acid) | 2014 | [3] |
| 2,2-dihydroxyindane-1,3-dione (ninhydrin) | 2014 | [3] |
| Cytosine | 2014 | [3] |
| Adeninium dinitrate | 2014 | [3] |
| Alanine 4-chlorobenzenesulfonic acid | 2014 | [49] |
| Phenylalanine 2,5-xylenesulfonic acid | 2014 | [49] |
| *N*-(2-methylbenzylidene)-phenylglycine amide | 2014 | [183] |
| 3-hydroxy-3-phenyl-2-propyl-2,3-dihydroisoindol-1-one | 2014 | [184] |

| | | |
|---|---|---|
| 3-hydroxy-2-isopropyl-3-phenyl-2,3-dihydroisoindol-1-one | 2014 | [184] |
| 2-(2-phenylethyl)-3-hydroxy-3-phenyl-2,3-dihydroisoindol-1-one | 2014 | [184] |
| 1,2-bis(*N*-benzoyl-*N*-methylamino)benzene | 2015 | [32] |
| 1,2-bis-(*N*-benzenesulfonyl-*N*-methylamino)benzene | 2015 | [32] |
| $[Ag(PS)_2]BF_4]$<br>(PS=(2(methylthio)ethyl)diphenyl-phosphine) | 2015 | [185] |
| $[Co(bpy)_3](PF_6)_2]$<br>(bpy=2,2'-bipyridine) | 2015 | [186] |
| (3,4-dimethoxyphenyl)-4-((4-methoxyphenyl)amino)butan-2-one | 2015 | [187] |
| γ polymorph of glycine | 2015 | [188] |
| 2-flouro-α-[(*E*)-(phenylmethylene)amino]-benzeneacetamide | 2015 | [50] |
| 2-((4-bromobenzylidene)amino)-2-(2-fluorophenyl)acetamide | 2015 | [50] |
| 5-nitrouracil | 2016 | [27] |

## *8.2. Homochiral Crystal Generation via Sequential Dehydration and Viedma Ripening – Supporting Information*

### 8.2.1. Materials and Methods

Cytosine (**1**) ([CAS 71-30-7], 6 % *ee* [CD(−)290 nm]) and potassium bromide ([7758-02-3]) were purchased from Sigma-Aldrich. 1,2-bis(N-benzoyl-N-methylamino)benzene (**2**) and 1,2-bis-(*N*-benzenesulfonyl-*N*-methylamino)benzene (**3**) were synthesized in a two-step reaction *via* the formation of a secondary anilide with subsequent *N*-methylation as described below (Figure 38 & 39). TLC was carried out on silica gel 60 $F_{254}$ with aluminum support. $^1$H-NMR spectra

were acquired on a Varian VNMR 500 MHz spectrometer. CD absorption spectra were recorded using a Jasco J-710 spectropolarimeter. X-ray powdered diffraction patterns were obtained using a Bruker D2 Phaser, Ni-filtered Cu Kα radiation was applied and a Lynxeye detector was used. Single crystal X-ray diffraction was run on a Bruker DUO system, which was either equipped with a Molybdenum Kα source (λ = 0.71073 Å), a graphite monochromator and an APEX II CCD detector or a system equipped with a Copper Kα microfocus source (λ = 1.54184 Å) and an APEX II CCD detector. Polarized light microscopy was performed on a Nikon SMZ1500 stereomicroscope. Mass spectroscopic analysis was completed using Quattro LC triple quadrupole mass spectrometer. DSC measurements were carried out using TA instruments, DSC Q2000 differential scanning calorimeter.

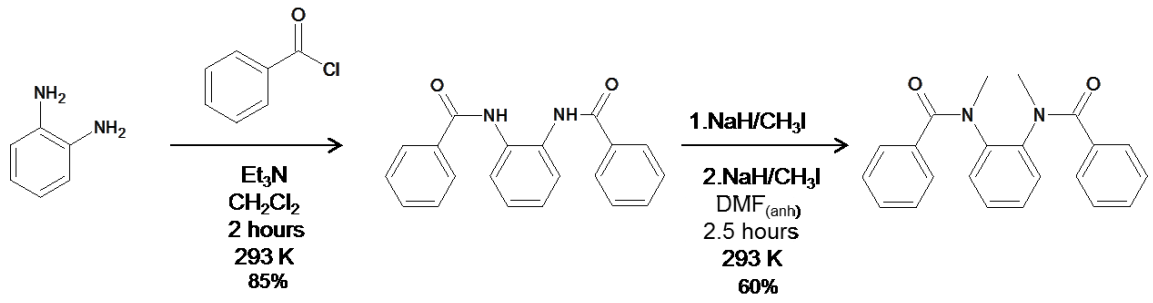


**Figure 38.** Reaction scheme for synthesis of **2**.

### 8.2.2. 1,2-bis(N-benzoyl-N-methylamino)benzene (2)

This compound was prepared using a similar protocol to that reported by Azumaya *et al.* (Figure 38).[84] A solution of *ortho*-phenylenediamine (1.1 g, 10 mmol) and triethylamine (3.5 mL, 25 mmol) in 50 mL of $CH_2Cl_2$ in a 250 mL round bottom flask was cooled in an ice bath. A solution of benzoyl chloride (2.32 mL, 20 mmol) in $CH_2Cl_2$ (50 mL) was subsequently added dropwise and the reaction mixture was stirred for an additional two hours at room temperature. The reaction mixture was washed with water (2 x 10 mL), dried with anhydrous $MgSO_4$ and evaporated to dryness. This intermediate product (2.689 g, 85%; $R_f$ = 0.54 (50:50 ethyl acetate: hexanes) was used as obtained for the subsequent methylation step. A suspension of sodium hydride (0.1967 g, 8.20 mmol) in anhydrous DMF was prepared. A solution of the intermediate product (1.297 g; 4.10 mmol) in anhydrous DMF (25 mL) was added to the suspension and the mixture was stirred at room temperature for 30 minutes. Iodomethane (0.255 mL; 4.10 mmol)

was subsequently added dropwise and the stirring continued for another hour. An additional aliquot of sodium hydride (0.198 g; 8.20 mmol) and iodomethane (0.255 mL; 4.10 mmol) was made. After one hour of stirring the solvent was removed under vacuum. The residue was diluted with $CH_2Cl_2$ and washed with 2 N HCl (10 mL), brine (10 mL) and water (10 mL). The organic layer was dried with anhydrous $MgSO_4$ and evaporated to dryness. Purification by silica chromatography (50:50 hexane: ethyl acetate) yielded the desired product (0.838 g, 60%): $R_f$ = 0.20 (50:50 hexane: ethyl acetate); $^1$H-NMR: A broadening of the *N*-methyl peaks between 2 and 4 ppm was observed when going from 25 to 50 °C. This conformational broadening is due to the increased *cis/trans* interconversion about the chiral axes (Ar-N bonds) as reported by Azumaya *et al.*,[84] MS (ESI): m/z 345.3 $[M+H]^+$ and m/z 367.3 $[M+Na]^+$

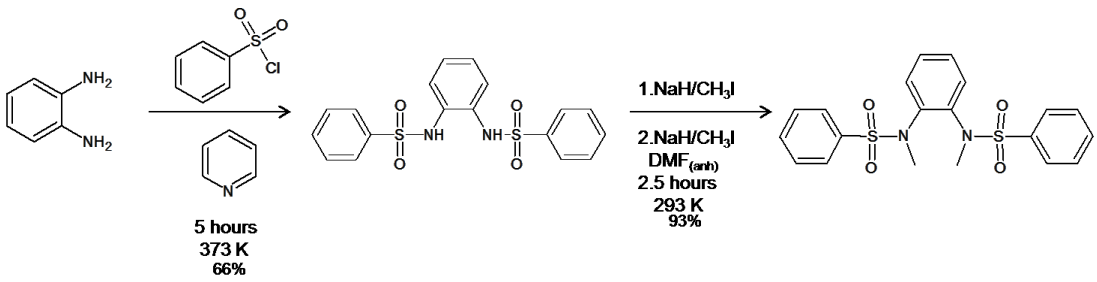


**Figure 39.** Reaction scheme for synthesis of **3**.

### 8.2.3. 1,2-bis-(phenylsulfonamido)benzene

The intermediate product was prepared using a similar protocol to that reported by Shang *et al.* whereas the final product was synthesized through a methylation step using a similar protocol to that reported by Azumaya *et al.* (Figure 39).[84,189] A solution of *ortho*-phenylenediamine (1.08 g, 0.01 mol) in pyridine (40 mL) was slowly added to a 100 mL round bottom flask containing a solution of benzenesulfonyl chloride (2.750 mL, 0.020 mol) in pyridine (0.808 mL, 0.010 mol). The reaction mixture was stirred under reflux at 100 °C for 5 hours. The reaction mixture was allowed to cool to room temperature and 150 mL of distilled water was added to precipitate the intermediate product. The crude product was filtered and washed with cold distilled water (10 mL) and dried under vacuum. Purification by silica chromatography (97.5:2.5 followed by 1:1 (toluene: ethyl acetate)) yielded the desired product (2.57 g, 66%): $R_f$ = 0.55 (1:1 toluene: ethyl acetate); m.p. = 190 °C (lit.,[190] 190.3-190.8 °C); $^1$H NMR (500 MHz, $CDCl_3$-d, $Me_4Si$) δ = 7.75 - 7.62 (2H, m, ph-H), 7.57 (1 H, d, *J* = 7.3 Hz, ph-

H), 7.49 - 7.41 (2H, m, ph-H), 7.06 (1 H, dd, $J$ = 3.4, 5.9 Hz, ph-H), 6.99 - 6.90 (1H, m, ph-H), 1.55 (3 H, s, N-H).

### 8.2.4. 1,2-bis-(*N*-benzenesulfonyl-*N*-methylamino)benzene (3)

1,2-bis-(phenylsulfonamido)benzene (1.4418 g, 0.0037 moles) was dissolved in anhydrous DMF and added to a suspension of NaH (0.1775 g, 0.0074 moles) in anhydrous DMF. The mixture was stirred for 30 minutes prior to the addition of iodomethane (0.231 mL, 0.0037 moles). The mixture was stirred at room temperature for 1 hour before another addition of NaH (0.1775 g, 0.0074 moles) and iodomethane (0.231 mL, 0.0037 moles). After an additional hour, excess solvent was removed under vacuum. Purification by silica chromatography (50:50 hexane: ethyl acetate) yielded the desired product (1.442 g, 93%): $R_f$ = 0.67; m.p. = 225 °C (lit.,[119] 223 °C); $^1$H NMR (500 MHz ,$CDCl_3$-d, $Me_4Si$) δ = 7.89 - 7.83 (4H, m, ph-H), 7.68 - 7.62 (2H, m, ph-H), 7.60 - 7.54 (4H, m, ph-H), 7.29 - 7.24 (8H, m, ph-H + $CDCl_3$ interference), 6.89 (2H, dd, $J$ = 3.4, 5.9 Hz, ph-H), 3.25 (6H, s, N-$CH_3$). Overlap of the chloroform peak with product signal at 7.29-7.24 ppm resulted in an increased integration (8 H), the actual integration for the peak is 2H. An additional peak at *ca.* 1.56 ppm is assigned to water within the sample.

### 8.2.5. Crystallization through Slow Evaporation

Crystals of **1**•$H_2O$ were grown through slow evaporation from water in a 12.5 cm by 6 cm crystallizing dish at room temperature. 1.0 g of **1** was dissolved in 130 mL of water with heating and stirring and subsequently covered with aluminum foil containing small perforations. Crystallization of **1**•$H_2O$ typically occurred within one week, resulting in crystals that were typically 2 x 0.5 x 0.25 cm in size.

Compound **2** was recrystallized with water-saturated ethyl acetate to obtain achiral crystals (*i.e.* **2**•*x*$H_2O$) and anhydrous ethyl acetate to obtain chiral crystals. The recrystallization was carried out in a 250 mL beaker covered with aluminum foil and placed on a bench top at room temperature. Depending on the desired speed of evaporation, the number of perforations on the aluminum foil covering the beaker varied. Crystal growth would normally occur within 1-2 weeks. A non-stochastic crystallization was observed, where there was a large preference for crystals with (-) CD signal ([CD(−)260 nm]). Achiral crystals of **2**•*x*$H_2O$ were typically 0.5 x 0.5 x 0.25 cm in size whereas the chiral crystals (**2**) were slightly larger. The crystals were viewed

under a microscope to isolate single crystals for subsequent measurements. **2**•$x$H$_2$O appeared to readily lose water as indicated by the emergence of white spots on the initially clear crystals. The dehydration of **2**•$x$H$_2$O was investigated by DSC and TGA measurements.

Compound **3** was recrystallized at room temperature from ethyl acetate in a 250 mL beaker. In the case of **3,** crystallization occurred rapidly and the evaporation of solvent was slowed down with aluminium foil. Typical crystals were 0.2 x 0.2 x 0.2 cm in size.

### 8.2.6. Differential Scanning Calorimetry

DSC thermograms were recorded using TA instruments, DSC Q2000 differential scanning calorimeter. Finely ground samples of **1**•H$_2$O (18.67 mg) and **2**•$x$H$_2$O (14.59 mg) were placed in an aluminum pan and subsequently crimped with an aluminum lid before sampling. An empty pan was used as a reference during the measurements. Different parameters were used for the heating cycle for each sample. The heating rate was 5 °C/min and 10 °C/min for **1**•H$_2$O and **2**•$x$H$_2$O, respectively. The heating ramp was carried out from 20 - 150 °C and 100 - 180 °C for **1**•H$_2$O and **2**•$x$H$_2$O, respectively (Figure 40).

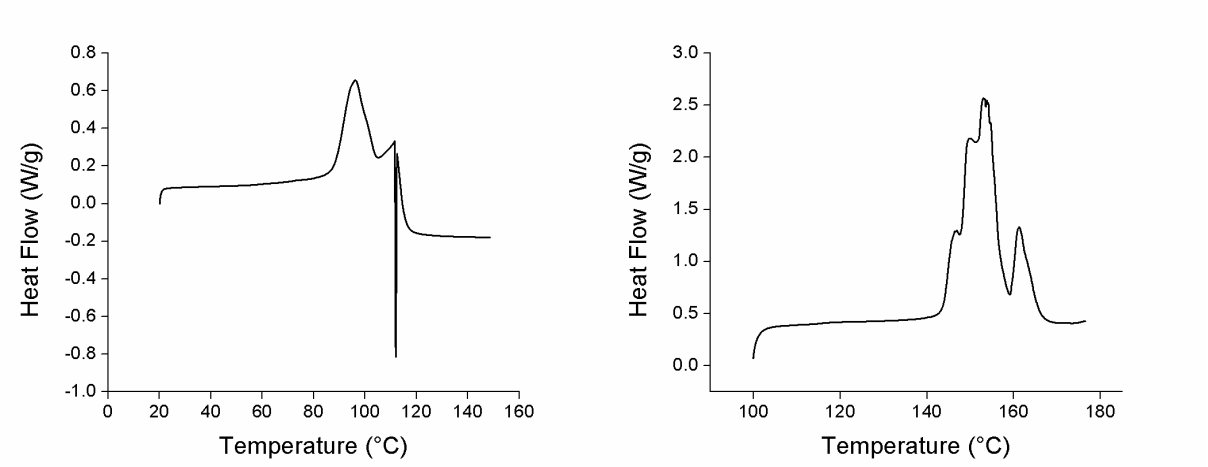


**Figure 40.** DSC thermogram of **1**•H$_2$O (A) and **2**•$x$H$_2$O (B).

### 8.2.7. Thermogravimetric Analysis

Thermal gravimetric analysis (TGA) analysis was performed on TGA 500 instrument. In a typical experiment, the crystal was carefully transferred to the furnace of the instrument where it was carefully weighed at 11.8820 mg. The sample was then heated under nitrogen through a

range of 25 ˚C – 200 ˚C, at a rate of 5 ˚C/min in order to determine the weight loss as a function of temperature (Figure 41).

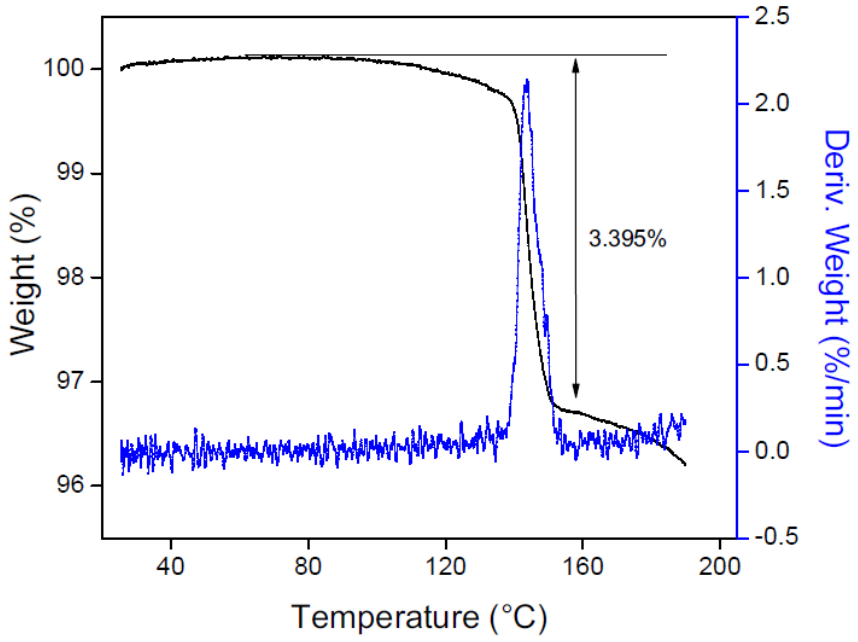


**Figure 41.** TGA thermogram of **2**•$x$H$_2$O. The total amount of water lost during the heating process was determined from the percentage of mass lost ((11.8820 mg of sample*0.03395 = 0.403394 mg; 22.3918 μmoles). This mass of water lost from **2**•$x$H$_2$O (0.403394 mg) was subtracted from total mass (11.8820 mg) to determine the mass of 2 (11.4786 mg; 33.3286 μmoles). The amount of water, x, in the hydrated crystal was calculated from the molar ratio of the water to 2 (22.3918 μmoles/33.3286 μm) to be 0.67**.**

### 8.2.8. Dehydration of Achiral Crystals

Dehydration of achiral crystals was carried out in a similar fashion for both **1**•H$_2$O and **2**•$x$H$_2$O. Achiral crystals were crushed with a mortar and pestle and placed in a 15 x 45 mm vial. The open vials were placed in a digitally controlled Chemglass aluminium heating block/stirrer (**2**•$x$H$_2$O was heated at 140 °C and **1**•H$_2$O was heated at 90 °C).[191] The hotplate was set at the desired temperature for 30 minutes to equilibrate and the sample was subsequently placed in the center wells of the heating block. The time required for the transformation from achiral crystals to chiral crystals was *ca.* 3 hours for **1**•H$_2$O and *ca.* 30 minutes for **2**•$x$H$_2$O. The transition between space groups was verified using X-ray powder diffraction. The presence of an

amorphous phase in the sample of **2** was responsible for the halo effect observed in the XRPD pattern, but this did not influence the subsequent Viedma amplification process (Figure 30c).

Face-selective dehydration was attempted by directly placing crystals (*ca.* 0.5 x 0.5 x 0.25 cm) of **2**•*x*$H_2O$ on the center of the hotplate at 140 °C. The most prominent face was placed against the hotplate until a structural change was observed *via* XRPD pattern or until the crystal melted. If the crystal is too small, there would be less face-selectivity but if the crystal is too big, the dehydration would take more time and chirality was not observed. This can be attributed to the development of an amorphous phase or lack of selectivity during dehydration.

### 8.2.9. X-ray Powder Diffraction

Achiral and chiral crystals were differentiated using XRPD, which also confirmed the transition between space groups upon dehydration. Samples were prepared and placed on a shallow well null sample holder. The sample was pressed flat with a glass plate to ensure an even layer and distribution of sample. The sample was run at room temperature using a 0.03° step and a count time of 0.5 s per step. A continuous scan mode was utilized. Patterns collected for samples without a literature reference are typically run from 0° to 90° in 2θ. **1**, **1**•$H_2O$, **2** and **2**•*x*$H_2O$ were run from 5° to 50° in 2θ. The sample time varied depending on the 2θ used for each sample.

### 8.2.10. Viedma Ripening

Samples were subjected to Viedma ripening using a modified Pine Industrial Company analytical rotator. Viedma ripening was carried out in a 5 mL sterile vial with a 20 mm Teflon-faced septum to prevent solvent evaporation. The vial contained 0.25 g of a racemic mixture of **1** or **2**, grinding media (3.0 g of 0.8 mm of YTZ® Zirconia ceramic beads), a 10 mm by 5 mm stir bar and 3 mL saturated solution and was sealed with a vial crimper. The stirring speed for Viedma ripening experiments was either 1500 rpm or 2400 rpm. The time required to reach homochirality for **1**, **2** and **3** was *ca.* 65 hours (2400 rpm), *ca.* 6 hours (1500 rpm), and *ca.* 24 hours (2400 rpm), respectively. Slurry samples (*ca.* 100 μL) were taken from the vial to estimate the time required to reach homochirality for **2** and **3**. Viedma ripening of **1** has previously been reported by our group.[3]

### 8.2.11. Circular Dichroism

Circular dichroism was used to generate calibration curves and to quantify the crystal chirality achieved through Viedma ripening of **1**, **2** and **3**. A Jasco J-710 spectropolarimeter was used to record the circular dichroism spectra. The KBr pellet method was used to prepare solid state samples. Using a mortar and pestle, 100 mg samples were prepared with varying ratios of oven dried KBr. Sample concentrations were 1.2, 1.0 and 1.0% (*wt/wt*) for **1**, **2** and **3**, respectively. The sample was then divided into two portions, and each was vacuum pressed for 30 seconds at *ca.* 10 tons while placed in an evacuable 13 mm pellet press from Pike Technologies. Each pellet was placed into the instrument using a homemade cardstock pellet holder. Typically, three runs were acquired per pellet. The position of the KBr pellet in the pellet holder was varied to ensure homogeneity of the sample. The pellet was rotated so that the circularly polarized light made contact with another position within the pellet. The pellet holder was placed at a specified location as close to the detector as possible. The resolution, accumulations and scan rate were set to 5 points/nm, 4 accumulations and 50 nm/min, respectively. Spectra were recorded from 270 nm to 380 nm for **1**, 240 nm to 340 nm for **2** and 250 nm to 320 nm for **3**. Variability in CD spectra is attributed mainly to pellet preparation. Preparing completely homogenous samples in each preparation was difficult and therefore replicate CD spectra are often variable.

### 8.2.12. Enantiomeric Excess Calibration Curves

CD calibration curves were generated to determine the enantiomeric excess in single crystal as well as Viedma ripening samples. Samples varying in enantiomeric excess were prepared by mixing appropriate ratios of left-handed and right-handed crystalline powder while maintaining a constant total weight. A calibration curve was generated by plotting the CD signal at a specified wavelength versus the enantiomeric excess of the standards. For each standard, multiple pellets were prepared and measured to determine the average CD signal and standard deviation. The calibration curves were subsequently used to determine the enantiomeric excess of the samples from Viedma ripening experiments. Chiral crystallites used as standards for the construction of calibration curves were obtained either by crushing single crystals obtained from slow evaporation (**2** and **3**) or from the crystalline powders generated by Viedma ripening (**1**). The

enantiomeric excess was calculated according to eq.1 where $m_{(+)}$ and $m_{(-)}$ are the weights of CD-positive and CD-negative crystals.

$$\%ee = \frac{m_{(+)} - m_{(-)}}{m_{(+)} + m_{(-)}} \times 100\%$$

Equation 2. Determination of enantiomeric excess

The CD values for the calibration curve were taken from 290 nm, 260 nm and 275 nm for **1**, **2** and **3**, respectively. The average CD signals and standard deviations were calculated based on 3 replicate measurements.

### 8.2.13. Polarized Light Microscopy

Polarized light microscopy of **3** was carried out on a Nikon SMZ1500 stereomicroscope. The polarizer was rotated clockwise to visualize the optical rotatory dispersion along the optic axis.

### 8.2.14. Characterization of 1,2-bis(*N*-benzenesulfonyl-*N*-methylamino)benze-ne

Crystals of **3** obtained *via* slow evaporation from ethyl acetate resulted in crystals with prominent (001) and (00-1)$(00\bar{1})$ faces. Chirality was determined through optical rotatory dispersion (ORD) using polarized light microscopy (Figure 42). This property is seen in various crystals found the tetragonal and hexagonal crystal systems.

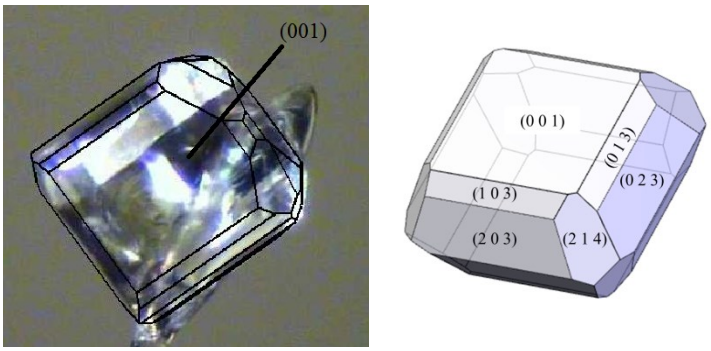


**Figure 42.** Indexed chiral crystal of **3** indicating face used for optical rotatory dispersion determined by single crystal X-ray diffraction (left) and indexed face simulated using WinXMorph™ software (right).[149]

Analysis of **3** crystals displayed an optical rotatory dispersion of blue-amber-clear which is indicative of a crystal with (+) CD signal ([CD(+)275 nm]) whereas an optical rotatory dispersion of amber-blue-clear is indicative of a crystal with (-) CD signal ([CD(−)275 nm]) (Figure 43). Crystals were harvested according to their respective color transitions and subsequently subjected to CD measurements to correlate CD transitions with ORD. Compound **3** crystallizes in enantiomorphic space groups, the resulting CD signal can be correlated to the space group in which the crystal is found. Single crystal X-ray diffraction was carried out to assign the absolute configuration to the CD signal. Crystals with (+) CD signal are representative of crystals that reside in space group $P4_12_12$ whereas crystals with (-) CD signal are representative of crystals that reside in space group $P4_32_12$, which agreed with previously reported results.[119]

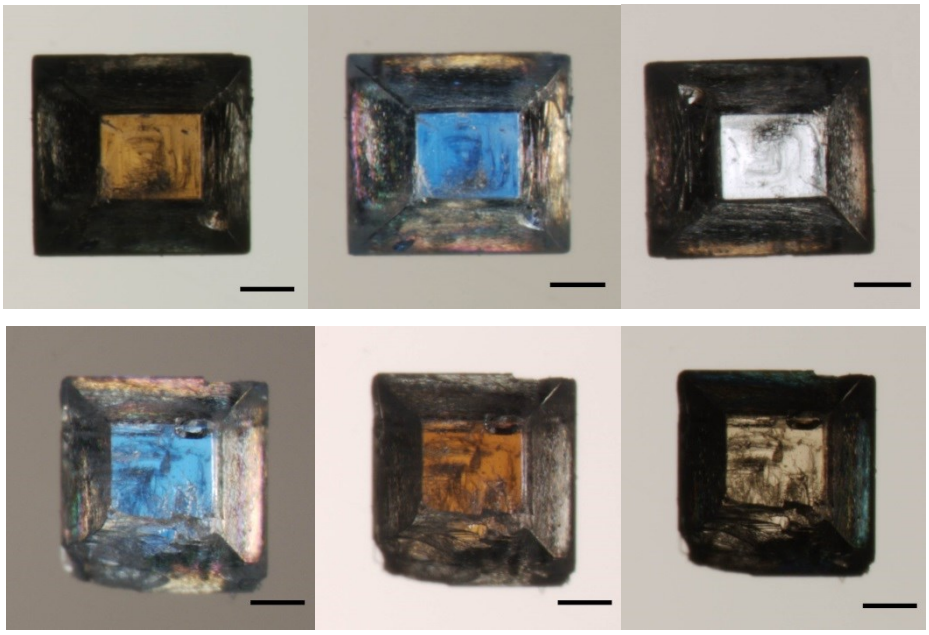

**Figure 43.** Transition observed upon analysis of chiral crystals of 1,2-bis-(*N*-benzenesulfonyl-*N*-methylamino)benzene using polarized light microscopy (rotating the analyzer clockwise). 1,2-bis-(*N*-benzenesulfonyl-*N*-methylamino)benzene crystals observed: (-) crystals (*top row)*, (+) crystals (*bottom-row*). Scale bar = 0.02 cm.

After manual separation of enantiomorphous crystals of **3,** attrition-enhanced deracemization was carried out. In an attempt to attain an initial enantiomeric excess of 0, equal amounts of chiral crystallites were mixed and finely ground to prepare the starting material for Viedma ripening. Compound **3** has been shown to reach homochirality within 24 hours. CD

measurements using chiral crystallites were used to generate a calibration curve to quantify enantiomeric excess of samples at various intervals during Viedma ripening experiments. Of 3 experiments, 1 experiment produced homochiral crystals with (-) CD signal ([CD(−)275 nm]) and 2 experiments produced homochiral crystals with (+) CD signal ([CD(−)275 nm]) (Figure 44).

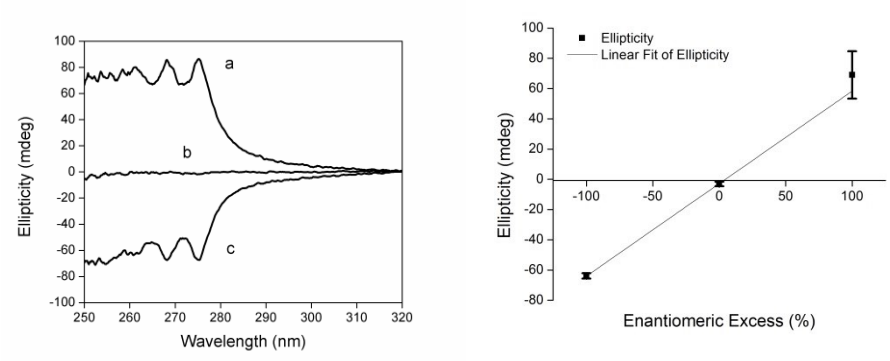


**Figure 44.** Left: Solid-state CD spectra of the chiral crystals of **3** in KBr: (b) After dehydration, (a) and (c) following Viedma ripening. Viedma ripening was carried out using 0.25 g of sample suspended in 3 mL of saturated solution in anhydrous ethyl acetate with 3 g of ceramic grinding media (0.8 mm) stirring at 2400 rpm for *ca.* 24 hours. Right: CD calibration of 3 in KBr prepared from mixtures of homochiral crystals ([CD(±)275 nm]).

### 8.2.15. Crystallographic Data

## 8.2.15.1. Analysis of Cambridge Structural Database (CSD)

The percentage of achiral molecules that crystallize as chiral crystals was determined through the use of Mercury 3.6, ConQuest 1.17, ChiralFinder and CSD 5.36 database (Updated 3 May 2015).[161,192–194] The entire database of crystal structures was probed for crystals that reside in Sohncke space groups using ConQuest. Upon opening ConQuest the following steps were taken to carry out the determination of crystal structures that crystallize in Sohncke space groups.

1) In the Build Queries tab, select Space Group
2) Adjust space group symmetry to "allows enantiopure substances (Sohncke)"
3) Click search, a new window appears with further search options
4) Leave filters as is and begin search
5) Total number of structures is eventually generated (127 397 structures), the entries were subsequently exported
6) To export entries go to File, Export entries as

7) A new window appears in which the following options were selected
    a. File type – CSD coordinate file
    b. All selected entries checkbox was selected
    c. Fractional and all coordinates checkbox was selected
8) Finally the entries were saved via file pop-up and a .cor file was generated

The next step was to run the results through ChiralFinder. ChiralFinder is a program which separates the entries into different categories: achiral structures, chiral structures, racemic structures, meso structures and error structures.[194]

1) Upon program start-up, a dialog box opens in which an input file name and output files directory is required.
2) The input file name must include the files location i.e C:\Desktop\File A\A.cor
3) The output file directory must end in a similar fashion *i.e.* C:\Desktop\File A\

The coordinate file generated through ConQuest was run through ChiralFinder and the total number of achiral molecules that crystallize as chiral crystals was generated. The value was subsequently divided by the total number of entries in the CSD 5.36 database (776 408). The value obtained was 5%.ChiralFinder also reports error structures which were not included in the calculations; these error structures were also included in the calculation to determine the error. To generate the possible error, two assumptions were made. The error structures can be all achiral structures or they can all be other structures, using that parameter an error of ± 2% was determined. Error structures are a result of files with atoms with too many bonds (atoms with more than 4 bonds or hydrogens with 2 bonds) or atoms with metal elements which cannot be run by ChiralFinder. Incomplete molecular structures due to missing hydrogen atoms also result in error structures.[194] ChiralFinder was not able to process the following entries: DOGMAP, BEQXEB, NUDVIS, BOBDEC, JEJWEB, JUBXIP, XUKNOH, YAWHAG. RANCEQ, PUXGOE and JUBXAH. To generate the total number of Sohncke structures that crystallized in the $P2_1$ or $P2_12_12_1$ space group. The initial search in ConQuest was adjusted to restrict the desired space group to either $P2_1$ or $P2_12_12_1$ while only allowing for enantiopure substance (Sohncke). Furthermore, the generated coordinate files can be processed through ChiralFinder to determine the amount of structures in the $P2_1$ and $P2_12_12_1$ space groups that crystallize from achiral molecules.

### 8.2.15.2. WinXMorph™

Crystal structure of **3** was generated using WinXMorph™ software.[149] Recreation of experimental crystal structure required the point symmetry as well as the corresponding faces. The refinement of the structure was carried out through manipulation of the face sizes as well as minor details (crystal fill color, edge color, *etc.*).

### 8.2.15.3. Simulated Single Crystal X-ray Diffraction

Single crystal data for **1**•$H_2O$ (CYTOSM), **1** (CYTSIN) and **3** (tka17112 & tka171101), which was used to simulate XRPD patterns, were obtained from the Cambridge Structural Database. Supplementary crystallographic data can be accessed free of charge from Cambridge Crystallographic Data Centre *via* www.ccdc.cam.ac.uk/data_request/cif.

### 8.2.15.4. Experimental Single Crystal X-ray Diffraction

**Achiral 1,2-bis(*N*-benzoyl-*N*-methylamino)benzene hydrate (2•0.59 $H_2O$):** A clear colourless rhomb-like specimen of $C_{22}H_{21.18}N_2O_{2.59}$, approximate dimensions 0.62 mm x 0.58 mm x 0.25 mm, was used for the X-ray crystallographic analysis. The X-ray intensity data were measured on a Bruker DUO system equipped with a Molybdenum Kα source (λ = 0.71073 Å), a graphite monochromator and an APEX II CCD detector. A total of 1464 frames were collected. The frames were integrated with the Bruker SAINT software package using a narrow-frame algorithm. The integration of the data using a monoclinic unit cell yielded a total of 21466 reflections to a maximum θ angle of 27.64° (0.77 Å resolution), of which 4267 were independent (average redundancy 5.031, completeness = 99.6%, $R_{int}$ = 3.36%, $R_{sig}$ = 2.30%) and 3714 (87.04%) were greater than $2\sigma(F^2)$. The final cell constants of a = 9.1639(9) Å, b = 21.320(2) Å, c = 10.0007(10) Å, β = 109.6520(10)°, volume = 1840.1(3) $Å^3$, are based upon the refinement of the XYZ-centroids of 9480 reflections above 20 σ(I) with 4.728° < 2θ < 55.28°. Data were corrected for absorption effects using the multi-scan method (SADABS). The ratio of minimum to maximum apparent transmission was 0.937. The calculated minimum and maximum transmission coefficients (based on crystal size) are 0.6985 and 0.7456. The structure was solved and refined using the Bruker SHELXTL software package, using the space group P 1 21/n 1, with Z = 4 for the formula unit, $C_{22}H_{21.18}N_2O_{2.59}$. The final anisotropic full-matrix least-squares refinement on $F^2$ with 247 variables converged at $R_1$ = 4.44%, for the observed data and $wR_2$ =

10.72% for all data. The goodness-of-fit was 1.083. The largest peak in the final difference electron density synthesis was 0.305 $e^-/Å^3$ and the largest hole was -0.222 $e^-/Å^3$ with an RMS deviation of 0.040 $e^-/Å^3$. On the basis of the final model, the calculated density was 1.281 $g/cm^3$ and F(000), 752 $e^-$.

Another crystal, which was freshly picked out of wet solution, refined to 0.78 water occupancy (**2**•0.78 $H_2O$, data not shown).

**Chiral 1,2-bis(*N*-benzoyl-*N*-methylamino)benzene (2):** A clear colourless rhomb-like specimen of $C_{22}H_{20}N_2O_2$, approximate dimensions 0.26 mm x 0.34 mm x 0.62 mm, was used for the X-ray crystallographic analysis. The X-ray intensity data were measured on a Bruker DUO system equipped with a Copper Kα microfocus source (λ = 1.54184 Å) and an APEX II CCD detector. A total of 3431 frames were collected. The frames were integrated with the Bruker SAINT software package using a narrow-frame algorithm. The integration of the data using an orthorhombic unit cell yielded a total of 13866 reflections to a maximum θ angle of 68.25° (0.83 Å resolution), of which 3414 were independent (average redundancy 4.062, completeness = 99.9%, $R_{int}$ = 4.55%, $R_{sig}$ = 3.68%) and 3312 (97.01%) were greater than $2\sigma(F^2)$. The final cell constants of a = 8.2418(7) Å, b = 14.0963(12) Å, c = 16.1962(13) Å, volume = 1881.7(2) $Å^3$, are based upon the refinement of the XYZ-centroids of 736 reflections above 20 σ(I) with 5.554° < 2θ < 137.6°. Data were corrected for absorption effects using the multi-scan method (SADABS). The ratio of minimum to maximum apparent transmission was 0.901. The calculated minimum and maximum transmission coefficients (based on crystal size) are 0.6789 and 0.7531. The structure was solved and refined using the Bruker SHELXTL software package, using the space group P 21 21 21, with Z = 4 for the formula unit, $C_{22}H_{20}N_2O_2$. The final anisotropic full-matrix least-squares refinement on $F^2$ with 238 variables converged at $R_1$ = 2.91%, for the observed data and $wR_2$ = 7.18% for all data. The goodness-of-fit was 1.060. The largest peak in the final difference electron density synthesis was 0.158 $e^-/Å^3$ and the largest hole was -0.127 $e^-/Å^3$ with an RMS deviation of 0.035 $e^-/Å^3$. On the basis of the final model, the calculated density was 1.216 $g/cm^3$ and F(000), 728 $e^-$.

**Chiral 1,2-bis-(*N*-benzenesulfonyl-*N*-methylamino)benzene (3):** A colorless block-like specimen of $C_{10}H_{10}NO_2S$, approximate dimensions 0.38 mm x 0.53 mm x 0.54 mm, was used for

the X-ray crystallographic analysis. The X-ray intensity data were measured on a Bruker DUO system equipped with a Molybdenum Kα source (λ = 0.71073 Å), a graphite monochromator and an APEX II CCD detector. A total of 1464 frames were collected. The frames were integrated with the Bruker SAINT software package using a narrow-frame algorithm. The integration of the data using a tetragonal unit cell yielded a total of 22948 reflections to a maximum θ angle of 27.71° (0.76 Å resolution), of which 2250 were independent (average redundancy 10.199, completeness = 100.0%, $R_{int}$ = 4.05%, $R_{sig}$ = 2.01%) and 2155 (95.78%) were greater than $2\sigma(F^2)$. The final cell constants of a = 8.3899(7) Å, b = 8.3899(7) Å, c = 27.226(2) Å, volume = 1916.4(4) $Å^3$, are based upon the refinement of the XYZ-centroids of 598 reflections above 20 σ(I) with 7.486° < 2θ < 58.27°. Data were corrected for absorption effects using the multi-scan method (SADABS). The ratio of minimum to maximum apparent transmission was 0.964. The calculated minimum and maximum transmission coefficients (based on crystal size) are 0.7184 and 0.7456. The structure was solved and refined using the Bruker SHELXTL Software Package, using the space group P 43 21 2, with Z = 8 for the formula unit, $C_{10}H_{10}NO_2S$. The final anisotropic full-matrix least-squares refinement on $F^2$ with 128 variables converged at $R_1$ = 2.71%, for the observed data and $wR_2$ = 7.29% for all data. The goodness-of-fit was 1.101. The largest peak in the final difference electron density synthesis was 0.195 $e^-/Å^3$ and the largest hole was -0.412 $e^-/Å^3$ with an RMS deviation of 0.067 $e^-/Å^3$. On the basis of the final model, the calculated density was 1.444 $g/cm^3$ and F(000), 872 $e^-$.

| | Achiral **(2**•0.59 $H_2O$**)** | Chiral **(2)** | Chiral **(3)** |
|---|---|---|---|
| CCDC deposition number | 1443506 | 1443507 | 1443508 |
| Empirical formula | $C_{22}H_{22}N_2O_3$ | $C_{22}H_{20}N_2O_2$ | $C_{10}H_{10}NO_2S$ |
| Formula weight | 354.99 | 344.40 | 208.25 |
| *T* (K) | 110(2) | 150(2) | 150(2) |
| Wavelength (Å) | 0.71073 | 1.54184 | 0.71073 |
| Crystal system | Monoclinic | Orthorhombic | Tetragonal |
| Space group | $P2_1/n$ | $P2_12_12_1$ | $P4_32_12$ |

| | | | |
|---|---|---|---|
| *Unit cell dimensions* | | | |
| a (Å) | 9.1639(9) | 8.2418(7) | 8.3899(7) |
| b (Å) | 21.320(2) | 14.0963(12) | 8.3899(7) |
| c (Å) | 10.0007(10) | 16.1962(13) | 27.226(2) |
| α (°) | 90 | 90 | 90 |
| β (°) | 109.6520(10) | 90 | 90 |
| γ (°) | 90 | 90 | 90 |
| $V$ (Å$^3$) | 1840.1(3) | 1881.7(2) | 1916.4(4) |
| $Z$ | 4 | 4 | 8 |
| $D_{calc}$ | 1.281 | 1.216 | 1.444 |
| Absorption coefficient (mm$^{-1}$) | 0.085 | 0.626 | 0.308 |
| F(000) | 752 | 728 | 872 |
| Crystal size (mm) | 0.62 x 0.58 x 0.25 | 0.26 x 0.34 x 0.62 | 0.38 x 0.53 x 0.54 |
| $\theta$ (°) | 1.91 – 27.64 | 4.16 – 68.25 | 2.54 – 27.71 |
| Index ranges | $h$ = -11→11 | $h$ = -9→9 | $h$ = -10→10 |
| | $k$ = -27→27 | $k$ = -16→16 | $k$ = -10→10 |
| | $l$ = -12→13 | $l$ = -19→19 | $l$ = -35→35 |
| Reflections collected | 21466 | 13866 | 22948 |
| Independent reflections | 4267 | 3414 | 2250 |
| Completeness ($\theta$) | 99.6% | 99.9% | 100% |
| Data/restraints/parameters | 4267/0/247 | 3414 / 0 / 238 | 2250 / 0 / 128 |
| Goodness of fit (GOF) on $F^2$ | 1.083 | 1.060 | 1.101 |
| Final R indices [$I > 2\sigma(I)$] (%) | $R_1$ = 4.44 | $R_1$ = 2.91 | $R_1$ = 2.71 |
| | $wR_2$ = 10.25 | $wR_2$ = 7.10 | $wR_2$ = 7.19 |
| R indices (all data) (%) | $R_1$ = 5.22 | $R_1$ = 3.00 | $R_1$ = 2.86 |
| | $wR_2$ = 10.72 | $wR_2$ = 7.18 | $wR_2$ = 7.29 |

| | | | |
|---|---|---|---|
| Flack parameter | n/a | -0.03(10) | -0.05(3) |
| Largest difference in peak and hole (e $Å^{-3}$) | 0.305 and -0.222 | 0.158 and -0.127 | 0.195 and -0.412 |

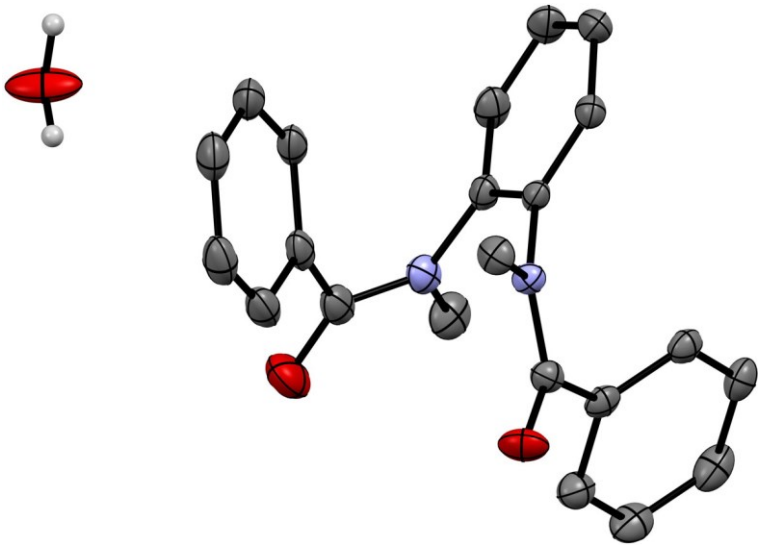

**Figure 45.** ORTEP representation of achiral **2**•0.59 $H_2O$ at 50% ellipsoid probability. H atoms except on water were omitted for clarity.

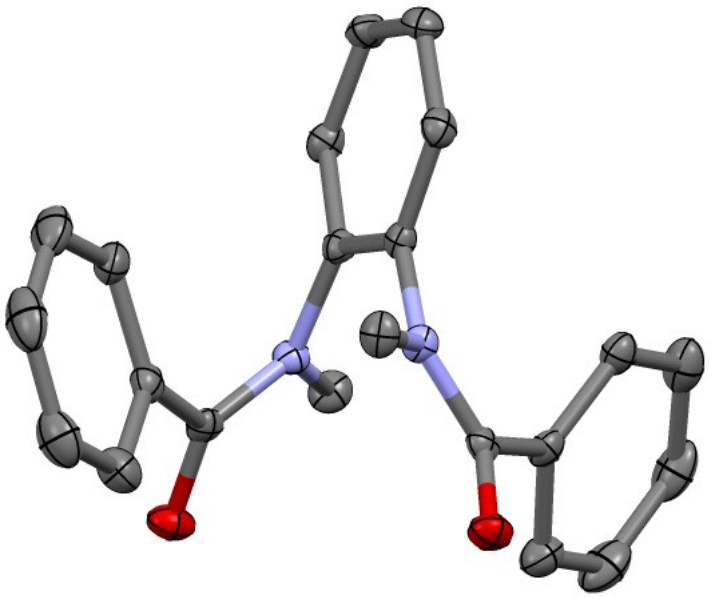

**Figure 46.** ORTEP representation of chiral **2** at 50% ellipsoid probability. H atoms were omitted for clarity.

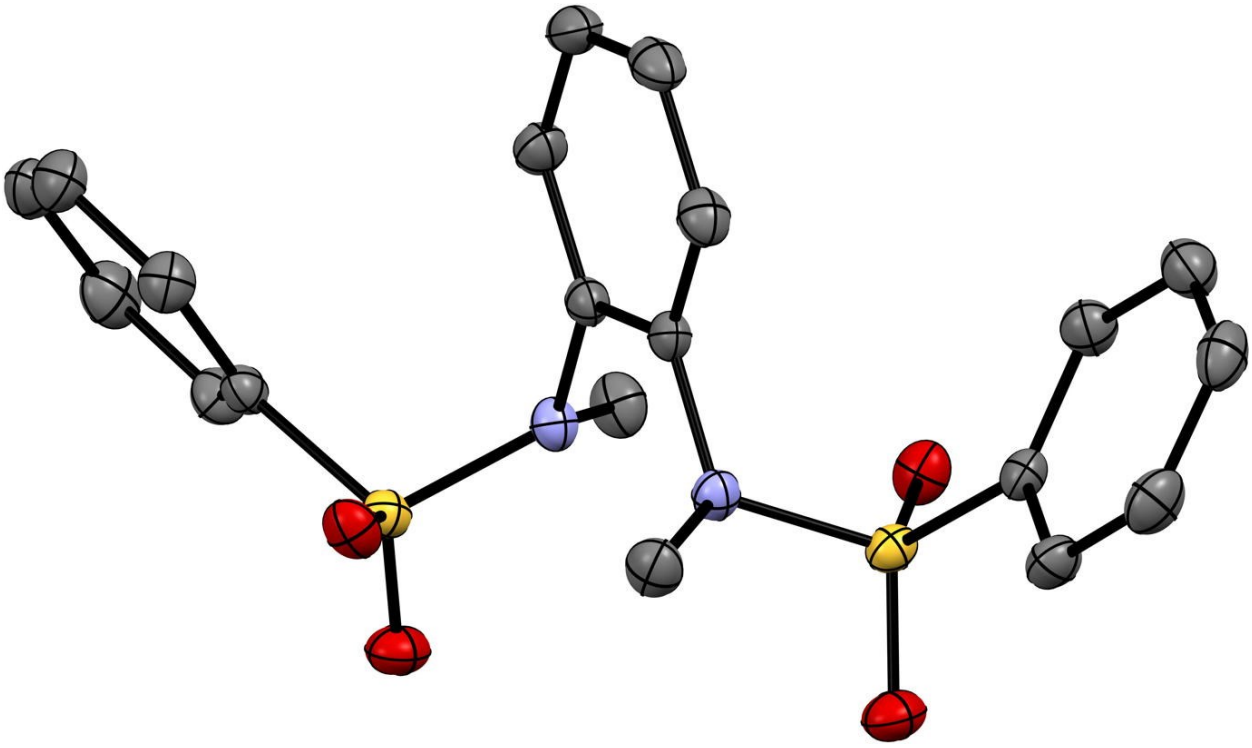

**Figure 47.** ORTEP representation of chiral **3** at 50% ellipsoid probability. H atoms were omitted for clarity.

## *8.3. 5-nitrouracil*

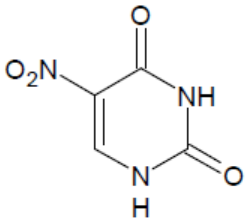


5-Nitrouracil

Slow crystallization of 5-nitrouracil from an aqueuous saturated solution resulted in the formation of multiple polymorphs. Polymorphs were formed with space group $P2_1/c$

(NURAMH), $P2_1/n$ (NIMFOE) and Pbca (NIMFOE01). Due to the presence of multiple polymorphs, the achiral hydrated 5-nitrouracil (NURAMH) was not obtained. Furthermore, dehydration of 5-nitrouracil monohydrate transforms the crystals to achiral crystals (NIMFOE or NIMFOE01) rather than the desired chiral form (NIMFOE02).[195]

Slow crystallization of 5-nitrouracil from a saturated acetonitrile solution resulted in the formation of the desired chiral crystals of 5-nitrouracil with space group $P2_12_12_1$ (Figure 48).[196] Crystals of 5-nitrouracil were too small to carry out single crystal CD analysis. CD measurements revealed that the crystallization process was stochastic. 5-nitrouracil (*ca.* 0.25 g) was taken from a crystallization dish, and CD measurements were taken of the grinded mixture. CD measurements showed baseline signal. Viedma ripening was carried out on this racemic conglomerate of 5-nitrouracil. All 4 experiments resulted in the formation of homochiral crystals with positive CD signal ([CD (+) 280 nm]) (Figure 49).

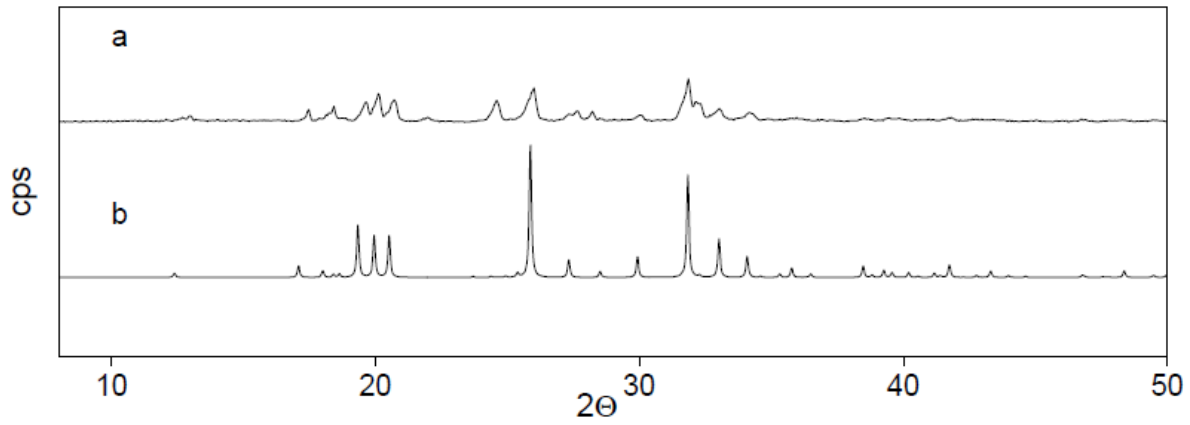


**Figure 48.** XRPD of chiral 5-nitrouracil. (a) Experimental XPRD of chiral 5-nitrouracil (b) XRPD of 5-nitrouracil generated from the CSD (NIMFOE02).

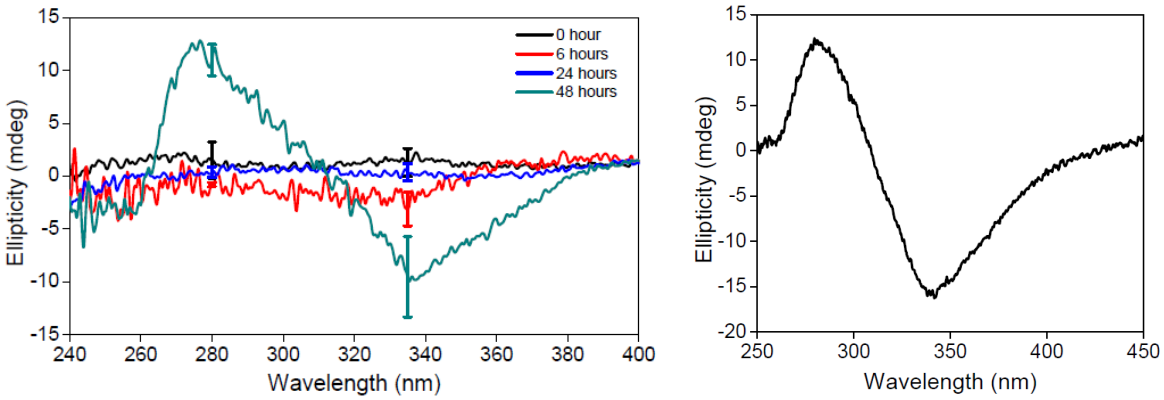


**Figure 49.** Left: Viedma ripening of 5-nitrouracil starting from 0.25 g of suspended in 1 mL of saturated solution in acetonitrile with 3 g of ceramic grinding media (0.8 mm) and stirring at 1200 rpm for *ca.* 48 hours. Right: Solid-state CD spectrum of a completed Viedma ripening experiment of 5-nitrouracil in KBr.

## 8.3.1. Experimental

### 8.3.1.1. Crystallization through Slow Evaporation

Crystals of 5-nitrouracil were grown through slow evaporation from a saturated solution in acetonitrile in crystallizing dishes (15 cm by 8 cm). 5-nitrouracil (*ca.* 0.50 g) was dissolved in acetonitrile (250 mL) with heating and stirring. Slow evaporation resulted in the formation of small crystals within 1-2 days.

### 8.3.1.2. Viedma Ripening

Viedma ripening of 5-nitrouracil was carried out with a modified analytical rotator. 5-nitrouracil (*ca.* 0.25 g), a magnetic stir bar (10 mm x 5 mm) and grinding media (3 g of 0.8 mm of YTZ® Zirconia ceramic beads) were suspended in a saturated solution of acetonitrile (1 mL) in a 10 mL microwave vial. The sample was stirred at 1200 rpm until the crystals attained homochirality (*ca.* 48 hours). Slurry samples (100 μL) were periodically removed to monitor the kinetics of the Viedma ripening process. Solid-state CD analysis was carried out by preparing 1.0% (*wt/wt*) samples in oven dried KBr. The KBr pellet was measured in a similar fashion to those of cytosine and 1,2-bis-(*N*-benzenesulfonyl-*N*-methylamino)benzene. The spectra were recorded

from 250 nm to 450 nm. Three pellets were measured for each time interval and three accumulations were taken for each pellet for each sampling of the Viedma ripening process.

## 8.4. Phloroglucinol

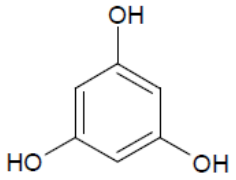


Phloroglucinol

Phloroglucinol is a compound that can form achiral hydrated crystals and chiral anhydrous crystals (Figure 50). The experimental procedure applied to both cytosine and 1,2-bis(*N*-benzoyl-*N*-methylamino)benzene can be applied to phloroglucinol. Slow crystallization of phloroglucinol dihydrate from a saturated aqueous solution results in the generation of achiral crystals of phloroglucinol dihydrate with space group Pnma.[196]

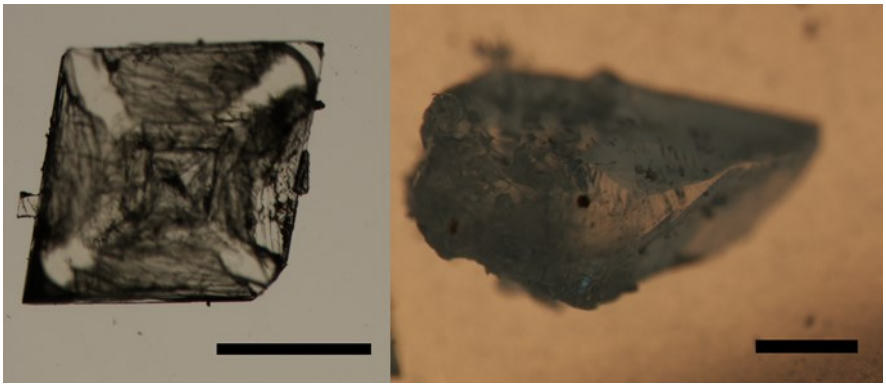

**Figure 50.** Left: Achiral hydrated crystal of phloroglucinol dihydrate. Right: Chiral anhydrous crystal of phloroglucinol. Scale bar: 0.5 mm.

Achiral crystals of phloroglucinol dihydrate were transformed to chiral anhydrous crystals through thermal dehydration inside an oven (*i.e.* 5h at 100 °C). [197] The phase transition from achiral hydrated crystal to chiral anhydrous crystals was confirmed using X-ray powder diffraction. Simulated patterns from single-crystal X-ray diffraction data obtained from the CSD were used to validate experimental XRPD data (Figure 51). Dehydration resulted in the

formation of a physical racemate of chiral crystals which was confirmed with a baseline signal in the solid-state circular dichroism (CD) spectrum. Chiral crystals of phloroglucinol with space group $P2_12_12_1$ can also be formed through sublimation under vacuum. [198] Sufficiently large single crystals of phloroglucinol were not obtained from the sublimation process.

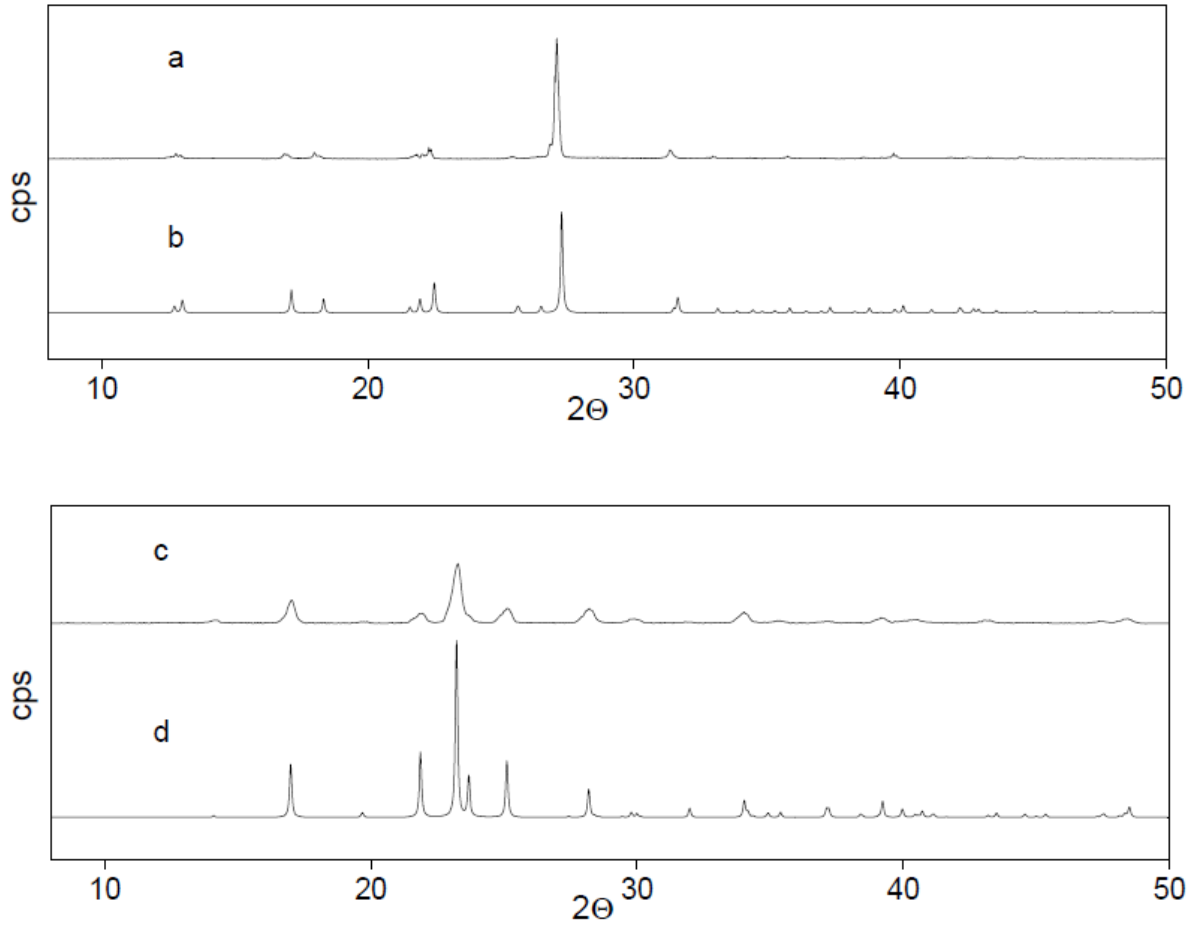


**Figure 51.** Transformation of phloroglucinol dihydrate (Pnma) to phloroglucinol ($P2_12_12_1$). (a) Experimental XRPD of phloroglucinol dihydrate, (b) XRPD of phloroglucinol dihydrate generated from the CSD (PHGLOH), (c) Experimental XRPD of phloroglucinol and (d) XRPD of phloroglucinol generated from the CSD (PHGLOL).

Two Viedma ripening experiments were carried out: one experiment resulted in homochiral crystals with negative CD signal whereas the second experiment resulted in homochiral crystals with positive CD signal (Figure 52).

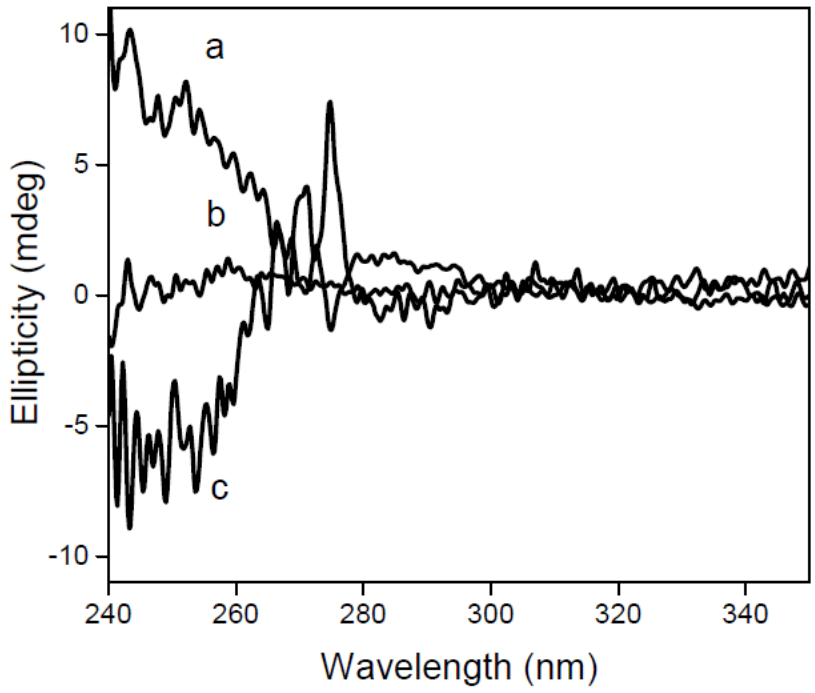


**Figure 52.** Solid-state CD spectra of chiral crystals of phloroglucinol in KBr: (b) after dehydration, (a) and (c) following Viedma ripening. Viedma ripening was carried out using 0.25 g sample suspended in 3 mL of saturated solution in acetonitrile with 3 g of ceramic grinding media (0.8 mm) stirring at 1200 rpm for *ca.* 4 days.

### 8.4.1. Experimental

#### 8.4.1.1. Crystallization through Slow Evaporation

Single crystals of phloroglucinol dihydrate were grown through slow evaporation from water in crystallizing dishes (15 cm by 8 cm). Phloroglucinol dihydrate (*ca.* 0.5 g) was dissolved in water (500 mL) with heating and stirring. Small crystals, typically 0.1 x 0.1 cm in size, formed within several days. Dehydrated crystals were also obtained through sublimation under vacuum (Figure 53). Phloroglucinol dihydrate (*ca.* 0.5 g) was placed in a sublimation apparatus and was heated at 160 °C under vacuum for 10 days. Sublimed phloroglucinol accumulated on the sides of the glass tube.

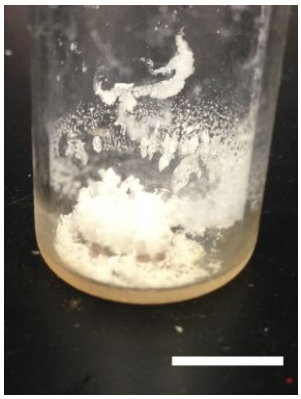

**Figure 53.** Sublimed phloroglucinol. Scale bar: 1 cm.

### 8.4.1.2. Dehydration of Achiral Crystals

Crystals of phloroglucinol dihydrate were placed in an open vial and heated in an oven to dehydrate the achiral crystals (5h at 100 °C). The transition to anhydrous chiral crystals was confirmed using X-ray powder diffraction.

### 8.4.1.3. Viedma Ripening

Viedma ripening of phloroglucinol was carried out using a modified analytical rotator. Phloroglucinol (*ca.* 0.25 g), a magnetic stir bar (10 mm x 5 mm) and grinding media (3 g of 0.8 mm of YTZ® Zirconia ceramic beads) were suspended in a saturated solution of acetonitrile (1 mL) in a x mLmicrowave vial. The sample was stirred at 1200 rpm until the crystals attained homochirality (*ca.* 4 days). Solid-state CD analysis was carried out by preparing 1.0% (*wt/wt*) samples in oven dried KBr. The samples were prepared and analyzed (CD) as described for 5-nitrouracil. The CD spectra were recorded from 240 nm to 350 nm. Three pellets were measured for each time interval and three accumulations were taken for each pellet for each sampling of the Viedma ripening process.